CAPITAL UNIVERSITY OF SCIENCE AND TECHNOLOGY, ISLAMABAD

Entropy Analysis of Peristalsis Fluid Models

by

Muhammad Nasir Abrar

A thesis submitted in partial fulfillment for the
degree of Doctor of Philosophy

in the
Faculty of Computing
Department of Mathematics

2020

Entropy Analysis of Peristalsis Fluid Models

By

Muhammad Nasir Abrar

(DMT143011)

Dr. Muhammad Usman, Professor,

University of Dayton, Ohio, USA,

(Foreign Evaluator 1)

Dr. Kambiz Vafai, Professor,

University of California, Riverside, USA,

(Foreign Evaluator 2)

Dr. Muhammad Sagheer

(Thesis Supervisor)

Dr. Muhammad Sagheer

(Head, Department of Mathematics)

Dr. Muhammad Abdul Qadir

(Dean, Faculty of Computing)

DEPARTMENT OF MATHEMATICS

CAPITAL UNIVERSITY OF SCIENCE AND TECHNOLOGY

ISLAMABAD

2020

Dedicated to

My Beloved Parents*,*

My Supporting Siblings*,*

&

My Lovely Wife*,*

Without whom none of my success

would be possible

CAPITAL UNIVERSITY OF SCIENCE & TECHNOLOGY
ISLAMABAD

Expressway, Kahuta Road, Zone-V, Islamabad
Phone:+92-51-111-555-666 Fax: +92-51-4486705
Email: info@cust.edu.pk Website: https://www.cust.edu.pk

CERTIFICATE OF APPROVAL

This is to certify that the research work presented in the thesis, entitled **"Entropy Analysis of Peristalsis Fluid Models"** was conducted under the supervision of **Dr. Muhammad Sagheer**. No part of this thesis has been submitted anywhere else for any other degree. This thesis is submitted to the **Department of Mathematics, Capital University of Science and Technology** in partial fulfillment of the requirements for the degree of Doctor in Philosophy in the field of **Mathematics**. The open defence of the thesis was conducted on **September 18, 2020**.

Student Name :   Muhammad Nasir Abrar
(DMT143011)

The Examining Committee unanimously agrees to award PhD degree in the mentioned field.

Examination Committee :

(a) External Examiner 1: Prof. Dr. Muhammad Ashraf
BZU, Mulatn

(b) External Examiner 2: Dr. Muhammad Kamran
Associate Professor
CUI, Wah Cantt Campus

(c) Internal Examiner : Dr. Muhammad Afzal
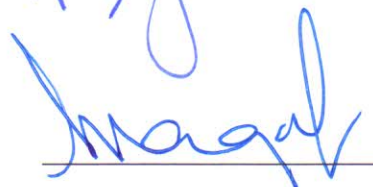Assistant Professor
CUST, Islamabad

Supervisor Name : Dr. Muhammad Sagheer
Professor
CUST, Islamabad

Name of HoD : Dr. Muhammad Sagheer
Professor
CUST, Islamabad

Name of Dean : Dr. Muhammad Abdul Qadir
Professor
CUST, Islamabad

AUTHOR'S DECLARATION

I, **Muhammad Nasir Abrar (Registration No. DMT-143011)**, hereby state that my PhD thesis titled, '**Entropy Analysis of Peristalsis Fluid Models**' is my own work and has not been submitted previously by me for taking any degree from Capital University of Science and Technology, Islamabad or anywhere else in the country/ world.

At any time, if my statement is found to be incorrect even after my graduation, the University has the right to withdraw my PhD Degree.

(Muhammad Nasir Abrar)

Dated: 18   September, 2020

Registration No : DMT-143011

PLAGIARISM UNDERTAKING

I solemnly declare that research work presented in the thesis titled "**Entropy Analysis of Peristalsis Fluid Models**" is solely my research work with no significant contribution from any other person. Small contribution/ help wherever taken has been duly acknowledged and that complete thesis has been written by me.

I understand the zero tolerance policy of the HEC and Capital University of Science and Technology towards plagiarism. Therefore, I as an author of the above titled thesis declare that no portion of my thesis has been plagiarized and any material used as reference is properly referred/ cited.

I undertake that if I am found guilty of any formal plagiarism in the above titled thesis even after award of PhD Degree, the University reserves the right to withdraw/ revoke my PhD degree and that HEC and the University have the right to publish my name on the HEC/ University Website on which names of students are placed who submitted plagiarized thesis.

(Muhammad Nasir Abrar)

Dated: 18 September, 2020

Registration No : DMT-143011

List of Publications

It is certified that the following publication(s) have been made out of the research work that has been carried out for this thesis:-

1. **M. N. Abrar**, M. Sagheer, and S. Hussain, "Entropy analysis of Hall current and thermal radiation influenced by cilia with single and multi wall carbon nanotubes" *Bulletin of Material Science*, vol. 42, https://doi.org/10.1007/s12034-019-1822-4, 2019.

2. **M. N. Abrar**, R. Ul Haq, M. Awais and I. Rashid, "Entropy analysis in a cilia transport of nanofluid under the influence of magnetic field" *Nuclear Engineering and Technology*, vol. 9, pp. 1680-1688, 2017.

3. **M. N. Abrar**, M. Sagheer, and S. Hussain, "Entropy formation analysis for the peristaltic motion of ferrofluids in the presence of Joule heating and fluid friction phenomena in a plumb duct" *Journal of Nanofluids*, vol. 8, pp. 1305-1313, 2019.

4. **M. N. Abrar**, M. Sagheer, and S. Hussain, "Entropy analysis of SWCNT & MWCNT flow induced by collecting beating of cilia with porous medium" *Journal of Central South University*, vol. 26, pp. 2109-2118, 2019.

Muhammad Nasir Abrar

(DMT143011)

Acknowledgements

Alhamdulliah, all praises to **Allah** for the strengths and His blessing in completing this thesis. I would like to express the deepest appreciation to my honorable and worthy supervisor **Prof. Dr. Muhammad Sagheer** for his valuable and constructive suggestion during the planning, development and completion of this research work and a special thanks for his kind, polite and welcoming nature.

Besides my supervisor, I would like to express my special thanks and respect to **Dr. Muhammad Awais** and **Dr. Shafqat Hussain** and **Dr. Rizwan Ul Haq** for their inspiration, patient guidance, support and encouragement throughout my research. I would also like to express my gratitude to **Dr. Rashid Ali** and **Dr. Muhammad Afzal** for their valuable guidance during synopsis preparation and positive criticism through out the research seminars.

For most, I would like to express my great gratitude to **Ammi** and **Abu**, and all other family members for their love, support, and sacrifices during this time period. Without them, this thesis would never have been written. I am very much thankful to my elder brother **Lt. Col. Muhammad Shakir Ullah** for his financial support, he is more than an ideal for me and a person of great ethics and support, without his support and motivation, I wouldn't be able to complete my Ph. D degree.

I cannot forget friends who went through hard times together, cheered me on, and celebrated each accomplishment: **Mr. Irfan Rashid**, **Engr. Imran Rashid**, **Dr. Umar Farooq**, **Dr. Rizwan Tariq**, **Mr. Basit Suhaib** and **Mr. Majid Awan**.

Finally, I thank with love to my wife: **Uzma Nasir**. Uzma has been my great companion during this period. She has been extremely supportive of me throughout this entire process and has made countless sacrifices to help me get to this point.

Abstract

In this thesis, it has been managed to analyze the entropy generation during the peristaltic transport of creeping viscous nanofluid in an axisymmetric channel. The peristaltic pumping is incorporated in frame of two basic scenarios: (i) a peristaltic wavelength is assumed to be very large compared with the channel width, and (ii) a sufficiently small Reynolds number is considered, which indicates inertia free flow. The flow is provoked as a result of metachronal waves, which are produced, when a group of cilia operate together. These metachronal waves moves together in the direction of an effective stroke to transport the fluid and transmit wavy or beating motion. The flow is assumed to be two dimensional, incompressible, and linear viscous (Newtonian). The momentum analysis is performed under the impact of various pertinent flow parameters such as Hall current, gravitational force, porous medium, transverse and inclined magnetic field with horizontal and vertical channel. Further, the energy analysis is performed in the presence of thermal radiation, viscous dissipation, Joule heating and internal heat source phenomena. All of the above body forces are taken along the horizontal, vertical and inclined channel flow. Moreover, entropy generation due to heat transfer, thermal radiation, viscous dissipation and magnetic effects has been encountered. The mathematical modeling is reflected in the form of a nonlinear coupled partial differential equations. The governing differential equations is transformed into ordinary differential equations by considering some suitable dimensionless variables. Exact solutions in the closed form have been computed for the momentum, pressure gradient and temperature profiles. Graphical results have been carried out to interpret the pertinent parameters of interest. The main goal i.e. the reduction of the entropy generation of the second law of thermodynamics is achieved by decreasing the magnitude of Brinkmann number, Hartmann number and dimensionless temperature difference. Fluid velocity is reduced by an increasing the magnitude of Hartmann number and Darcy number. Further, the trapping phenomenon is also portrayed through streamlines pattern for certain flow parameters.

Contents

List of Figures

List of Tables

Abbreviations

CNTs	Carbon Nanotubes
MWCNTs	Multi Wall Carbon Nanotbes
MHD	Magnetohydrodynamics
MRI	Magnetic Resonance Imaging
SWCNTs	Single Wall Carbon Nanotubes
SAE	Society of Automotive Engineering

Symbols

Al_2O_3 Aluminum oxide

α Measure of the eccentricity of the elliptical motion

α^* Coefficient of linear thermal expansion

a Electric charge

Br Brinkmann number

Be Bejan number

B_0 Applied magnetic field

β Wave number

cP Centipoise

CuO Copper oxide

Cu Copper

c_p Specific heat

c Wave speed

Da Darcy number

ΔP Pressure rise

∇ Differential operator

Eg Entropy number

e Mean radius of the tube

ϵ Wave amplitude

E_H Entropy due to heat transfer

E_{Rn} Entropy due to thermal radiation

E_M Entropy due to magnetic field

E_V Entropy due to viscous dissipation

Fe_3O_4	Magnetite
F	Mean flow rate
γ	Ratio of nanolayer thickness to the original particle
Gr	Grashof number
g	Acceleration due to gravity
Ha	Hartmann number
J_h	Joule heating
k_{CNT}	Thermal conductivity of carbon nanotubes
k_{bf}	Thermal conductivity of base fluid
k_s	Thermal conductivity of solid nanoparticles
k^*	Rosseland mean absorption coefficient
k_{nf}	Effective thermal conductivity
λ	Wavelength
Λ	Dimensionless temperature difference
D/Dt	Material derivative
μ	Dynamic viscosity
m	Hall parameter
μ_{nf}	Effective dynamic viscosity
ν	Kinematics viscosity
n_a	Number density of electrons
Ω	Internal heat source parameter
P	Pressure
dp/dz	Pressure gradient
ϕ	Solid volume fraction
$\bar{\Phi}$	Viscous dissipation
Q_0	Internal heat source coefficient
Q	Flow rate
ρc_p	Heat capacity of the material
Re	Reynolds number
$\bar{R}$	Radial direction in fixed framed
du/dy	Rate of shear deformation

Rn	Radiation parameter
ρ_{nf}	Effective density
$(\rho c_p)_{nf}$	Heat capacitance
ρ	Density
$\bar{r}$	Radial direction in wave frame
S_G	Volumetric entropy generation
S_g	Characteristic entropy generation
σ	Electric conductivity
σ^*	Stefan-Boltzmann constant
Θ	Angle of inclination
θ	Dimensionaless temperature component
τ	Shear stress
TiO_2	Titanium dioxide
T	Temperature
$\bar{u}$	Dimensional velocity elements in the radial direction
w	Dimensionaless velocity component
$\bar{w}$	Dimensional velocity elements in the axial direction
$\bar{z}$	Axial direction in wave frame
$\bar{Z}$	Axial direction in fixed framed
Z_0	Reference position of cilia

Chapter 1

Introduction

This chapter provides comprehensive literature review of fluid, entropy, peristalsis, nanofluid, magnetohydrodynamics and porous medium to the reader in order to have excellent understating of this thesis.

1.1 Background

The recent developments in science and technology have classified the fluid flow models into two categories; the hydraulic systems which deal with the development of experimental studies and the hydrodynamics that deals with the theoretical studies. A few characteristics of physical interest of the hydraulics and the hydrodynamics are density, viscosity, temperature, pressure, etc. Due to such characteristics both the hydraulics and the hydrodynamics are merged into a single discipline called the fluid mechanics. It has countless practical applications in mechanical industry, chemical industry, bio-medical industry, etc. In mechanics, the fluid flow is organized as compressible (all gases) and incompressible (all liquids) flow on the basis of density. On the broader side there are basically two types of flow; the internal and external flows. If a fluid flows thorough confined boundaries; it is known as an internal flow such as flow in ducts, nozzles, pipes, and vessels, otherwise the flow is known as an external flows such as ocean flow,

flow over an airplane. All of these flow categories are of tremendous importance in our daily life. Flow of any fluid flowing is not as much smooth as it is seen. There are numerous factors influencing the progression of fluid (e.g viscosity, density, and velocity of the fluid) and thus energy is not fully transferred into work. In modern physics, 2nd law of thermodynamics is used to calculate this loss in terms of entropy.

The mechanics of every engineering machine containing thermofluid strongly relies upon the structure and the running temperature of the functioning fluid. Since the energy transfer is an irreversible mechanism, therefore, for the outstanding performance of system, it is mandatory to scrutinize the entropy of fluid system. The 2nd law of thermodynamics is used to scrutinize the irreversibilities in a system in terms of entropy. When the transfer of heat takes place through a chemical reaction, fluid friction and finite temperature, it causes an irreversibility in the system, which generates entropy. The entropy comprises of two principal parts: 1 - the thermal irreversibility and 2 - the energy losses due to frictional factors. From a birds eye view, entropy appears as a result of the heat transport. Physically, when the heat transfer takes place, some supplementary changes happen at a molecular level such as resistance, vibration, unstained expansion, displacement and spin moment which cause the loss of effective heat and thus energy cannot be transmitted effectively into work. It should be noted that this type of energy fall cannot be earned back, therefore entropy is also called the measure of irreversibilities. The entropy generation is associated with a number of energy related applications such as geothermal power systems, cooling of modern electronic systems and solar power collectors.

The latest studies have demonstrated that the second law investigation approach is an effective and productive approach for reducing the system entropy. Firstly, Bejan [1] described the science of entropy in energy transport and in flow systems. Robert [2], Xu et al. [3], Bejan [4], Nada [5], Qudais and Nada [6], Naterer and Camberos [7], Mahmud and Fraser [8], Nada [9], Romatschke [10], Aksoy [11],

Srinivasacharya and Bindu [12], Kamran et al. [13], Hussain et al. [14], Anjum et al. [15], Saleem and El-Aziz [16], etc, have contributed significantly in this useful area of entropy analysis by considering different physical and engineering scenarios. The analysis of entropy generation in peristaltic flows has attracted the attention of many researchers in last two decades.

Peristalsis is a procedure of pumping the fluid, when a progressive wave shrinkage or development proliferates along the boundaries of the tube possessing a fluid. In this pumping process, the fluid moves like the sinusoidal waves travelling along the walls in the direction of their propagation during the contraction/expansion of the wave. This process of pumping the fluid is significant in multiple fields of sciences, including physiological, engineering and biochemical industry [17]. The requirement of peristalsis emerges, when it is that fascinating to evade utilizing any moving unit inside the structure, for example, pistons in the pumping mechanism. Further, the peristaltic transport is a normal phenomenon of shifting the substance inside empty solid structures by progressive constriction of their strong fibers. It happens in gulping nourishment through the throat, development of chyme, transport of urine and lymph in the lymphatic vessel. In fluid transport, the peristaltic pumping has turned out very purposeful over short distances avoiding the fluid from being contaminated. The fundamental principle of peristalsis for the transport of fluids has been practiced by the engineers in the manufacturing of multiple industrial and biological instruments involving roller, finger pumps, blood pumps and dialysis machines [18]. The mechanism of peristaltic flow is also applied in the nuclear industry for the movement of caustic fluids, where the mixing of fluid with the component of machines is restricted. Some more expolarity investigations in this broader area can be found in Weinberg et al. [19], Srivastava and Srivastava [20], Siddiqui et al. [21], Srivastava and Saxena [22], Srinivasacharya et al. [23], Srinivas and Pushparaj [24], Vajravelu et al. [25], Tripathi [26], Kamel et al. [27], Hayat et al. [28], Mekheimer et al. [29], Ellahi et al [30], etc.

In the last decade, as the energy crises are emerging rapidly, there has been a massive need for new techniques which can increase the thermal efficiency of the

working fluid and thus reduce the overall energy crises. In order to overcome the energy crises, the vibration phenomenon [31], micro channels [32], wavy surfaces [33], etc are developed by the researchers and engineers to reinforce the heat transfer rate.

In 1995, Choi [34] initially introduced the term nanofluid which describes that the heat transfer rate can be strengthened by boosting the thermal attitude of the base fluids. Actually, the base fluids, like pure water, lubricants etc., possess a finite heat transfer strength, because of their low thermal abilities, on contrary, the nanoparticles hold dramatically higher thermal strength as compared to the base fluids. Moreover, nanofluids offer their potential application in pharmaceutical industry such as drug delivery microchip [35], nanomedicine applications of nanogels [36], in detergents industry [37, 38], and in cooling industry [39]. It is a very common practice in circumpolar world where the temperature is almost less then 40° throughout the years to use nanoparticles with water as a heat transfer fluid in order to maintain the daily life activities.

Based on the these useful applications of nanoparticle, several studies in this direction have been undertaken using different flow conditions. Flow induced by linear stretching with convective heating was presented by Makinde and Aziz [40]. Stagnation point flow under the influence of porous medium was studied by Alsaedi et al. [41]. Brownian motion and thermophoresis effects over an exponential stretching surface were demonstrated by Nadeem and Lee [42]. Characteristics of unsteady flow over an infinite plate were examined by Turkyilmazoglu and Pop [43]. Natural convection flow under the action of MHD was discussed by Sheikholeslami et al. [44]. Third grade nanofluid flow in the presence of unifrom MHD and the Maxwell model for the convective cooling were studied by Awais et al. [45, 46]. Consequences of forced convection heat transfer in an annuls and free convection heat transfer in a cubic cavity was presented by Sheikholeslami et al. [47, 48].

Impulsive motion of free convective flow under the influence of thermal radiation

was analyzed by Das and Jana [49]. Mixed convection flow in a symmetric duct was introduced by Abbasi et al. [50]. The impact of thermal radiation in a flow of suspended nanoparticles was demonstrated by Hayat et al. [51]. A comprehensive review of the under study solid nanoparticles i.e. carbon nanotubes, titanium dioxide and magnetite is provided in next three paragraphs.

Carbon nanotubes fall in a new class of nanocarrier structures, which are responsible for enhancing the thermal performance of the conventional fluids. CNTs are best fitted in the group of fullerene structures and incorporate amazing carbon particles which contain high length to diameter ratio. These marvelous characteristics of carbon nanotubes make them interesting. The structure of CNTs gives them absolutely surprising electrical and physical properties. CNTs take the form of cylindrical carbon molecules and have unique characteristics such as electrical and thermal conductivity, electron emission, energy storage, expansion, and aspect ratio. These characteristics make them highly advantageous in a number of applications in molecular electronics, thermal materials, structural materials, fabrics, fibers, catalyst supports, biomedical, water filtration, conductive plastics and ceramics. Carbon nanotubes were first found by Iijima [52]. Moreover, carbon nanotubes are subdivided into two unique classes; the single wall carbon nanotubes (SWCNT) and the multi wall carbon nanotubes (MWCNT). Apart from their rare existence, CNTs find their utilization as added substance in structural materials, for instance, golf stub, water-boat, airship, and engine-bicycles. Also, CNTs are extensively used in electrical gadgets [53, 54], compound goods [55, 56] hydrogen stockpiling [57, 58] and many others. Thermally, CNTs hold immense thermal abilities. As far as electrical properties are concerned, CNTs can be either metallic or semiconducting, dependent upon the presentation of the network with respect to the tube center. The transport properties of nanofluids are not just susceptible on volume fraction of nanoparticle, these also depend upon the particle shape, size and mixture combinations, etc. Earlier studies clearfy clarify that the thermal properties as well as the viscous nature of fluid can be improved by considering the nanofluid instead of the conventional fluids. The subject of heat transfer with nanofluids is investigated by many e.g., Nallusamy et al. [59],

Sabhia et al. [60], Eshgarf et al. [61], Baratpour et al. [62], Akbar et al. [63], Bahiraei et al. [64], shahsavani et al. [65], etc.

Titanium dioxide (TiO_2) nanoparticles achieve their best performance in biological, chemical and environmental engineering, for instance, in drugs, foodstuff, skin goods, toothpastes, skin care products, cosmetic, sunscreens, paints, nail polishes, plastics, printing inks, and ceramic glazes. These nanoparticles have great potential for remediation of waste water. Furthermore, they also reduce the probability of skin tumors, skin smolder, and untimely maturing. Based on the above applications of TiO_2 nanoparticles, several studies in this direction have been undertaken using different flow conditions like application of free convection was given by Dongsheng and Yulong [66], heat transport analysis of natural convection was presented by Wen et al. [67], heat transport enhancement in a tube was investigated by Duangthongsuk et al. [68], thermal efficiency of heat pipes was experminetally studied by Saleh et al. [69], energy transport analysis of Nusselt number in a duct was studied by Arulprakasajothi et al. [70], etc.

The magnetite (Fe_3O_4) offers its potential applications in biological, chemical and environmental engineering, for instance, high gradient magnetic separation [71], pharmaceutical transport [72], restoration of harmful wastes [73], magnetic resonance technology [74], safe drinking water [75], antimicrobial behavior [76], crude petroleum collector for oil spills [77], anticorrosion coatings [78]. Moreover, food and health authorities endorse the clinical utilization of magnetite due to its diverse characteristics and compatibility with medical science as it naturally exists in the human body organs, like heart, spleen, liver, etc. Based on the above useful applications of magnetite nanoparticles, the subject of nanofluids with different geometries has been discussed by a very big number of researchers e.g. Hiergeist and Andr [79], Odenbach [80], Voelker and Odenbach [81], Xuan et al. [82], Jafari and Tynj [83], Rosensweig and Ronald [84], and Sandeep et al. [85].

In modern physics, magnetic field is applied to the flowing fluid in order to manage the flow. Magnetohydrodynamics describes the study of motion of electrically conducting fluid e.g. liquid metals and plasmas. The basics of MHD was first given

by Hannes Alfven [86]. In the plenty of industrial mechanisms, magnetic effects are used to mix up, pump, levitate and heat liquid metals. The earth's magnetic field, insulating the surface from toxic radiation, is generated by the motion of the earths liquid core. Sunspots and solar flares are generated by the solar magnetic field which influences the formation of stars from interstellar gas clouds. We use the word Magnetohydrodynamics (MHD) for all of these phenomena, where the magnetic field and the velocity field are coupled, given that there is an electrically conducting and non-magnetic fluid. The MHD peristaltic flow is very meaningful in biological systems having conductive fluids, such transport phenomena are blood pumps, magnetic resonance imaging (MRI), aimed transport of medicines by means of magnetic units as drug carriers and blood therapy. These interesting engineering applications of MHD, have pulled the consideration of mathematicians and engineers. Several studies on MHD peristaltic transport with different flow geometries have been undertaken. Flow through homogenous porous medium in a planer channel with insulated walls was investigated by Mekheimer and Al-Arabi [87]. Two dimensional flow of Johnson-Segalman fluid along the walls of a flexible duct was presented by Elshahed and Haroun [88]. The peristalsis flow analysis of viscous fluid in a vertical tube was examined by Mekheimer and Elmaboud [89]. Heat transfer analysis of MHD persitaltic flow along the walls of an asymmetric channel was examined by Srinivas and Kothandapani [90]. Exact solution of MHD peristaltic flow over a symmetric channel was studied by Nadeem and Akram [91]. Mixed convective flow over a vertical porous medium was studied by Srinivas and Muthuraj [92]. Flow of an Oldroyd-B fluid in symmetric duct was studied by Zakaria and Amin [93]. Analysis of MHD, viscous dissipation and Joule heating inside the compliant walls was studied by Hayat et al. [94]. The magnetite nanofluid flow over an asymmetric channel was explained by Prakash et al. [95].

In any engineering procedure, there are many ways to increase the rate of heat transfer, one of them is using porous media in heat transfer appliances. Porous materials come across everywhere in daily life, in technology and in nature. A material or structure must posses these two properties in order to entitle as a porous medium: i) it must contain spaces, so-called voids or pores, free of solids,

embedded in the solid or semi-solid matrix. ii) It must be permeable to a variety of fluids, i.e., fluids should be able to penetrate through one face of a sample of material and emerge on the other side. The process of using porous material has been the core subject of multiple studies and has taken a rational appreciation. This appreciation is because of the fact that this type of structure is highly acceptable in many engineering applications, such as thermal insulation, oil flow, ground water, power stations, etc. Porous medium is specially applied in such kinds of engineering devices, where the cooling or heating is mandatory [96].

The scope of this thesis is to analyze the entropy generation during the peristaltic transport of nanofluids. Motivated by the significance and fascinating applications of peristaltic pumping in a flow system, peristalsis flow is considered. Chapter 2 provides introduction to some important terminologies. The detail analysis of entropy generation in the presence of Hall current and thermal radiation induced by cilia waves in a vertical tube is given in chapter 3. Chapter 4 covers the entropy analysis of cilia transport under the influence of magnetic field in a horizontal tube. Chapter 5 gives the detailed analysis of entropy formation during the peristaltic movement of ferrofluids in the presence of Joule heating and viscous dissipation phenomena. The entropy analysis of SWCNT and MWCNT flow induced by collecting beating of cilia in porous medium is given in chapter 6. Chapter 7 is focused on the concluding remarks of this thesis.

Chapter 2

Preliminaries

2.1 Introduction

This chapter contains some basic definitions of fluid flow, fundamental concepts and ideas of fluid and dimensionless numbers regarding the presented work.

2.1.1 Fluid [97]

"A substance in the liquid or gas phase is referred to as a fluid. Distinction between a solid and a fluid is made on the basis of the substance's ability to resist an applied shear (or tangential) stress that tends to change its shape. A solid can resist an applied shear stress by deforming, whereas a fluid deforms continuously under the influence of shear stress, no matter how small. In solids stress is proportional to strain, but in fluids stress is proportional to strain rate. When a constant shear force is applied, a solid eventually stops deforming, at some fixed strain angle, whereas a fluid never stops deforming and approaches a certain rate of strain".

2.1.2 Stress [97]

"Stress is defined as force per unit area and is determined by dividing the force by the area upon which it acts. The normal component of the force acting on a surface per unit area is called the normal stress, and the tangential component of

a force acting on a surface per unit area is called shear stress). In a fluid at rest, the normal stress is called pressure".

2.1.3   Mechanics [97]

"Mechanics is the oldest physical science that deals with both stationary and moving bodies under the influence of forces. The branch of mechanics that deals with bodies at rest is called statics, while the branch that deals with bodies in motion is called dynamics. The subcategory fluid mechanics is defined as the science that deals with the behavior of fluids at rest (fluid statics) or in motion (fluid dynamics), and the interaction of fluids with solids or other fluids at the boundaries. Fluid mechanics is also referred to as fluid dynamics by considering fluids at rest as a special case of motion with zero velocity (see Figure 2.1)".
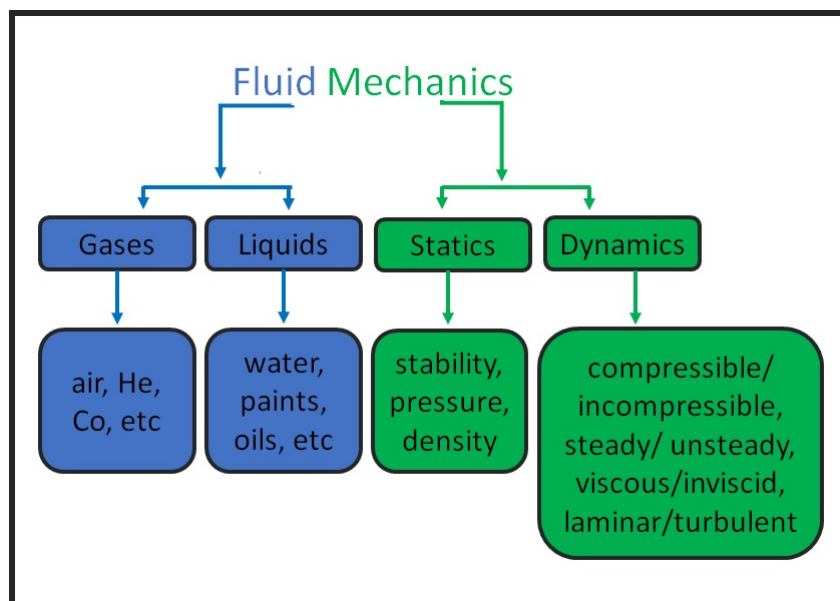
FIGURE 2.1: Fluid mechanics flow chart

2.1.4   Viscosity [97], [98], [99]

"Viscosity is a quantitative measure of a fluids resistance to flow. More specifically, it determines the fluid strain rate that is generated by a given applied shear stress. We can easily move through air, which has very low viscosity. Movement is more difficult in water, which has 50 times higher viscosity then air. Still more resistance is found in Society of Automotive Engineers (SAE) 30 oil, which is 300 times more

viscous than water. Fluids may have a vast range of viscosities. The viscosity of liquids decreases with the increase of temperature and while the viscosity of gases increases with the increase of temperature. Viscosity is caused by cohesive forces between the molecules in liquids and by molecular collisions in gases. There is no fluid with zero viscosity, and thus all fluid flows involve viscous effects to some degree (see Figure 2.2). Flows in which the frictional effects are significant are called viscous flows.

Mathematically:

$$\mu = \frac{\tau}{\left(\dfrac{du}{dy}\right)},$$

(2.1)

where μ is called the constant of proportionality, and is known as the coefficient of dynamic viscosity or only viscosity, τ is the shear stress and du/dy represents the velocity gradient or rate of shear deformation. Thus viscosity is also defined as shear stress required to produce unit area of strain. The unit of viscosity is centipoise (cP). The viscosity of water at 20°C is 1 centipoise".
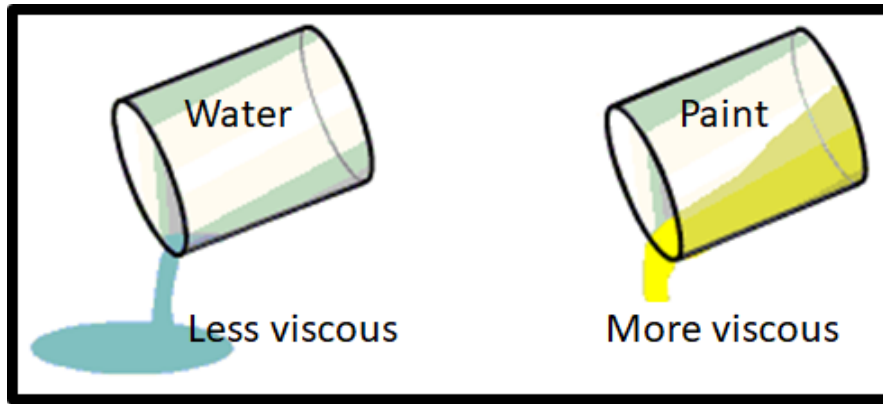
FIGURE 2.2: Viscosity

2.1.5 Kinematics Viscosity [99]

"It is defined as the ratio between dynamic viscosity and density if fluid. It is denoted by Greek letter ν. Thus, mathematically,

$$\nu = \frac{\text{viscosity}}{\text{density}} = \frac{\mu}{\rho},$$

(2.2)

the SI unit of kinematics viscosity is m^2/sec".

2.1.6   Newton's Law of Viscosity [99]

"It states that shear stresses (τ) on a fluid element layer is directly proportional to the rate shear strain. The constant of proportionality is called the coefficient of viscosity.

Mathematically, it is expressed as given by the equation:

$$\tau = \mu \frac{du}{dy}, \tag{2.3}$$

in the above equation, μ is the viscosity and $\frac{du}{dy}$ is the deformation rate. Fluids which obey the above relation are known as Newtonian fluids and the fluids which do not obey the above relations are called non-Newtonian fluids".

2.1.7   Thermodynamic Properties of a Fluid [98]

"The three most common thermodynamic properties of a fluid are:

2.1.7.1   Pressure [98]

The pressure (P) is the most dynamic variable in fluid mechanics. Pressure is defined as a normal force exerted by a fluid per unit area. We speak of pressure only when we deal with a gas or a liquid. The counterpart of pressure in solids is normal stress. Differences or gradients in pressure often drive a fluid flow, especially in ducts.

2.1.7.2   Temperature [98]

Temperature (T) is a measure of the kinetic energies of the particles such as the molecules or atoms of a substance. In a liquid or gas, the kinetic energy of the molecules is due to their random translational motion as well as their vibrational and rotational motions. The higher the temperature, the faster the molecules move and the higher the number of such collisions, and the better the heat transfer.

2.1.7.3   Density [98]

The density of a fluid, denoted by ρ, is its mass per unit volume. Density is highly

variable in gases and increases nearly proportionally to the pressure level. The most liquid flows are treated analytically as nearly incompressible".

2.1.8 Uniform and Non-uniform Flows [98]

"The flow is said to be uniform if the magnitude and direction of flow velocity are the same at every point and flow is said to be non-uniform if the velocity is not the same at each point of the flow, at a given instant (see Figure 2.3)".
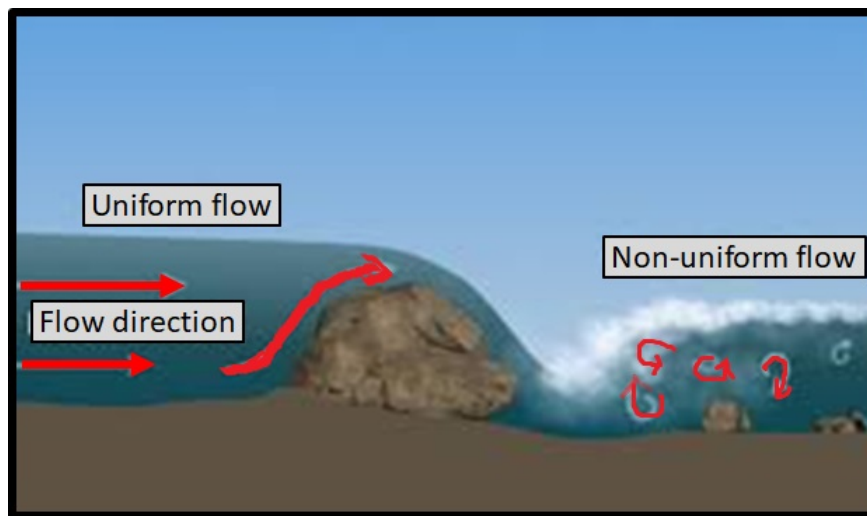
FIGURE 2.3: Uniform and non-uniform flows

2.1.9 Steady and Unsteady Flows [98]

"A flow whose flow state expressed by velocity, pressure, density, etc, at any position, does not change with time, is called a steady flow. A flow whose flow state does change with time is called an unsteady flow".

2.1.10 Compressible and Incompressible Flows [98]

"Flow in which variations in density are negligible is termed as incompressible other wise it is called compressible. The most common example of compressible flow is the flow of gases, while the flow of liquids may frequently be treated as incompressible. Mathematically,

$$\frac{D\rho}{Dt} = 0,$$ (2.4)

where ρ denotes the fluid density and $\frac{D}{Dt}$ is the material derivative given by

$$\frac{D}{Dt} = \frac{\partial}{\partial t} + V.\nabla, \tag{2.5}$$

in above equation, V denotes the velocity of the flow and ∇ is the differential operator. In Cartesian coordinate system, ∇ is given as:

$$\nabla = \frac{\partial}{\partial x}\hat{i} + \frac{\partial}{\partial y}\hat{j} + \frac{\partial}{\partial z}\hat{k}". \tag{2.6}$$

2.1.11 Types of Fluid [99]

"The fluids may be classified into following five types (see Figure 2.4):

2.1.11.1 Ideal Fluid [99]

A fluid which is incompressible and having no viscosity, is known as ideal fluid. Ideal fluid is only an imaginary fluid as all the fluids, which exist, have some viscosity.

2.1.11.2 Real Fluid [99]

A fluid, which possesses viscosity, is known as real fluid. All the fluids, in actual practice, are real fluid.

2.1.11.3 Newtonian Fluid [99]

A real fluid, in which the shear stress is directly proportional to rate of shear strain (or velocity gradient), is known as Newtonian fluid.

2.1.11.4 Non-Newtonian Fluid [99]

A real fluid, in which the shear stress is not directly proportional to rate of shear strain (or velocity gradient), known as non-Newtonian fluid.

2.1.11.5 Ideal Plastic Fluid [99]

A fluid, in which the shear stress is more than the yield value and shear stress

is proportional to the rate of shear strain (velocity gradient), is known as ideal plastic fluid (also called Bingham plastic fluid)".
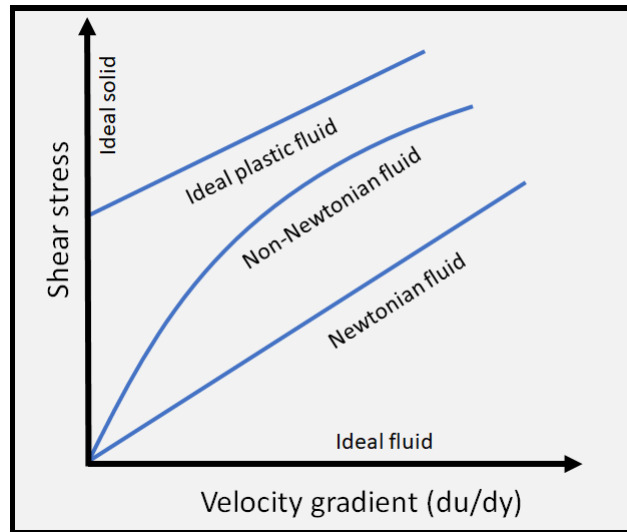
FIGURE 2.4: Types of fluid

2.1.12 Boundary Layer Flow [98]

"The concept of boundary layer was first introduced by Ludwig Prandtl, a German aerodynamicist, in 1904. Prandtl introduced the basic idea of the boundary layer in the motion of a fluid over a surface. Boundary layer is a flow layer of fluid close to the solid region of the wall in contact, where the viscosity effects are significant (see Figure 2.5). The flow in this layer is usually laminar. The boundary layer thickness is the measure of the distance apart from the surface. There are two types of boundary layers:

2.1.12.1 Hydrodynamic (Velocity) Boundary Layer [98]

A region of a fluid flow, where the transition from zero velocity at the solid surface to the free stream velocity at some extent far from the surface in the direction normal to the flow takes place in a very thin layer, is known as the hydrodynamic boundary layer.

2.1.12.2 Thermal Boundary Layer [98]

The heat transfer exchange surface and the free stream a liquid or a gaseous

agent for heat transfer. From wall to free stream we come across the change of temperature of heat transfer agent. It increases from wall to the main stream. The surface temperature is assumed to be equal to the temperature of the fluid layer closed to the wall inside the boundary and this temperature is equal to the temperature of the bulk at some point in the fluid".
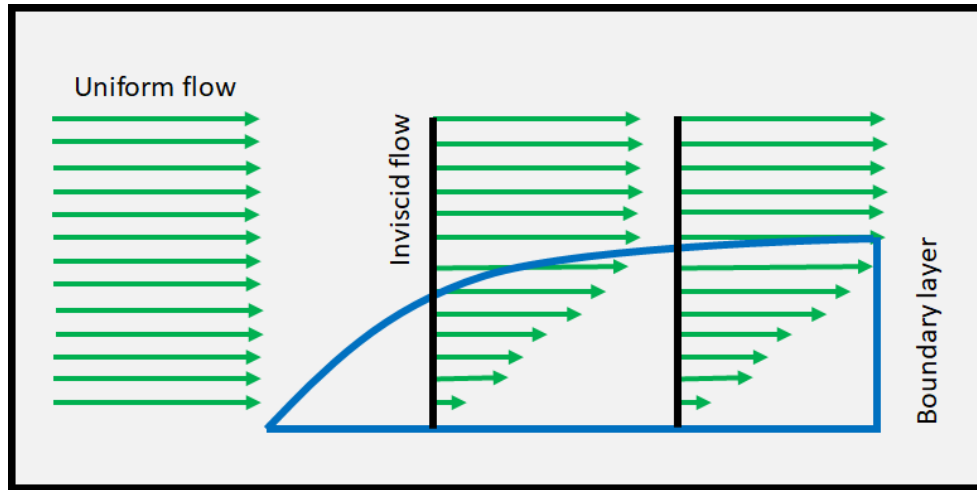
FIGURE 2.5: Boundary layer flow

2.1.13 Nanofluid [101]

"A nanofluid is the mixture of nanoparticles suspended in the base fluid. It is an advanced heat transfer fluid that possesses superior heat transfer properties. Recent developments in nanotechnology bring out fluids that possess better thermal properties than conventional fluids. The inherent properties like the larger relative surface area of nanoparticles and superior thermal conductivity makes them a choice for thermal engineers over conventional fluid. A suspended nanoparticle significantly improves heat transfer capabilities and stability of the suspension. Nanofluids possess wide range of possibilities as it can enhance heat transfer performance in comparison to that of pure liquids and hence can be considered as next generation heat transfer fluids. The most recent popular nanoparticles which are used to produce nanofluids are aluminum oxide (Al_2O_3), copper oxide (CuO), copper (Cu). While the most common base fluids which are being employed for producing nanofluids are water, oil, decene, acetone and ethylene glycol".

2.1.14 Magnetohydrodynamics [102]

"Magnetohydrodynamics describe the study of motion of electrically conducting fluid (e.g. liquid metals and Plasmas) in the presence of a magnetic field. The key hypothesis behind magnetohydrodynamic is that magnetic fields can generate current in a moving conductive fluid, which sequentially produce a force on the fluid and also alter the magnetic field itself. The basic equations of magnetohydrodynamics have been proposed by Hannes Alfven, who realized the importance of the electric currents carried by a plasma and the magnetic field they generate. Alfven combined the equations of fluid dynamics with Faradays and Amperes laws of electrodynamics, thus obtaining a novel mathematical theory, which helped understanding space plasmas in earth and planetary magnetospheres, as well as the physics of the sun, solar wind, and stellar atmospheres".

2.1.15 Heat Transfer [100]

"Heat is the form of energy that can be transferred from one system to another as a result of temperature difference. The basic requirement for heat transfer is the presence of a temperature difference (see Figure 2.6). There can be no net heat transfer between two mediums that are at the same temperature. The temperature difference is the driving force for heat transfer, just as the voltage difference is the driving force for electric current flow and pressure difference is the driving force for fluid flow. The rate of heat transfer in a certain direction depends on the magnitude of the temperature gradient (the temperature difference per unit length or the rate of change of temperature) in that direction. The larger the temperature gradient, the higher the rate of heat transfer".

2.1.16 The First Law of Thermodynamics [100]

"The first law of thermodynamics, also known as the conservation of energy principle, states that energy can neither be created nor destroyed; it can only change forms. The conservation of energy principle (or the energy balance) for any system undergoing any process may be expressed as follows: The net change (increase or
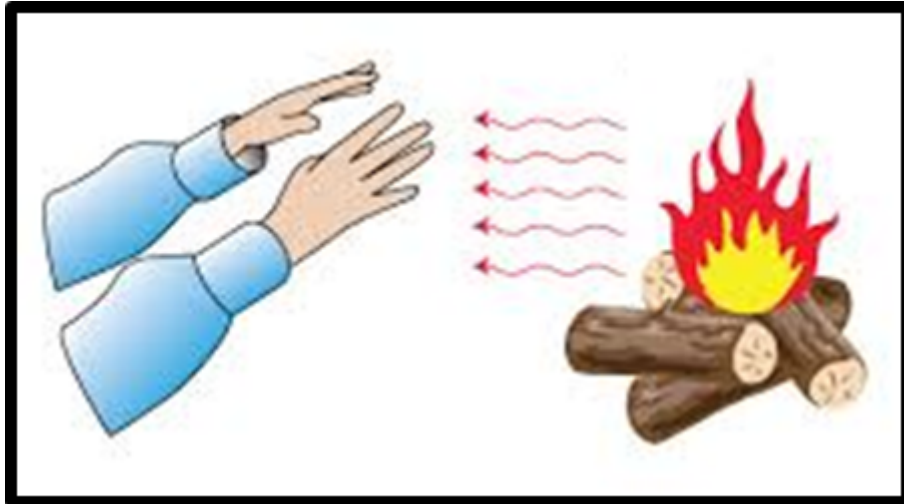
FIGURE 2.6: Heat transfer

decrease) in the total energy of the system during a process is equal to the difference between the total energy entering and the total energy leaving the system during that process".

2.1.17 Thermal Conductivity [100]

"The rate of heat transfer through a unit thickness of the material per unit area per unit temperature difference. The thermal conductivity of a material is a measure of the ability of the material to conduct heat. A high value for thermal conductivity indicates that the material is a good heat conductor, and a low value indicates that the material is a poor heat conductor or insulator".

2.1.18 Specific Heat [100]

"The product ρc_p, which is frequently encountered in heat transfer analysis, is called the heat capacity of a material. Both the specific heat (c_p) and the heat capacity (ρc_p) represent the heat storage capability of a material. But c_p expresses it per unit mass, whereas ρc_p expresses it per unit volume".

2.1.19 Entropy [103]

"Entropy is a Greek terms means change. It is a measure of disorder or randomness of molecular motion of the system (see Figure 2.7). It is a thermal property of

a system, which remains constant as long as no heat enters or leaves the system. Entropy of a system increases if heat flows into the system at constant temperature and decreases, if leaves the system at constant temperature. Noted that such kind of energy loss can not be regained so system and surrounding cannot come to its initial state without doing any extra work on it be. Therefore, entropy is called the measure of irreversibilities. In nature there is no reversible process due to friction and heat transfer. So every thermodynamic process is irreversible".
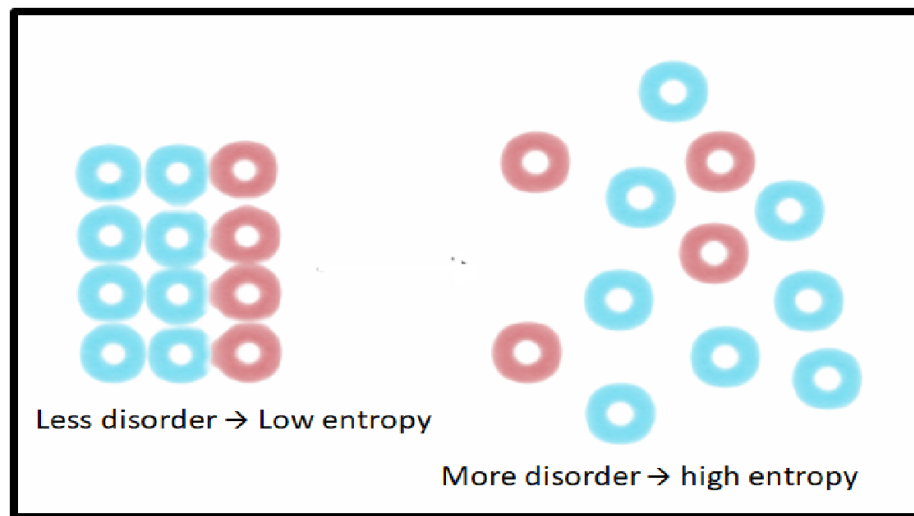
FIGURE 2.7: Entropy

2.1.20 Peristalsis [100]

Peristalsis means centrifugally symmetric tightening and slackening of muscles which proliferates in the form of a wave (see Figure 2.8). Peristalsis commonly occurs in the digestive system of living organisms to propel food material, gastro-intestinal tract, the bile tube, etc. Peristaltic transport happens, when the fluid moves as a result of a sinusoidal wave travel on the tube walls in the direction of their propagation during the contraction and expansion of the wave. This fundamental principle of peristalsis for the transport of fluids has been practiced by the engineers in the manufacturing of multiple industrial and biological instruments involving roller, finger pumps, blood pumps in heart lung and dialysis machines. The mechanism of peristaltic flow is also applied in the nuclear industry for the movement of corrosive fluids, where the connection of the fluid with the machinery is restricted.
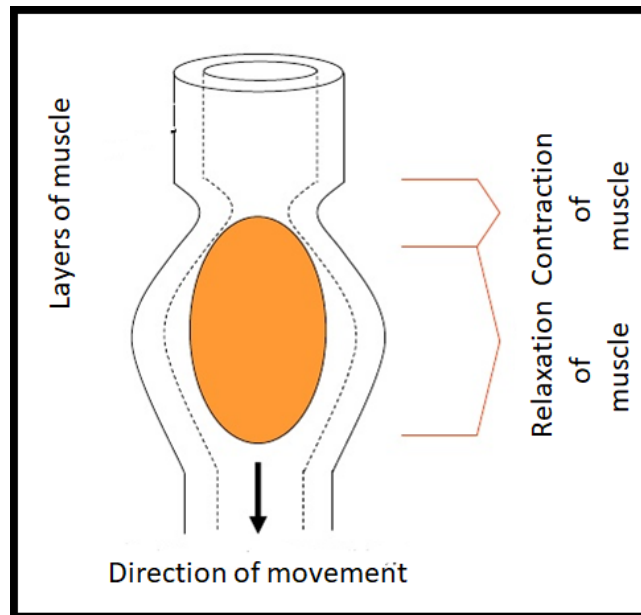
FIGURE 2.8: Mechanism of peristalsis

2.1.21 Dimensionless Physical Quantities [104]

"In physics and mathematics, dimensionless physical quantities have been widely used. Some of these quantities, which are usefull in this thesis are:

2.1.21.1 Reynolds Number [104]

Reynolds Number (Re) expresses the ratio of the fluid inertia force to that of molecular friction (viscosity). It characterizes the hydrodynamic conditions for viscous fluid flow. It determines the character of the flow (laminar, turbulent and transient flows).

2.1.21.2 Bejan Number [104]

Bejan number (Be) expresses the ratio of heat transfer unreturnability to the total unreturnability caused by heat transfer and fluid friction.

2.1.21.3 Entropy Generation Number [104]

Entropy number (Eg) characterizes the fluid entropy change in laminar streaming of viscous incompressible fluid through an inclined canal with isothermic walls. It was determined from the analysis of the second law of thermodynamics.

2.1.21.4 Hartmann Number [104]

Hartmann number (Ha) expresses the ratio of the induced electrodynamic (magnetic) force to the hydrodynamic force of the viscosity. It characterizes the magnetic field influence on the flow of viscous, electrically conducting fluid. With small Ha values, the motion proceeds as if no magnetic field were acting. With great Ha values, the viscosity forces act only on a thin layer of the electrically conducting fluid (ionized gas) which adheres closely to a by-passed wall surface.

2.1.21.5 Brinkmann Number [104]

Brinkmann number (Br) expresses the ratio of the heat arising due to viscous friction of a fluid to the heat transferred by molecular conduction. It characterizes the heat conduction in viscous fluid flow. For high fluid viscosity values and low thermal conductivity values (e.g. molten polymers), the value is $Br \gg 1$".

Chapter 3

Entropy Analysis of Hall Current and Thermal Radiation Influenced by Cilia with Suspended CNTs

3.1   Introduction

This chapter investigates the significance of creeping viscous nanofluid in an axisymmetric channel influenced by metachronical waves containing MHD and Hall current. Heat transport analysis is also computed along with the impact of thermal radiation and internal heat source phenomena. Mathematical formulations have been established which result into a set of coupled partial differential equations. The governing system is transformed into a system comprising of ordinary differential equations by considering the similarity transformation. Exact solution in the closed form is computed for the obtained nonlinear system of coupled ordinary differential equations. Moreover, entropy development because of energy transfer, thermal radiation, and magnetic effects has been encountered. Graphical

results have been carried out to interpret sundry parameters of interest. Streamlines are also graphed against the multi wall carbon nanotubes. For the validation of our results, a comparison table is presented. It is also seen that the entropy of the system increases whereas the Bejan number reduces by an increment in the Brinkmann number.

3.2   Mathematical Analysis

In this study, consideration has been given to peristaltic transport of Newtonian flow of carbon nanotubes in a flexible duct. Metachronical waves are developed by wavy motion of cilia, which directs the flow. Uniform magnetic field B_0 is applied in the transverse direction. The cylindrical coordinate system $(\bar{R}, \bar{Z})$ has been introduced to present the geometry of the problem. Figure 3.1 depicts the systematic view of the under discussion peristaltic fluid flow.
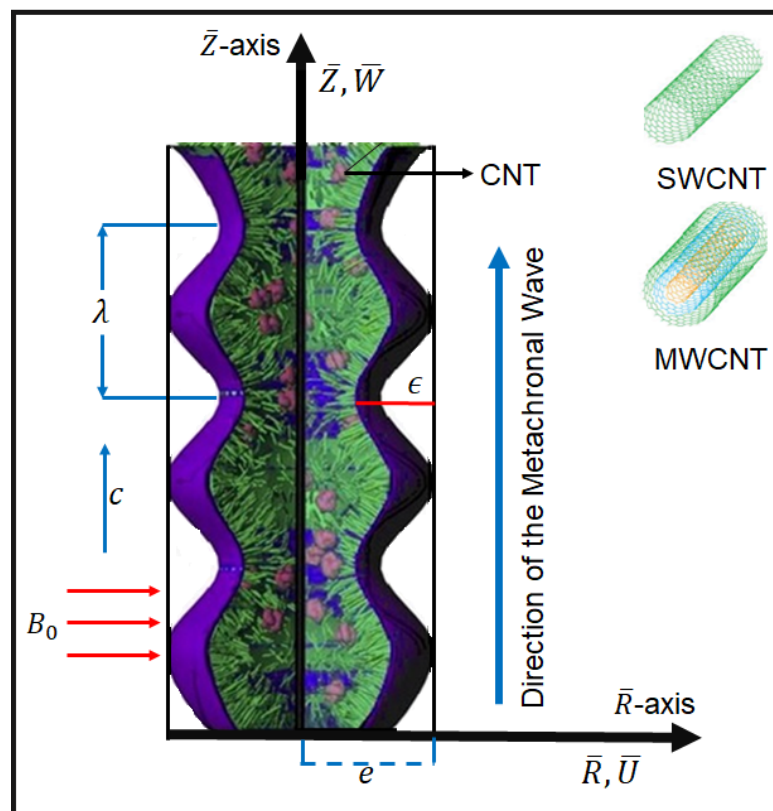
FIGURE 3.1: Geometrical view of the physical model

The shape of the cilia tips is supposed to obey the following pattern [105, 106]:

$$\left.\begin{aligned}
\bar{R} = \bar{h} = \bar{f}\left(\bar{Z}, \bar{t}\right) = e + e\epsilon \cos\left(\frac{2\pi}{\lambda}(\bar{Z} - c\bar{t})\right), \\
\bar{Z} = \bar{g}\left(\bar{Z}, \bar{Z}_0, \bar{t}\right) = e + e\epsilon\alpha \sin\left(\frac{2\pi}{\lambda}(\bar{Z} - c\bar{t})\right),
\end{aligned}\right\} \tag{3.1}$$

where e denotes the mean radius of the tube, ϵ the wave amplitude, Z_0 the reference position of cilia, c the wave speed, λ the wavelength, and α the measure of the eccentricity. No slip condition indicates that the cilia tips and fluid closed to it, have equal velocity, thus radial and axial velocities are given as:

$$\left.\begin{aligned}
\bar{U} = \left(\frac{\partial\bar{R}}{\partial\bar{t}}\right)_{\bar{Z}_0} = \left(\frac{\partial\bar{f}}{\partial\bar{t}}\right) + \left(\frac{\partial\bar{f}}{\partial\bar{Z}}\right)\left(\frac{\partial\bar{Z}}{\partial\bar{t}}\right) = \left(\frac{\partial\bar{f}}{\partial\bar{t}}\right) + \left(\frac{\partial\bar{f}}{\partial\bar{Z}}\right)\bar{W}, \\
\bar{W} = \left(\frac{\partial\bar{Z}}{\partial\bar{t}}\right)_{\bar{Z}_0} = \left(\frac{\partial\bar{g}}{\partial\bar{t}}\right) + \left(\frac{\partial\bar{g}}{\partial\bar{Z}}\right)\left(\frac{\partial\bar{Z}}{\partial\bar{t}}\right) = \left(\frac{\partial\bar{g}}{\partial\bar{t}}\right) + \left(\frac{\partial\bar{g}}{\partial\bar{Z}}\right)\bar{W},
\end{aligned}\right\} \tag{3.2}$$

combining (3.1) and (3.2), the radial and axial velocities of the cilia are given as:

$$\left.\begin{aligned}
\bar{U} = \frac{\left(\frac{2\pi}{\lambda}\right)\left[\epsilon\alpha c e \sin\left(\frac{2\pi}{\lambda}(\bar{Z} - c\bar{t})\right)\right]}{1 - \frac{2\pi}{\lambda}\left[\epsilon\alpha e \cos\left(\frac{2\pi}{\lambda}\left(\bar{Z} - c\bar{t}\right)\right)\right]}, \\
\bar{W} = \frac{\left(\frac{-2\pi}{\lambda}\right)\left[\epsilon\alpha c e \cos\left(\frac{2\pi}{\lambda}(\bar{Z} - c\bar{t})\right)\right]}{1 - \frac{2\pi}{\lambda}\left[\epsilon\alpha e \cos\left(\frac{2\pi}{\lambda}\left(\bar{Z} - c\bar{t}\right)\right)\right]}.
\end{aligned}\right\} \tag{3.3}$$

The governing bounadry layer equations for the laminar, viscous nanofluid flow in a fixed frame are given as [107]:

$$\frac{\partial\bar{U}}{\partial\bar{R}} + \frac{\bar{U}}{\bar{R}} + \frac{\partial\bar{W}}{\partial\bar{Z}} = 0. \tag{3.4}$$

$$\rho_{nf}\left[\frac{\partial\bar{U}}{\partial\bar{t}} + \bar{U}\frac{\partial\bar{U}}{\partial\bar{R}} + \bar{W}\frac{\partial\bar{U}}{\partial\bar{Z}}\right] = -\frac{\partial\bar{P}}{\partial\bar{R}} + \mu_{nf}\left[2\frac{\partial^2\bar{U}}{\partial\bar{R}^2} + \frac{2}{\bar{R}}\left(\frac{\partial\bar{U}}{\partial\bar{R}} - \frac{\bar{U}}{\bar{R}}\right)\right]$$
$$+ \mu_{nf}\left[\frac{\partial}{\partial\bar{Z}}\left(\frac{\partial\bar{U}}{\partial\bar{R}}\right) + \frac{\partial^2\bar{W}}{\partial\bar{Z}^2}\right]$$
$$- \frac{\sigma_{bf}B_0^2}{1 + m^2}\left[\bar{U} - m\bar{W}\right]. \tag{3.5}$$

$$\rho_{nf}\left[\frac{\partial \bar{W}}{\partial \bar{t}} + \bar{U}\frac{\partial \bar{W}}{\partial \bar{R}} + \bar{W}\frac{\partial \bar{W}}{\partial \bar{Z}}\right] = -\frac{\partial \bar{P}}{\partial \bar{Z}} + 2\mu_{nf}\left[\frac{\partial^2 \bar{W}}{\partial \bar{Z}^2} + \frac{1}{\bar{R}}\left(\frac{\partial \bar{U}}{\partial \bar{Z}} + \frac{\partial \bar{W}}{\partial \bar{R}}\right)\right]$$
$$+ \mu_{nf}\left[\frac{\partial}{\partial \bar{R}}\left(\frac{\partial \bar{U}}{\partial \bar{Z}} + \frac{\partial \bar{W}}{\partial \bar{R}}\right)\right]$$
$$- \frac{\sigma_{bf}B_0^2}{1+m^2}\left[\bar{W} + m\bar{U}\right] + \rho_{bf}\,g\,\alpha^*\left(\bar{T} - \bar{T}_0\right). \quad (3.6)$$

$$(\rho c_p)_{nf}\left[\frac{\partial \bar{T}}{\partial \bar{t}} + \bar{U}\frac{\partial \bar{T}}{\partial \bar{R}} + \bar{W}\frac{\partial \bar{T}}{\partial \bar{Z}}\right] = k_{nf}\left[\frac{1}{\bar{R}}\frac{\partial}{\partial \bar{R}}\left(\bar{R}\frac{\partial \bar{T}}{\partial \bar{R}}\right) + \frac{\partial^2 \bar{T}}{\partial \bar{Z}^2}\right] + Q_0$$
$$+ \frac{16\sigma^* T_\infty^3}{3k^*}\left[\frac{1}{\bar{R}}\frac{\partial}{\partial \bar{R}}\left(\bar{R}\frac{\partial \bar{T}}{\partial \bar{R}}\right)\right]. \quad (3.7)$$

The flow is unsteady in a fixed frame of reference $(\bar{R}, \bar{Z})$, whereas the flow develops to be steady in a wave frame $(\bar{r}, \bar{z})$. The following variables are meaningful to convert the flow from unsteady to steady flow.

$$\bar{Z} = \bar{z} + c\bar{t}, \quad \bar{R} = \bar{r}, \quad \bar{P}(\bar{Z}, \bar{R}, \bar{t}) = \bar{p}(\bar{z}, \bar{r}, \bar{t}), \quad (3.8)$$

where the velocities between the two frames are:

$$\bar{U} = \bar{u}, \quad \bar{W} = \bar{w} + c. \quad (3.9)$$

The derived fundamental system of equations after invoking the above variables, is of the form:

$$\frac{\partial \bar{u}}{\partial \bar{r}} + \frac{\bar{u}}{\bar{r}} + \frac{\partial \bar{w}}{\partial \bar{z}} = 0, \quad (3.10)$$

$$\rho_{nf}\left[\bar{u}\frac{\partial \bar{u}}{\partial \bar{r}} + (\bar{w}+c)\frac{\partial \bar{u}}{\partial \bar{z}}\right] = \mu_{nf}\left[2\frac{\partial^2 \bar{u}}{\partial \bar{r}^2} + \frac{2}{\bar{r}}\left(\frac{\partial \bar{u}}{\partial \bar{r}} - \frac{\bar{u}}{\bar{r}}\right) + \frac{\partial}{\partial \bar{z}}\left(\frac{\partial \bar{u}}{\partial \bar{r}}\right) + \frac{\partial^2 \bar{w}}{\partial \bar{z}^2}\right]$$
$$- \frac{\sigma_{bf}B_0^2}{1+m^2}\left[\bar{u} - m(\bar{w}+c)\right] - \frac{\partial \bar{p}}{\partial \bar{r}}, \quad (3.11)$$

$$\rho_{nf}\left[\bar{u}\frac{\partial \bar{w}}{\partial \bar{r}} + (\bar{w}+c)\frac{\partial \bar{w}}{\partial \bar{z}}\right] = 2\mu_{nf}\left[\frac{\partial^2 \bar{w}}{\partial \bar{z}^2} + \frac{1}{\bar{r}}\left(\frac{\partial \bar{u}}{\partial \bar{z}} + \frac{\partial \bar{w}}{\partial \bar{r}}\right) + \frac{\partial}{\partial \bar{r}}\left(\frac{\partial \bar{u}}{\partial \bar{z}} + \frac{\partial \bar{w}}{\partial \bar{r}}\right)\right]$$
$$+ \rho_{bf}g\alpha^*\left(\bar{T} - \bar{T}_0\right) - \frac{\sigma_{bf}B_0^2}{1+m^2}\left[(\bar{w}+c) + m\bar{u}\right] - \frac{\partial \bar{p}}{\partial \bar{z}}, \quad (3.12)$$

$$(\rho c_p)_{nf} \left[\bar{u} \frac{\partial \bar{T}}{\partial \bar{r}} + (\bar{w} + c) \frac{\partial \bar{T}}{\partial \bar{z}} \right] = k_{nf} \left[\frac{1}{\bar{r}} \frac{\partial}{\partial \bar{r}} \left(\bar{r} \frac{\partial \bar{T}}{\partial \bar{r}} \right) + \frac{\partial^2 \bar{T}}{\partial \bar{z}^2} \right] + Q_0$$
$$+ \frac{16 \sigma^* T_\infty^3}{3 k^*} \left[\frac{1}{\bar{r}} \frac{\partial}{\partial \bar{r}} \left(\bar{r} \frac{\partial \bar{T}}{\partial \bar{r}} \right) \right]. \tag{3.13}$$

The boundary conditions are:

$$\left. \begin{aligned} & w'(r) = 0, \quad \theta'(r) = 0, && \text{at } r = 0, \\ & w = \frac{-2\pi\epsilon\alpha\beta\cos(2\pi z)}{1 - 2\pi\epsilon\alpha\beta\cos(2\pi z)} - 1, \quad \theta = 0 \quad \text{at } r = h(z) = 1 + \epsilon\cos(2\pi z). \end{aligned} \right\} \tag{3.14}$$

Here $\bar{u}$ and $\bar{w}$ are the velocity elements in the radial ($\bar{r}$) and axial ($\bar{z}$) directions respectively, σ the electric conductivity, B_0 the applied magnetic field, α^* the coefficient of linear thermal expansion, Q_0 the internal heat source coefficient, g the acceleration due to gravity, m the Hall parameter, ρ_{nf} the effective density, μ_{nf} the effective viscosity, $(\rho c_p)_{nf}$ the heat capacitance, σ^* the Stefan-Boltzmann constant, k^* the Rosseland mean absorption coefficient, and k_{nf} the effective thermal conductivity, given as [108]:

$$\left. \begin{aligned} & (\rho c_p)_{nf} = (1 - \phi)(\rho c_p)_{bf} + \phi(\rho c_p)_{CNT}, \\ & \rho_{nf} = (1 - \phi)\rho_{bf} + \phi\rho_{CNT}, \quad \mu_{nf} = \mu_{bf}(1 - \phi)^{-2.5}, \\ & k_{nf} = k_{bf} \left(\frac{(1 - \phi) + \dfrac{2\phi k_{CNT}}{k_{CNT} - k_{bf}} log \left(\dfrac{k_{CNT} + k_{bf}}{2 k_{bf}} \right)}{(1 - \phi) + \dfrac{2\phi k_{bf}}{k_{CNT} - k_{bf}} log \left(\dfrac{k_{CNT} + k_{bf}}{2 k_{bf}} \right)} \right), \end{aligned} \right\} \tag{3.15}$$

where the subscripts bf, s and nf represents the base fluid, solid nanoparticles and nanofluid, respectively. Thermophysical properties [109, 110] of the base fluids and nanoparticles are given in Table 3.1. The following transformations are found successful to convert the model into the dimensionless form.

$$r = \frac{\bar{r}}{e}, \; z = \frac{\bar{z}}{\lambda}, \; w = \frac{\bar{w}}{c}, \; u = \frac{\lambda \bar{u}}{ec}, \; p = \frac{e^2 \bar{p}}{c \lambda \mu_{bf}}, \; t = \frac{c\bar{t}}{\lambda}, \; \theta = \frac{(\bar{T} - \bar{T}_0)}{T_0}, \tag{3.16}$$

where a is the electric charge, n_a the number density of electrons. Substituting (3.16) into (3.10)-(3.13), the mathematical model gets the following form.

$$A_1 \, Re \, \beta^3 \left[u \frac{\partial u}{\partial r} + (w+1) \frac{\partial u}{\partial z} \right] = - \frac{\partial p}{\partial r} + \beta^2 \left[\frac{2}{(1-\phi)^{2.5}} \right] \left[\frac{\partial^2 u}{\partial r^2} + \frac{1}{r} \frac{\partial u}{\partial r} - \frac{u}{r^2} \right]$$
$$+ \left[\frac{\beta^3}{(1-\phi)^{2.5}} \right] \left[\frac{\partial^2 u}{\partial r \partial z} + \frac{\partial^2 w}{\partial z^2} \right]$$
$$- \beta \frac{Ha^2}{1+m^2} [\beta \, u - m(w+1)], \qquad (3.17)$$

$$A_1 \, Re \, \beta \left[u \frac{\partial w}{\partial r} + (w+1) \frac{\partial w}{\partial z} \right] = \frac{1}{(1-\phi)^{2.5}} \left[\frac{1}{r} \left(\beta^2 \frac{\partial u}{\partial z} + \frac{\partial w}{\partial r} \right) + \beta^2 \frac{\partial^2 u}{\partial r \partial z} \right]$$
$$- \frac{\partial p}{\partial z} + \beta^2 \left[\frac{1}{(1-\phi)^{2.5}} \right] \frac{\partial^2 w}{\partial z^2} + Gr \, \theta(r)$$
$$- \frac{Ha^2}{1+m^2} (w+1 + \beta \, m \, u) + \frac{1}{(1-\phi)^{2.5}} \frac{\partial^2 w}{\partial r^2}, \qquad (3.18)$$

$$(\rho c_p)_{nf} \, e \, c \, \beta \left[u \frac{\partial \theta}{\partial r} + (w+1) \frac{\partial \theta}{\partial z} \right] = k_{nf} \left[\frac{\partial^2 \theta}{\partial r^2} + \frac{1}{r} \frac{\partial \theta}{\partial r} + \beta^2 \frac{\partial^2 \theta}{\partial z^2} \right] + \frac{Q_0 \, e^2}{T_0}$$
$$+ \frac{16 \sigma^* T_\infty^3}{3 k^*} \left[\frac{\partial^2 \theta}{\partial r^2} + \frac{1}{r} \frac{\partial \theta}{\partial r} \right], \qquad (3.19)$$

where

$$\left. \begin{array}{l} Ha^2 = \dfrac{\sigma_{bf} B_0^2 e^2}{\mu_{bf}}, \; Gr = \dfrac{\rho_{bf} \, g \, \alpha^* e^2 T_0}{c \mu_{bf}}, \; m = \dfrac{\sigma_{bf} B_0}{a n_a}, \; \beta = \dfrac{e}{\lambda}, \; h = \dfrac{\bar{h}}{e}, \\[3mm] Rn = \dfrac{4\sigma^*}{k^* k_{bf}} T_\infty^3, \quad \Omega = \dfrac{Q_0 e^2}{k_{bf} T_0}, \quad Re = \dfrac{e \, \rho_{bf}}{\mu_{bf}}, \quad A_1 = 1 - \phi + \phi \, \dfrac{\rho_s}{\rho_{bf}}. \end{array} \right\} \qquad (3.20)$$

Here ϕ is the solid volume fraction, Gr the Grashof number, Ω the internal heat source and Rn the radiation parameter. To attain the general solution of the Eqs. (3.17)-(3.19), we shall restrict this study under the assumptions of long wavelength i.e. $(\lambda \to \infty)$ and low Reynolds number i.e. $(Re \ll 1)$. The set of Eqs. (3.17)-(3.19) after employing the above assumptions is reduced to the following set of equations:

$$\frac{dp}{dr} = 0, \qquad (3.21)$$

$$\frac{dp}{dz} - \frac{1}{(1-\phi)^{2.5}} \left(\frac{1}{r} \frac{dw}{dr} + \frac{d^2 w}{dr^2} \right) + \frac{Ha^2}{1+m^2} (w+1) - Gr \, \theta(r) = 0, \qquad (3.22)$$

$$\frac{d^2 \theta}{dr^2} \left(\Psi_{3.1} + \frac{4}{3} Rn \right) + \frac{1}{r} \frac{d\theta}{dr} \left(\Psi_{3.1} + \frac{4}{3} Rn \right) + \Omega = 0. \qquad (3.23)$$

The boundary conditions are given as:

$$\left.\begin{array}{ll} w'(r) = 0, \quad \theta'(r) = 0, & \text{at } r = 0, \\[2mm] w = \dfrac{-2\pi\epsilon\alpha\beta\cos(2\pi z)}{1 - 2\pi\epsilon\alpha\beta\cos(2\pi z)} - 1, \quad \theta = 0 & \text{at } r = h(z) = 1 + \epsilon\cos(2\pi z). \end{array}\right\} \quad (3.24)$$

TABLE 3.1: Thermophysical properties of base fluids and nanoparticles.

Physical properties	$\rho(kg/m^3)$	$c_p(J/kgK)$	$k(W/mK)$
Water	997.1	4179	0.613
SWCNT	2600	425	6600
MWCNT	1600	796	3000
Engine Oil	884	1910	0.144
Ethylene Glycol	1110	2382	0.256

3.2.1 Second Law Analysis

Non-equilibrium situation emerges as a result of exchange of momentum, temperature and magnetic effects within the fluid and at the walls which motivates a continuous entropy generation. The volumetric entropy generation term (S_G) can be calculated as follows [111]:

$$S_G = \frac{1}{\bar{\theta}_0^2} \left(\overbrace{k_{nf} \left(\frac{\partial \bar{T}}{\partial \bar{r}}\right)^2}^{E_H} + \overbrace{\frac{16\sigma^* T_\infty^3}{3k^*} \left(\frac{\partial \bar{T}}{\partial \bar{r}}\right)^2}^{E_{Rn}} \right) + \overbrace{\frac{\sigma_{bf} B_0^2}{\bar{\theta}_0(1 + m^2)} \left((\bar{w} + c) + m\bar{u}\right)^2}^{E_M},$$

$$(3.25)$$

Eq. (3.25) reflects the contribution of three different factors causing the entropy generation. These factors are heat transfer E_H, the thermal radiation E_{Rn}, and the magnetic field E_M. Entropy gives the degree of disorder of the system and its surroundings and the rate of dimensionless entropy formation is given by

$$E_G = \frac{S_G}{S_g} = \left[\Psi_{3.1} + \frac{4}{3}Rn\right] \left(\frac{\partial \theta}{\partial r}\right)^2 + \Lambda\, Br \left[\frac{Ha^2}{1 + m^2}\right] (w + 1)^2, \qquad (3.26)$$

where

$$
\left.\begin{aligned}
S_g &= \frac{k_{bf} T_0^2}{\bar{\theta}_0^2 e^2}, \\
\Lambda &= \frac{\bar{\theta}_0}{T_0}, \\
Br &= \frac{c^2 \mu_{bf}}{k_{bf} T_0}.
\end{aligned}\right\}
\tag{3.27}
$$

Here Λ is the dimensionless temperature difference and Br the Brinkmann number. To figure out the irreversibility distribution, another diemnsionaless number, Bejan number Be, was introduced by Bejan [1] and is given as:

$$
Be = \frac{E_H}{E_H + E_{Rn} + E_M}.
\tag{3.28}
$$

3.3 Exact Solutions

This section reflects the exact solutions to the coupled ordinary differential Eqs. (3.22) and (3.23) together with the wall condition (6.24). The governing boundary layer equations incorporates momentum and energy equation. The exact analytical solution to the ordinary differential system is obtained by using a computational software called "MATHEMATICA".

3.3.1 Mechanism to Reach Solution of the Temperature Equation

- Introduction of the reduction of order scheme:

    - Order of the differential equation is reduced by introducing the dummy variable:
    $$
    y(r) = \frac{d\theta}{dr} \quad \text{and} \quad y'(r) = \frac{d^2\theta}{dr^2}.
    $$

    - 1st order differential equation is obtained.

- As a crucial step in the solution of the differential equation, integrating factor is applied.

- Convert the solution into the form containing the original variable.

- The closed form solution for the temperature distribution is:

$$
\theta(r, z) = \left(\cfrac{3\left(h^2 - r^2\right)}{12\left(\cfrac{(1-\phi) + \cfrac{2\phi k_{CNT}}{k_{CNT} - k_{bf}} log\left(\cfrac{k_{CNT} + k_{bf}}{2k_{bf}}\right)}{(1-\phi) + \cfrac{2\phi k_{bf}}{k_{CNT} - k_{bf}} log\left(\cfrac{k_{CNT} + k_{bf}}{2k_{bf}}\right)}\right) + 16Rn} \right) \Omega. \quad (3.29)
$$

3.3.2 Mechanism to Reach Solution of the Momentum Equation

- Assume the trial solution in the form:

$$
w(r) = \sum_{n=0}^{\infty} b_n r^{x+n}, \quad b_0 \neq 0, \quad r > 0.
$$

- Substitute $w(r)$, $w'(r)$ and $w''(r)$ in the momentum equation:

- Work out the constants b_0, b_1, $b_2...b_n$.

- The closed form exact solution for the momentum profile is:

$$
w(r, z) = \left(\frac{1+m^2}{Ha}\right)\left(\Psi_{3.2} + \cfrac{\left(\cfrac{Ha}{1+m^2} + \left[\Psi_{3.3} + \cfrac{dp}{dz}\right]\Psi_{3.4}\right)\Psi_{3.10}}{\Psi_{3.4}\, {}_0F_1\left[\left(\cfrac{Ha}{1+m^2}\right)\cfrac{h^2}{4\left(1-\phi\right)^{2.5}}\right]}\right). \quad (3.30)
$$

The flow rate is described as:

$$Q = 2 \int\limits_0^{h(z)} r w(r) dr. \tag{3.31}$$

Now using (3.30) into (3.31), we have solution of dp/dz i.e.

$$\frac{dp}{dz} = \left(\frac{\Psi_{3.5}\Psi_{3.7} + 8h^2 \, {}_0F_2\left[\left(\frac{Ha}{1+m^2} \right) \frac{h^2}{4\left(1-\phi\right)^{2.5}} \right] \left(4\Psi_{3.8} + 3\Psi_{3.9} \right)}{\left(\frac{Ha}{1+m^2} \right)^2 h^4 \Psi_{3.4} \left(\left(1-\phi\right)^{2.5} \right)^2 \Psi_{3.11}} \right). \tag{3.32}$$

where the expression for $(\Psi_i, i = 3.1 - 3.11)$ are given as:

$$\Psi_{3.1} = \left(\frac{(1-\phi) + \dfrac{2\phi k_{CNT}}{k_{CNT} - k_{bf}} log\left(\dfrac{k_{CNT} + k_{bf}}{2k_{bf}} \right)}{(1-\phi) + \dfrac{2\phi k_{bf}}{k_{CNT} - k_{bf}} log\left(\dfrac{k_{CNT} + k_{bf}}{2k_{bf}} \right)} \right),$$

$$\Psi_{3.2} = \left(\frac{Ha}{1+m^2} \right) + \frac{3\left(h^2 - r^2\right)\Omega}{4(3\Psi_{3.1} + 4Rn)} Gr - \frac{dp}{dz},$$

$$\Psi_{3.3} = \frac{Ha}{1+m^2} - \frac{3\left(h^2 - r^2\right)\Omega}{4(3\Psi_{3.1} + 4\,Rn)} Gr,$$

$$\Psi_{3.4} = \left(1 - 2\pi\alpha\,\beta\,\epsilon\,\cos(2\pi\,z)\right),$$

$$\Psi_{3.5} = -\Psi_{3.4}\,{}_0F_1\left[\left(\frac{Ha}{1+m^2} \right) \frac{h^2}{4\left(1-\phi\right)^{2.5}} \right] 32 \left(\frac{Ha}{1+m^2} \right)^2 \left(F + h^2 \right),$$

$$\Psi_{3.6} = Rn(1-\phi)^{2.5} - 3Grh^2\left(-8 + \left(\frac{Ha}{1+m^2} \right) h^2(1-\phi)^{2.5} \right),$$

$$\Psi_{3.7} = \Psi_{3.6}\Omega 24 \left(\frac{Ha}{1+m^2} \right)^2 \left(F + h^2 \right) (1-\phi)^{2.5}\,\Psi_{3.1},$$

$$\Psi_{3.8} = \left(\frac{Ha}{1+m^2} \right)^2 Rn\left(-1 + \Psi_{3.4} \right)(1-\phi)^{2.5} + 3Gr\Psi_{3.4}\Omega$$

$$\Psi_{3.9} = \left(\frac{Ha}{1+m^2} \right)^2 \left(-1 + \Psi_{3.4} \right)(1-\phi)^{2.5}\,\Psi_{3.1},$$

$$\Psi_{3.10} = {}_0F_1\left[\left(\frac{Ha}{1+m^2} \right) \frac{r^2}{4\left(1-\phi\right)^{2.5}} \right],$$

$$\Psi_{3.11} = {}_0F_3\left[\left(\frac{Ha}{1+m^2} \right) \frac{h^2}{4\left(1-\phi\right)^{2.5}} \right] (3\Psi_{3.1} + 4Rn).$$

The mean flow rate can be calculated as

$$F = Q - \left[0.5 + \frac{\epsilon^2}{4}\right], \tag{3.33}$$

3.4   Results

This section encloses the physical aspects of various significant parameters on velocity field, temperature field, pressure gradient, thermal conductivity and streamlines.

Table 3.2 and 3.3 are prepared to validate our numerical results. An excellent comparison is found between the present results and those of Akbar and Butt [112]. Results are obtained by keeping $Rn = 0.0 = m$ and the rest of the parameters the same as in [112].

Effects of Hartmann number Ha on $w(r, z)$ are shown in Figures 3.2 and 3.3 for SWCNT and MWCNT respectively. It is recorded that as Ha increases, there is a decrease in the fluid velocity. From the physical point of view, an increase in the magnetic field accelerates the strength of the Lorentz force, which is an opposing force, therefore additional resistance is offered to the fluid motion which consequently reduces the flow velocity.

The effect of flow rate Q on $w(r, z)$ is shown in Figures 3.4 and 3.5 for SWCNT and MWCNT respectively. It is found that Q is directly proportional to the flow field. Moreover, the fluid earns its maximum velocity at the middle i.e. $r = 0.0$ and minimum near the ciliated walls.

The impact of thermal radiation Rn on $\theta(r, z)$ is plotted in Figures 3.6 and 3.7 for SWCNT and MWCNT respectively. It is seen that the fluid energy reduces as there is an increase in Rn. Physically, an advancement in the radiative parameter Rn increases the mean absorption coefficient k^* which reduces the fluid temperature significantly.

The impact of Ω on $\theta(r, z)$ is depicted in Figure 3.8 and 3.9 for SWCNT and MWCNT respectively. It is found that Ω is directly proportional to $\theta(r, z)$. Moreover, the fluid earns its maximum energy at the middle i.e. $r = 0.0$ and minimum

near the walls. Futhermore, no temperature variation is seen, when Ω is kept zero. The impact of α on dp/dz against the axial direction is shown in Figures 3.10 and 3.11 for single and multi wall carbon nanotubes, respectively. Response of dp/dz to a variation in β against the axial direction is displayed in Figures 3.12 and 3.13 respectively. It is depicted that the pressure gradient distribution is small for α and β in the regions $[-1, -0.75]$, $[-0.25, 0.25]$ and $[0.75, 1]$, whereas huge pressure gradient is recorded in $[-0.75, -0.25]$ and $[0.25, 0.75]$. Physically, small pressure gradient regions indicate the area through which fluid can pass easily without facing a trouble, whereas large pressure gradient regions will resist the fluid to pass. Thermal conductivity is the ability of a material to conduct heat. We can clearly see a meaningful variation in the thermal conductivities of these basefluids, where the pure water having the maximum and engine oil having the minimum thermal conductivity for both SWCNT and MWCNT as depicted in Figures 3.14 and 3.15. In Figures 3.16 and 3.17, attention has been given to observe the behavior of entropy for the increasing magnitude of Brinkmann number Br against SWCNT and MWCNT. It is seen that, entropy of the system grows rapidly with an enhancement in Br. Physically, as Br increases, heat transfer influences the fluid viscosity within the tube, increasing the entropy of the system. Maximum entropy is noted at the center i.e. at $r = 0$.

Figures 3.18 and 3.19 show the influence of the dimensionless temperature difference Λ on the entropy. It is visualized that entropy of flow develops for higher magnitude of Λ.

Figures 3.20 and 3.21 show that an increment in Br causes a reduction in Be at the center, whereas an increment close to the ciliated walls can be noticed. Bejan number is a decreasing function of Λ as noticed from Figures 3.22 and 3.23. It is because of the fact that the heat transfer irreversibility is small as compared with the total irreversibility.

A very attractive phenomenon in peristaltic movement, called trapping, is shown with respect to a change in various parameters. In Figures **??** and **??**, it is clear that with an increment in the magnitude of α, the bolus size reduces, however the number of trapped bolus grows. Figures **??** and **??** reflect that the bolus size

increases rapidly, however the number of trapped bolus start decreasing.
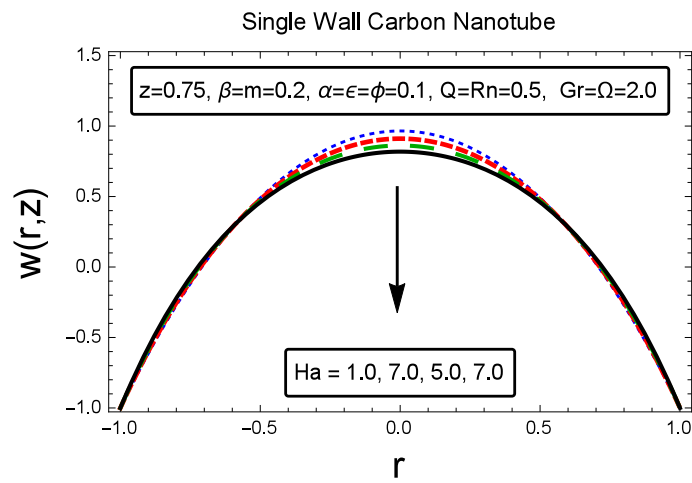
FIGURE 3.2: The impact of Ha on $w(r,z)$
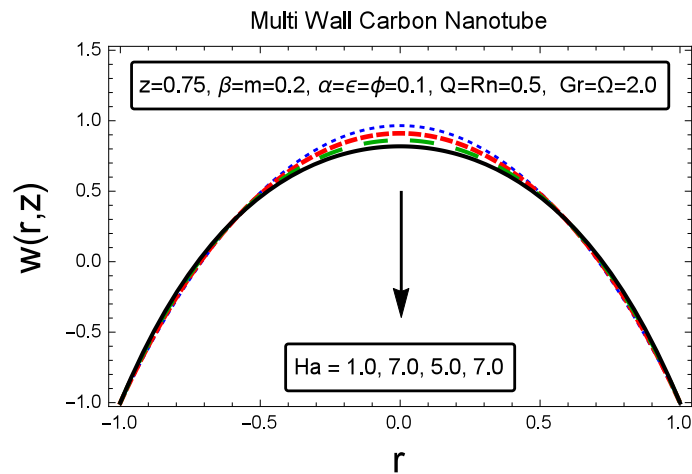
FIGURE 3.3: The impact of Ha on $w(r,z)$
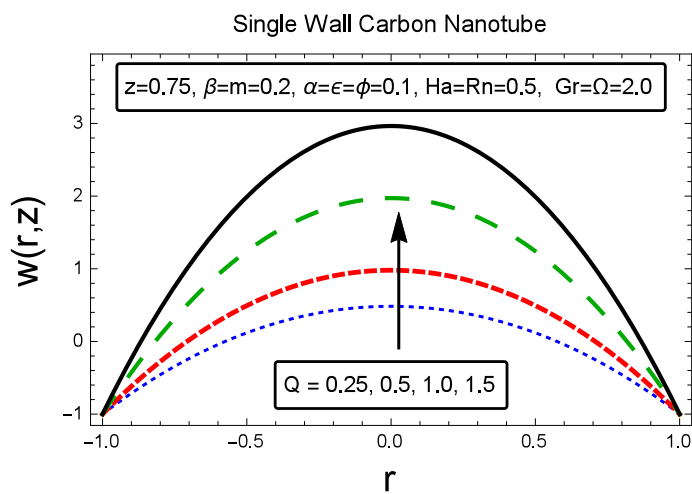
FIGURE 3.4: The impact of Q on $w(r,z)$

Multi Wall Carbon Nanotube

z=0.75, β=m=0.2, α=ϵ=ϕ=0.1, Ha=Rn=0.5, Gr=Ω=2.0

Q = 0.25, 0.5, 1.0, 1.5
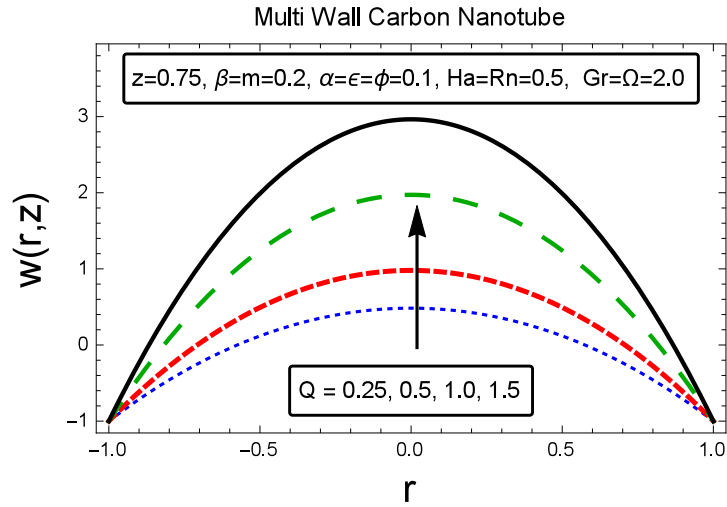
FIGURE 3.5: The impact of Q on $w(r,z)$

Single Wall Carbon Nanotube

z = 0.75, ϵ = 0.1, ϕ = 0.1, Ω = 2.0

Rn = 1.0, 5.0, 10.0, 15.0
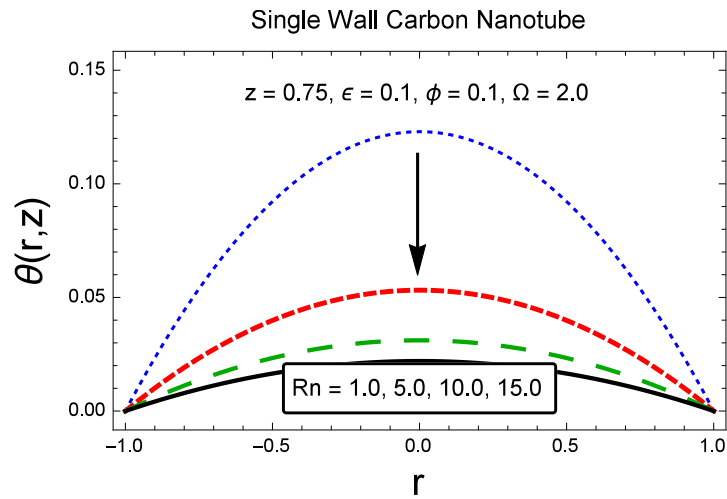
FIGURE 3.6: The impact of Rn on $\theta(r,z)$

Multi Wall Carbon Nanotube

z = 0.75, ϵ = 0.1, ϕ = 0.1, Ω = 2.0

Rn = 1.0, 5.0, 10.0, 15.0
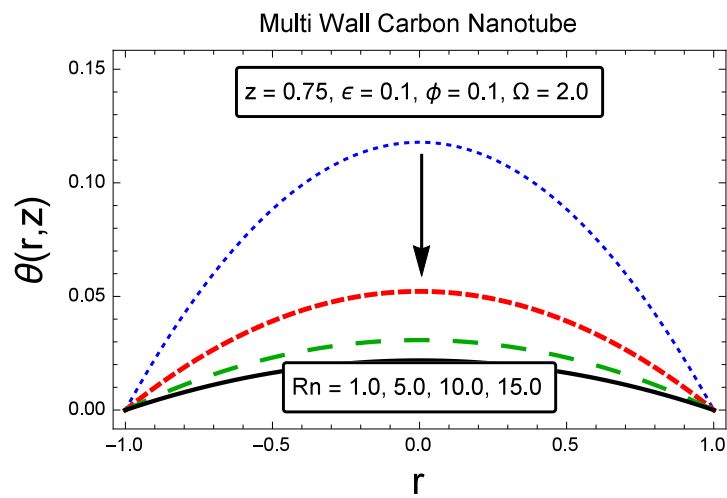
FIGURE 3.7: The impact of Rn on $\theta(r,z)$
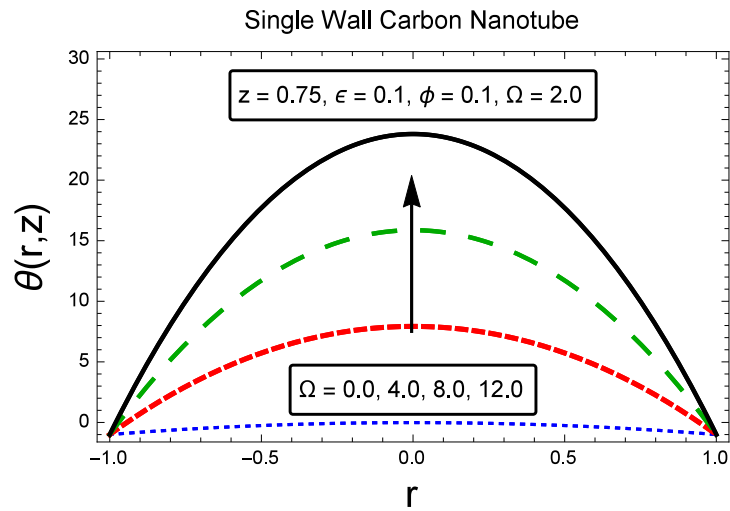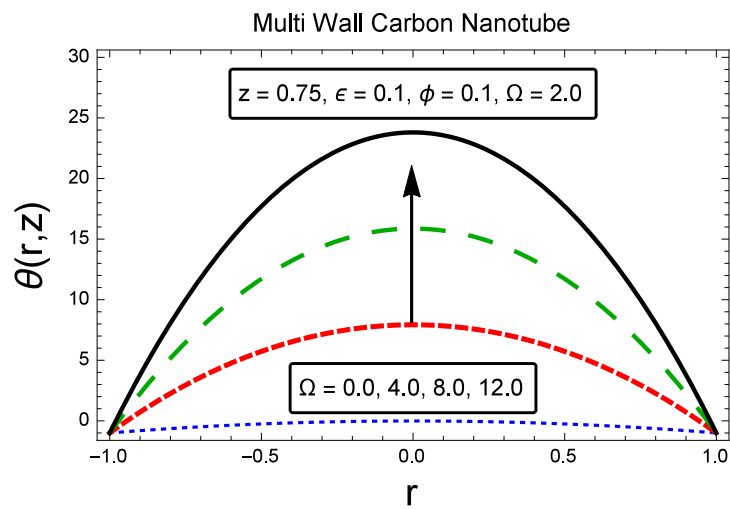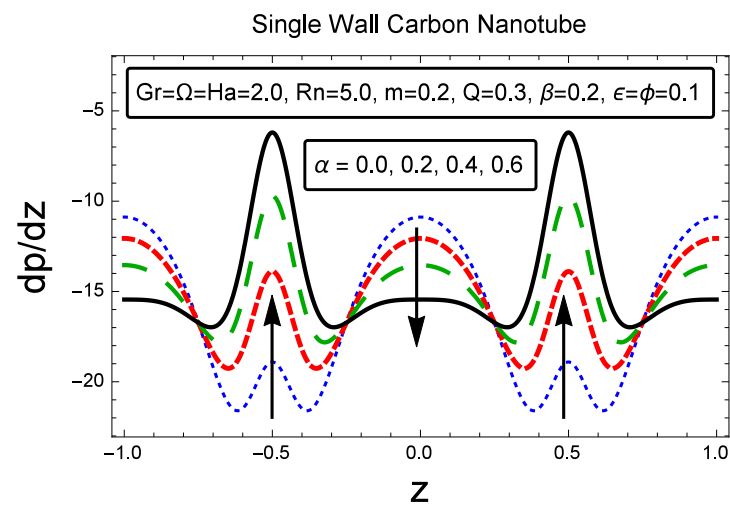
Single Wall Carbon Nanotube

FIGURE 3.8: The impact of Ω on $\theta(r,z)$

Multi Wall Carbon Nanotube

FIGURE 3.9: The impact of Ω on $\theta(r,z)$

Single Wall Carbon Nanotube

FIGURE 3.10: The impact of α on dp/dz

Multi Wall Carbon Nanotube

Gr=Ω=Ha=2.0, Rn=5.0, m=0.2, Q=0.3, β=0.2, ϵ=ϕ=0.1

α = 0.0, 0.2, 0.4, 0.6

FIGURE 3.11: The impact of α on dp/dz

Single Wall Carbon Nanotube

Gr=Ω=Ha=2.0, Rn=5.0, m=0.2, Q=0.3, β=0.2, ϵ=ϕ=0.1

β = 0.0, 0.5, 1.0, 1.5

FIGURE 3.12: The impact of β on dp/dz

Multi Wall Carbon Nanotube

Gr=Ω=Ha=2.0, Rn=5.0, m=0.2, Q=0.3, β=0.2, ϵ=ϕ=0.1

β = 0.0, 0.5, 1.0, 1.5
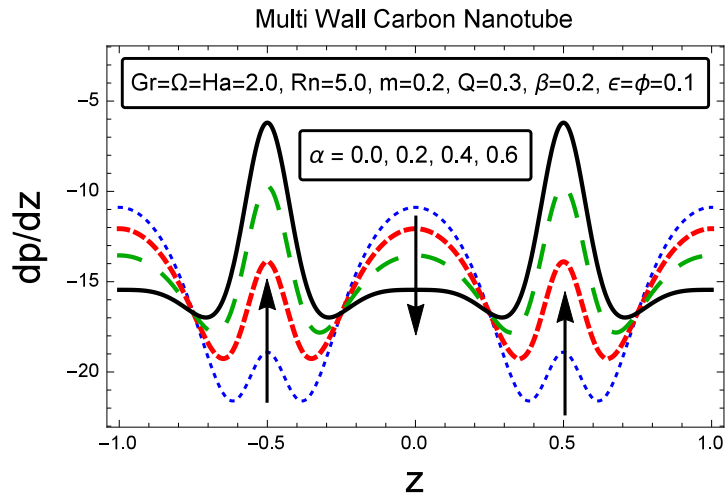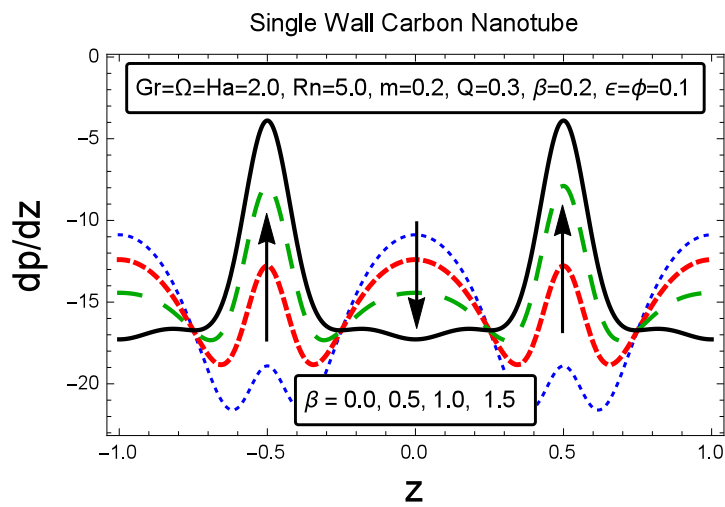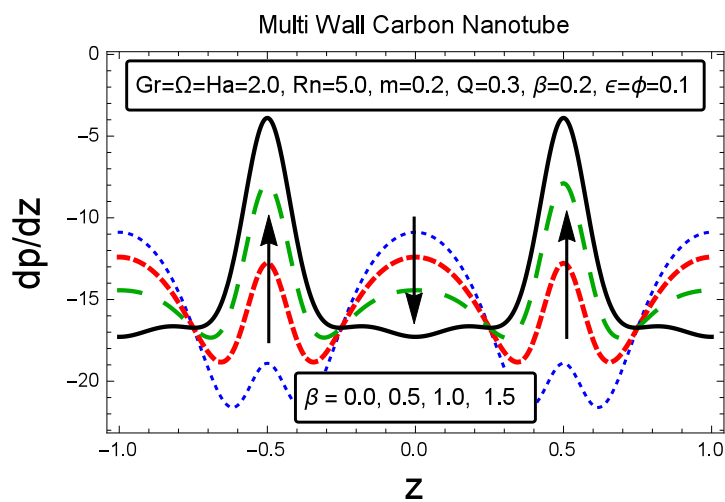
FIGURE 3.13: The impact of β on dp/dz
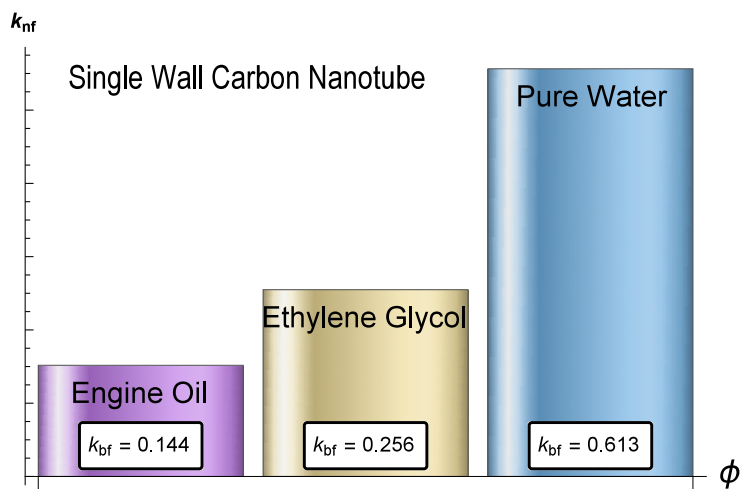
FIGURE 3.14: The impact of base fluids on k_{nf}
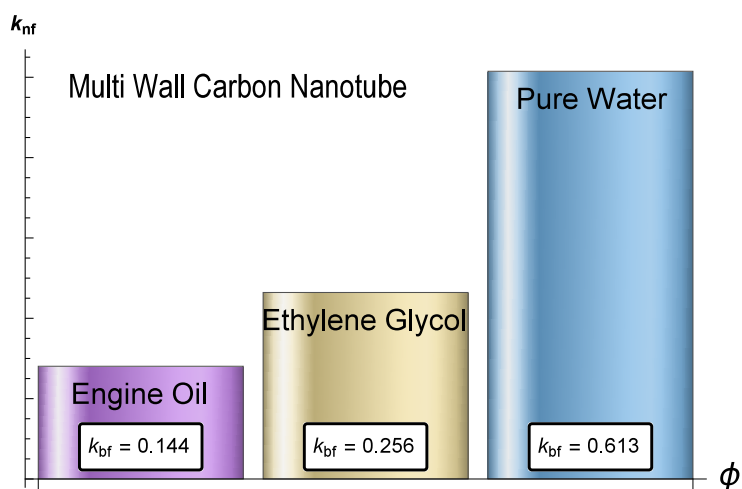
FIGURE 3.15: The impact of base fluids on k_{nf}

FIGURE 3.16: The impact of Br on Eg
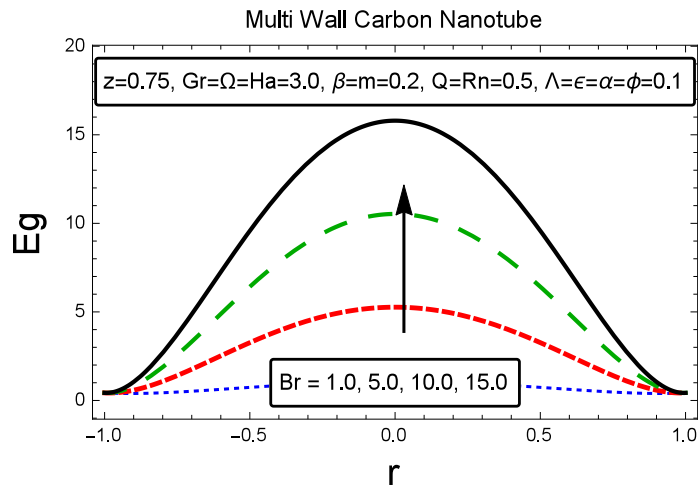
FIGURE 3.17: The impact of Br on Eg
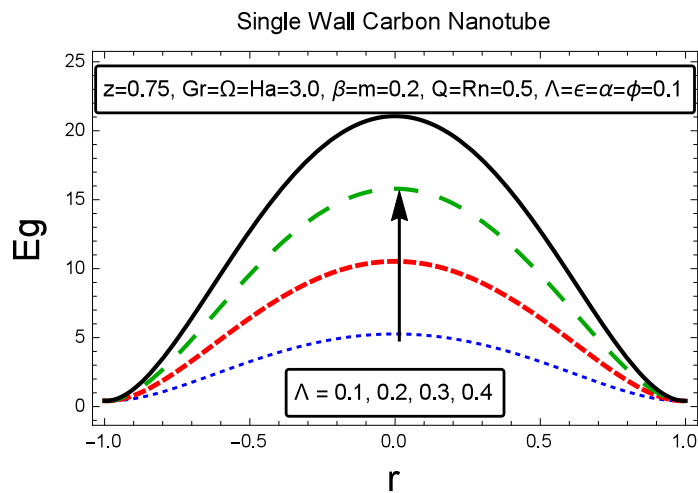
FIGURE 3.18: The impact of Λ on Eg

FIGURE 3.19: The impact of Λ on Eg
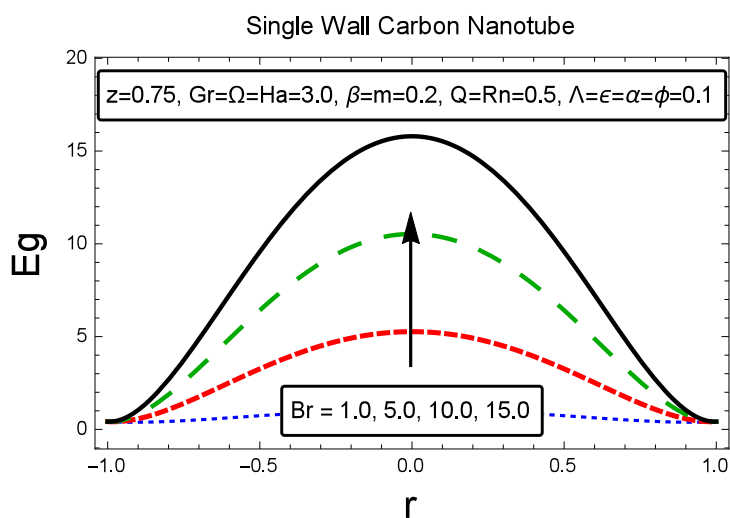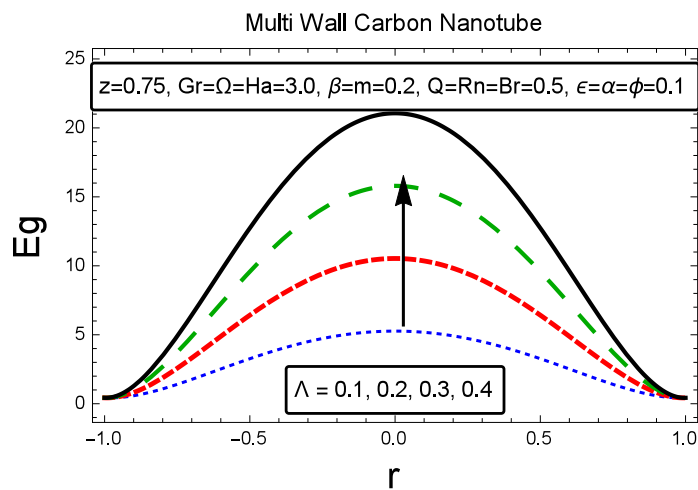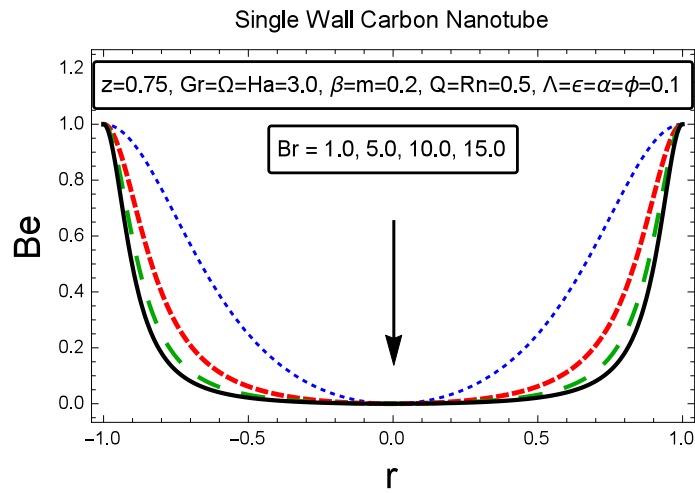
FIGURE 3.20: The impact of Br on Be
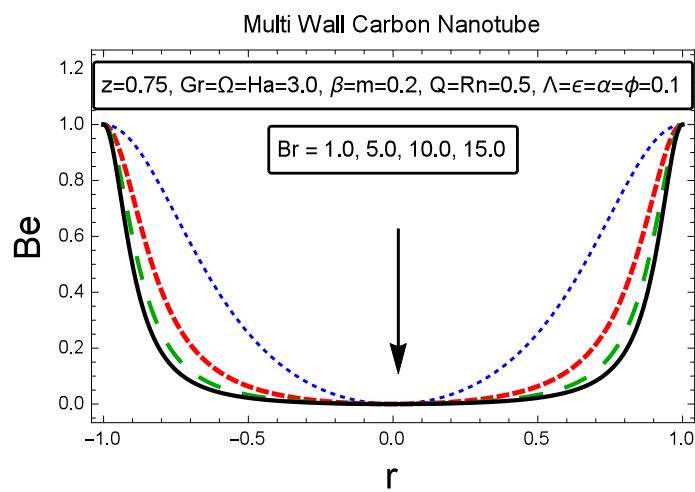
FIGURE 3.21: The impact of Br on Be
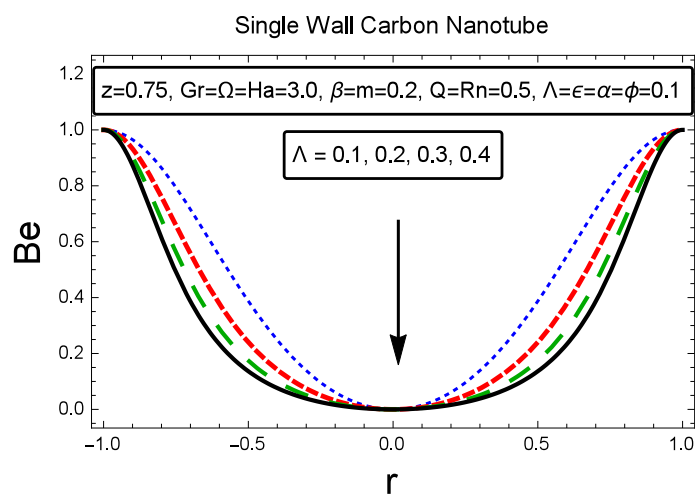
FIGURE 3.22: The impact of λ on Be
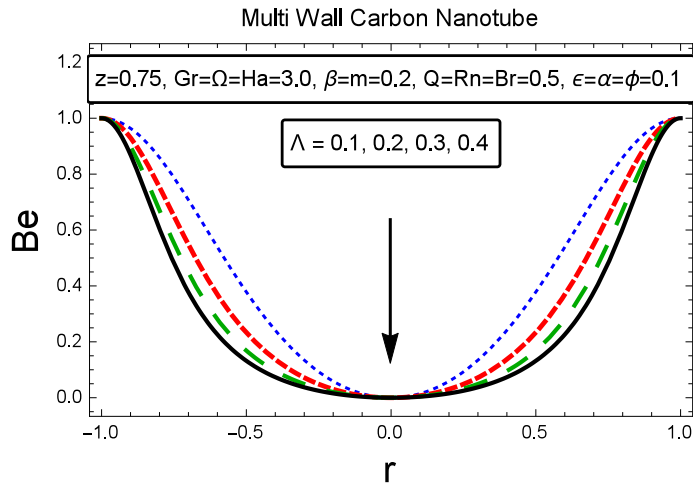
FIGURE 3.23: The impact of λ on Be
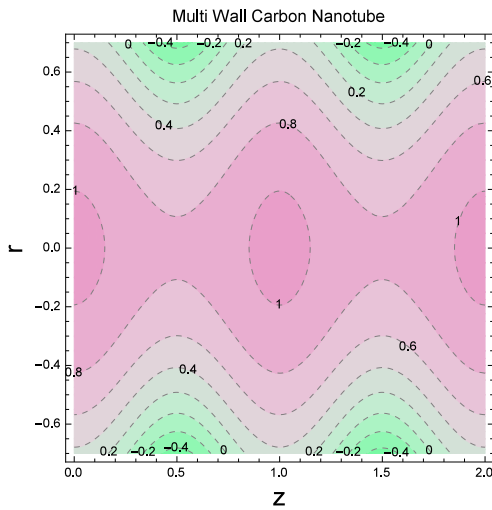
Fig. 3.24: Streamlines for $Q = 0.2$ Fig. 3.25: Streamlines for $\alpha = 2.0$
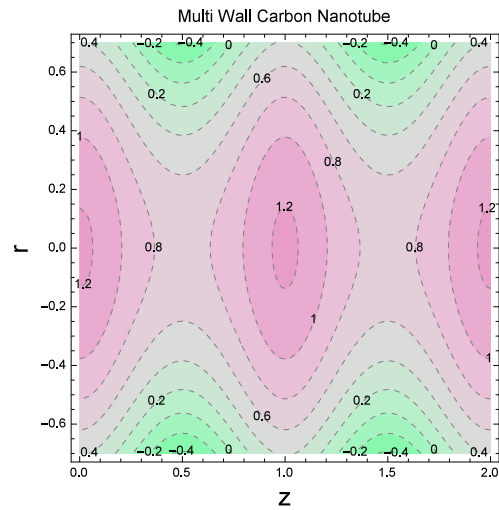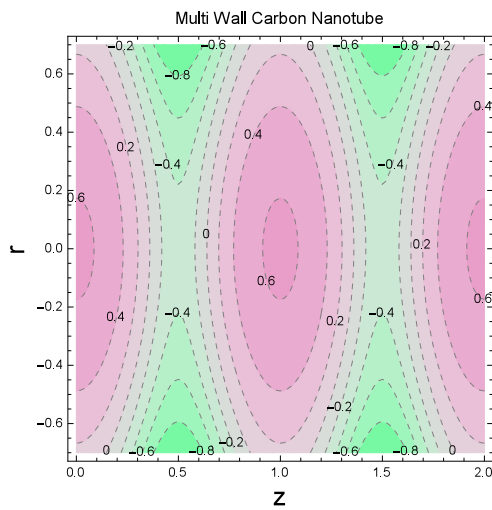
Fig. 3.26: Streamlines for $Q = 0.2$ Fig. 3.27: Streamlines for $Q = 0.4$
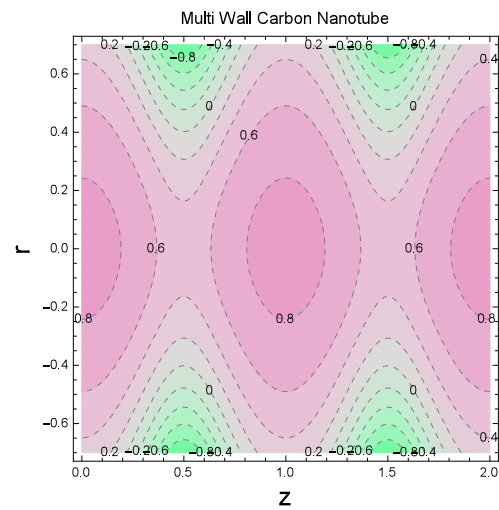
TABLE 3.2: Numerical computation of the velocity against SWCNT with $\epsilon = 0.1, \alpha = 0.1, \beta = 0.2, \Omega = 0.5, z = 0.5, \phi = 0.3, Rn = 0.0, m = 0.0$.

Q	M	Gr	$w(r,z)$ Present solution			$w(r,z)$ Akbar and Butt [112]		
			$r = 0.0$	$r = 0.25$	$r = 0.5$	$r = 0.0$	$r = 0.25$	$r = 0.5$
0.3	2.0	0.5	0.448967	0.346254	0.030112	0.448954	0.346236	0.0301363
0.4			0.689396	0.569413	0.200434	0.689394	0.569486	0.200482
0.5			0.929843	0.792723	0.370835	0.929834	0.792735	0.370827
	1.0		0.968034	0.819956	0.660112	0.968022	0.819977	0.660109
	3.0		0.872516	0.751459	0.367037	0.872505	0.751464	0.367044
	5.0		0.729409	0.646107	0.354189	0.729404	0.646104	0.354192
		1.0	0.729441	0.646183	0.354199	0.729435	0.646127	0.354194
		3.0	0.729567	0.646209	0.354212	0.729559	0.646217	0.354204
		5.0	0.729698	0.646312	0.354209	0.729683	0.646307	0.354214

TABLE 3.3: Numerical computation of the velocity against MWCNT with $\epsilon = 0.1, \alpha = 0.1, \beta = 0.2, \Omega = 0.5, z = 0.5, \phi = 0.3, Rn = 0.0, m = 0.0$.

Q	M	Gr	$w(r,z)$ Present solution			$w(r,z)$ Akbar and Butt [112]		
			$r = 0.0$	$r = 0.25$	$r = 0.5$	$r = 0.0$	$r = 0.25$	$r = 0.5$
0.3	2.0	0.5	0.448945	0.346256	0.0301398	0.448957	0.346239	0.0301365
0.4			0.689378	0.569467	0.200425	0.689397	0.569488	0.200482
0.5			0.929824	0.792745	0.370882	0.929837	0.792738	0.370827
	1.0		0.968045	0.819945	0.372923	0.968026	0.819979	0.372998
	3.0		0.872512	0.751447	0.367068	0.872508	0.751466	0.367044
	5.0		0.729402	0.646104	0.354199	0.729407	0.646106	0.354192
		1.0	0.729439	0.646129	0.354189	0.729441	0.646131	0.354195
		3.0	0.729568	0.646219	0.354201	0.729576	0.646229	0.354205
		5.0	0.729715	0.646313	0.354209	0.729711	0.646327	0.354216

Chapter 4

Entropy Analysis in a Cilia Transport of Nanofluid under the Influence of Magnetic Field

4.1 Introduction

In this chapter, an analysis of the entropy generation is performed during the cilia transport of water-based titanium dioxide nanoparticles in the presence of viscous dissipation. Moreover, thermal heat flux is considered at the surface of a channel with ciliated walls. Mathematical formulation is established in terms of a system comprising of nonlinear partial differential equations. The governing system is transformed into ordinary differential equations by considering the similarity transformation. Exact solution in the closed form has been computed for the obtained system of equations. Graphical illustrations for the emerging flow parameters such as Hartman number Ha, Brinkmann number Br, radiation parameter Rn and flow rate Q have been prepared. The main goal i.e. the reduction of the entropy generation of the second law of thermodynamics is achieved by decreasing the magnitude of Br, Ha and Λ.

4.2 Mathematical Analysis

Let us consider ciliary transport of two dimensional axisymmetric flow of a titanium dioxide water nanofluid in a horizontal tube. The inner layer of the duct is ciliated with metachronal waves. Flow is provoked as a result of these metachronal waves, which are formed due to wavy or beating motion cilia. A uniform magnetic field of strength B_0 is applied at an inclination angle Θ. It is an angle between a magnetic field line and axial axis which is measured in anticlockwise direction. Heat transfer is targeted to be analyzed in the presence of viscous dissipation effect.
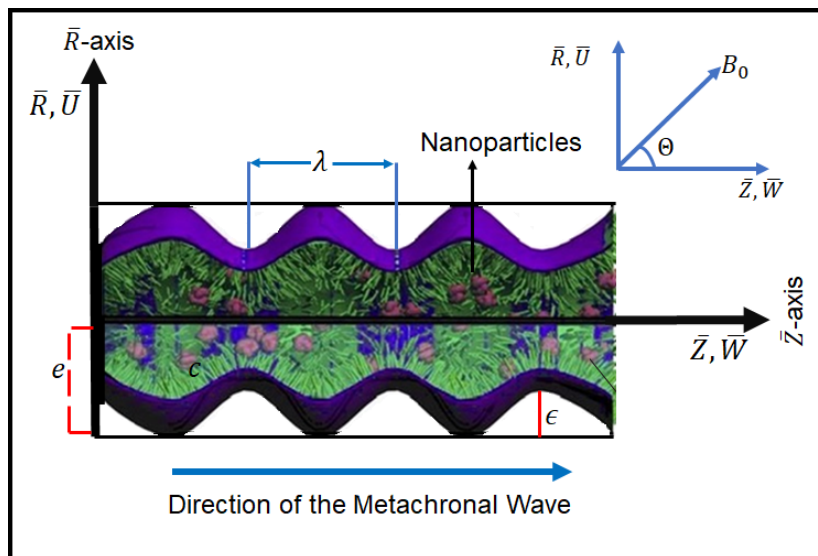
FIGURE 4.1: Geometry of the problem

The shape of the cilia tips is supposed to obey the following pattern [105]-[106]:

$$\left.\begin{array}{l} \bar{R} = \bar{h} = \bar{f}\left(\bar{Z}, \bar{t}\right) = e + e\epsilon \cos\left(\dfrac{2\pi}{\lambda}(\bar{Z} - c\bar{t})\right), \\[3mm] \bar{Z} = \bar{g}\left(\bar{Z}, \bar{Z}_0, \bar{t}\right) = e + e\epsilon\alpha \sin\left(\dfrac{2\pi}{\lambda}(\bar{Z} - c\bar{t})\right), \end{array}\right\} \tag{4.1}$$

where e denotes the mean radius of the tube, ϵ the wave amplitude, Z_0 the reference position of cilia, λ the the wavelength, α the measure of the eccentricity, and c the wave speed. No slip condition is assumed which implies that the cilia tips and the fluid closed to it, have equal velocity. Therefore the radial and axial velocities are

given as:

$$\left. \begin{aligned} \bar{U} &= \left(\frac{\partial \bar{R}}{\partial \bar{t}}\right)_{\bar{Z}_0} = \left(\frac{\partial \bar{f}}{\partial \bar{t}}\right) + \left(\frac{\partial \bar{f}}{\partial \bar{Z}}\right)\left(\frac{\partial \bar{Z}}{\partial \bar{t}}\right) = \left(\frac{\partial \bar{f}}{\partial \bar{t}}\right) + \left(\frac{\partial \bar{f}}{\partial \bar{Z}}\right)\bar{W}, \\ \bar{W} &= \left(\frac{\partial \bar{Z}}{\partial \bar{t}}\right)_{\bar{Z}_0} = \left(\frac{\partial \bar{g}}{\partial \bar{t}}\right) + \left(\frac{\partial \bar{g}}{\partial \bar{Z}}\right)\left(\frac{\partial \bar{Z}}{\partial \bar{t}}\right) = \left(\frac{\partial \bar{g}}{\partial \bar{t}}\right) + \left(\frac{\partial \bar{g}}{\partial \bar{Z}}\right)\bar{W}. \end{aligned} \right\} \tag{4.2}$$

Combining (4.1) and (4.2), the radial and axial velocities of the cilia are given as:

$$\left. \begin{aligned} \bar{U} &= \frac{\left(\frac{2\pi}{\lambda}\right)\left[\epsilon\alpha c e \sin\left(\frac{2\pi}{\lambda}(\bar{Z} - c\bar{t})\right)\right]}{1 - \frac{2\pi}{\lambda}\left[\epsilon\alpha e \cos\left(\frac{2\pi}{\lambda}\left(\bar{Z} - c\bar{t}\right)\right)\right]}, \\ \bar{W} &= \frac{\left(\frac{-2\pi}{\lambda}\right)\left[\epsilon\alpha c e \cos\left(\frac{2\pi}{\lambda}(\bar{Z} - c\tilde{t})\right)\right]}{1 - \frac{2\pi}{\lambda}\left[\epsilon\alpha e \cos\left(\frac{2\pi}{\lambda}\left(\bar{Z} - c\bar{t}\right)\right)\right]}. \end{aligned} \right\} \tag{4.3}$$

The fundamental boundary layer equations in the fixed frame can be written as [107]:

Continuity equation:

$$\frac{\partial \bar{U}}{\partial \bar{R}} + \frac{\bar{U}}{\bar{R}} + \frac{\partial \bar{W}}{\partial \bar{Z}} = 0. \tag{4.4}$$

Momentum equation in radial direction:

$$\rho_{nf}\left[\frac{\partial \bar{U}}{\partial \bar{t}} + \bar{U}\frac{\partial \bar{U}}{\partial \bar{R}} + \bar{W}\frac{\partial \bar{U}}{\partial \bar{Z}}\right] = -\frac{\partial \bar{P}}{\partial \bar{R}} + \mu_{nf}\left[2\frac{\partial^2 \bar{U}}{\partial \bar{R}^2} + \frac{2}{\bar{R}}\left(\frac{\partial \bar{U}}{\partial \bar{R}} - \frac{\bar{U}}{\bar{R}}\right)\right]$$
$$+ \mu_{nf}\left[\frac{\partial}{\partial \bar{Z}}\left(\frac{\partial \bar{U}}{\partial \bar{R}}\right) + \frac{\partial^2 \bar{W}}{\partial \bar{Z}^2}\right]. \tag{4.5}$$

Momentum equation in axial direction:

$$\rho_{nf}\left[\frac{\partial \bar{W}}{\partial \bar{t}} + \bar{U}\frac{\partial \bar{W}}{\partial \bar{R}} + \bar{W}\frac{\partial \bar{W}}{\partial \bar{Z}}\right] = -\frac{\partial \bar{P}}{\partial \bar{Z}} + 2\mu_{nf}\left[\frac{\partial^2 \bar{W}}{\partial \bar{Z}^2} + \frac{1}{\bar{R}}\left(\frac{\partial \bar{U}}{\partial \bar{Z}} + \frac{\partial \bar{W}}{\partial \bar{R}}\right)\right]$$
$$+ \mu_{nf}\left[\frac{\partial}{\partial \bar{R}}\left(\frac{\partial \bar{U}}{\partial \bar{Z}} + \frac{\partial \bar{W}}{\partial \bar{R}}\right)\right]$$
$$- \sigma_{bf}B_0^2\cos(\Theta)\left(\bar{W} + c\right). \tag{4.6}$$

Energy equation:

$$(\rho c_p)_{nf}\left[\frac{\partial \bar{T}}{\partial \bar{t}} + \bar{U}\frac{\partial \bar{T}}{\partial \bar{R}} + \bar{W}\frac{\partial \bar{T}}{\partial \bar{Z}}\right] = \left[k_{nf} + \frac{16\sigma^* T_\infty^3}{3k^*}\right]\frac{1}{\bar{R}}\frac{\partial}{\partial \bar{R}}\left(\bar{R}\frac{\partial \bar{T}}{\partial \bar{R}}\right) + k_{nf}\left[\frac{\partial^2 \bar{T}}{\partial \bar{Z}^2}\right]$$

$$+ \mu_{nf}\left[2\left(\frac{\partial \bar{U}}{\partial \bar{Z}}\right)^2 + 2\left(\frac{\partial \bar{W}}{\partial \bar{R}}\right)^2\right] + Q_0$$

$$+ \mu_{nf}\left(\frac{\partial \bar{U}}{\partial \bar{R}} + \frac{\partial \bar{W}}{\partial \bar{Z}}\right)^2. \tag{4.7}$$

The flow is unsteady in a fixed frame of reference $(\bar{R}, \bar{Z})$, whereas it develops to be a steady flow in a wave frame $(\bar{r}, \bar{z})$. The following variables are meaningful to move the flow regime from unsteady to steady.

$$\left.\begin{array}{l} \bar{Z} = \bar{z} + c\bar{t} \\[2mm] \bar{R} = \bar{r} \\[2mm] \bar{P}(\bar{Z}, \bar{R}, \bar{t}) = \bar{p}(\bar{z}, \bar{r}, \bar{t}), \end{array}\right\} \tag{4.8}$$

the velocities inside the two frames are:

$$\left.\begin{array}{l} \bar{U} = \bar{u}, \\[2mm] \bar{W} = \bar{w} + c. \end{array}\right\} \tag{4.9}$$

The derived fundamental system of equations after invoking the above variables, is of the form:

$$\frac{\partial \bar{u}}{\partial \bar{r}} + \frac{\bar{u}}{\bar{r}} + \frac{\partial \bar{w}}{\partial \bar{z}} = 0, \tag{4.10}$$

$$\rho_{nf}\left[\bar{u}\frac{\partial \bar{u}}{\partial \bar{r}} + (\bar{w} + c)\frac{\partial \bar{u}}{\partial \bar{z}}\right] = \mu_{nf}\left[2\frac{\partial^2 \bar{u}}{\partial \bar{r}^2} + \frac{2}{\bar{r}}\left(\frac{\partial \bar{u}}{\partial \bar{r}} - \frac{\bar{u}}{\bar{r}}\right) + \frac{\partial}{\partial \bar{z}}\left(\frac{\partial \bar{u}}{\partial \bar{r}}\right) + \frac{\partial^2 \bar{w}}{\partial \bar{z}^2}\right]$$

$$- \frac{\partial \bar{p}}{\partial \bar{r}}, \tag{4.11}$$

$$\rho_{nf}\left[\bar{u}\frac{\partial \bar{w}}{\partial \bar{r}} + (\bar{w} + c)\frac{\partial \bar{w}}{\partial \bar{z}}\right] = 2\mu_{nf}\left[\frac{\partial^2 \bar{w}}{\partial \bar{z}^2} + \frac{1}{\bar{r}}\left(\frac{\partial \bar{u}}{\partial \bar{z}} + \frac{\partial \bar{w}}{\partial \bar{r}}\right) + \frac{\partial}{\partial \bar{r}}\left(\frac{\partial \bar{u}}{\partial \bar{z}} + \frac{\partial \bar{w}}{\partial \bar{r}}\right)\right]$$

$$- \sigma_{bf}B_0^2\cos(\Theta)(\bar{w} + c) - \frac{\partial \bar{p}}{\partial \bar{z}}, \tag{4.12}$$

$$(\rho c_p)_{nf}\left[\bar{u}\frac{\partial \bar{T}}{\partial \bar{r}} + (\bar{w}+c)\frac{\partial \bar{T}}{\partial \bar{z}}\right] = \left[k_{nf} + \frac{16\sigma^* T_\infty^3}{3k^*}\right]\frac{1}{\bar{r}}\frac{\partial}{\partial \bar{r}}\left(\bar{r}\frac{\partial \bar{T}}{\partial \bar{r}}\right) + k_{nf}\left[\frac{\partial^2 \bar{T}}{\partial \bar{z}^2}\right]$$

$$+ \mu_{nf}\left[2\left(\frac{\partial \bar{w}}{\partial \bar{r}}\right)^2 + \left(\frac{\partial \bar{u}}{\partial \bar{r}} + \frac{\partial \bar{w}}{\partial \bar{z}}\right)^2\right]$$

$$+ 2\mu_{nf}\left(\frac{\partial \bar{u}}{\partial \bar{z}}\right)^2 + Q_0. \tag{4.13}$$

The boundary conditions are given as:

$$\left.\begin{array}{ll} \dfrac{\partial w}{\partial r}=0, \quad \dfrac{\partial \theta}{\partial r}=0, & \text{at } r=0, \\[2mm] w = \dfrac{-2\pi\epsilon\alpha\beta\cos(2\pi z)}{1-2\pi\epsilon\alpha\beta\cos(2\pi z)}-1, \quad \theta=0 & \text{at } r=h(z)=1+\epsilon\cos(2\pi z), \end{array}\right\} \tag{4.14}$$

where $\bar{u}$ and $\bar{w}$ are the velocity elements in the $\bar{r}$ and $\bar{z}$ directions, respectively. Further, B_0 represents the magnetic field, Θ the angle of inclination and Q_0 the internal heat generation coefficient. Further, the physical properties of the nanofluid are given as [113]:

$$\left.\begin{array}{l} \mu_{nf} = \dfrac{\mu_{bf}}{(1-\phi)^{2.5}}, \\[3mm] \rho_{nf} = (1-\phi)\rho_{bf} + \phi\rho_s, \\[3mm] (\rho c_p)_{nf} = (1-\phi)(\rho c_p)_{bf} + \phi(\rho c_p)_s, \\[3mm] k_{nf} = \dfrac{k_s + 2k_{bf} + 2\left(k_s - k_{bf}\right)\phi\left(1+\gamma\right)^3}{k_s + 2k_{bf} - 2\left(k_s - k_{bf}\right)\phi\left(1+\gamma\right)^3}k_{bf}, \end{array}\right\} \tag{4.15}$$

where γ represents the ratio of the nanolayer thickness to the original particle radius.

TABLE 4.1: Thermophysical properties of H_2O and TiO_2 ([114, 115]).

item	$\rho(kg/m^3)$	$c_p(J/kgK)$	$k(W/mK)$
TiO_2	4250.0	686.2	8.9538
H_2O	997.1	4179.0	0.613

Now introducing the following dimensionless transformations, which are fruitful to transform the partial differential equation into ordinary differential equation:

$$
\left.
\begin{aligned}
&r = \frac{\bar{r}}{e}, \;\; z = \frac{\bar{z}}{\lambda}, \;\; u = \frac{\lambda \bar{u}}{ec}, \;\; p = \frac{e^2 \bar{p}}{c\lambda \mu_{bf}}, \;\; h = \frac{\bar{h}}{e}, \;\; Br = \frac{c^2 \mu_{bf}}{k_{bf} T_0}, \\
&Re = \frac{e\rho_{bf}}{\mu_{bf}}, \;\; w = \frac{\bar{w}}{c}, \;\;\; \beta = \frac{e}{\lambda}, \;\; Ha^2 = \frac{e^2 B_0^2 \sigma_{bf}}{\mu_{bf}}, \;\; \Omega = \frac{Q_0 e^2}{k_{bf} T_0}, \\
&\theta = \frac{(\bar{T} - \bar{T}_0)}{T_0}, \;\; Rn = \frac{16\sigma^*}{3k^* k_{bf}} T_\infty^3.
\end{aligned}
\right\}
\tag{4.16}
$$

Substituting (4.16) into Eqs. (4.10)-(4.13), we obtain the following non-dimensional system:

$$
A_1 \, Re \, \beta^3 \left[u\frac{\partial u}{\partial r} + (w+1)\frac{\partial u}{\partial z} \right] = -\frac{\partial p}{\partial r} + \beta^2 \left[\frac{2}{(1-\phi)^{2.5}} \right] \left[\frac{\partial^2 u}{\partial r^2} + \frac{1}{r}\frac{\partial u}{\partial r} - \frac{u}{r^2} \right]
$$
$$
+ \left[\frac{\beta^3}{(1-\phi)^{2.5}} \right] \left[\frac{\partial^2 u}{\partial r \partial z} + \frac{\partial^2 w}{\partial z^2} \right], \tag{4.17}
$$
$$
A_1 \, Re \, \beta \left[u\frac{\partial w}{\partial r} + (w+1)\frac{\partial w}{\partial z} \right] = -\frac{\partial p}{\partial z} + \beta^2 \left[\frac{1}{(1-\phi)^{2.5}} \right] \frac{\partial^2 w}{\partial z^2}
$$
$$
+ \frac{2}{(1-\phi)^{2.5}} \left[\frac{1}{r}\left(\beta^2 \frac{\partial u}{\partial z} + \frac{\partial w}{\partial r} \right) + \beta^2 \frac{\partial^2 u}{\partial r \partial z} + \frac{\partial^2 w}{\partial r^2} \right]
$$
$$
- Ha^2 \cos(\Theta)\,(w+1), \tag{4.18}
$$
$$
(\rho c_p)_{nf}\, e\, c\, \beta \left[u\frac{\partial \theta}{\partial r} + (w+1)\frac{\partial \theta}{\partial z} \right] = k_{nf} \left[\frac{\partial^2 \theta}{\partial r^2} + \frac{1}{r}\frac{\partial \theta}{\partial r} + \beta^2 \frac{\partial^2 \theta}{\partial z^2} \right] + \frac{Q_0\, e^2}{T_0}
$$
$$
+ \mu_{nf} \left[\frac{2c^2}{T_0}\left(\frac{\partial w}{\partial r} \right)^2 \right] + \frac{16\sigma^* T_\infty^3}{3k^*}\left[\frac{\partial^2 \theta}{\partial r^2} + \frac{1}{r}\frac{\partial \theta}{\partial r} \right]
$$
$$
+ \mu_{nf}\, c^2 \left[2e^2 \left(\frac{\partial u}{\partial z} \right)^2 + \left(\frac{\partial u}{\partial r} \right)^2 + \left(\frac{\partial w}{\partial z} \right)^2 \right] \beta^2
$$
$$
+ 2\left[\frac{\partial u}{\partial r}\frac{\partial w}{\partial z} \right] \beta^2, \tag{4.19}
$$

where

$$
A_1 = 1 - \phi + \phi\,\frac{\rho_s}{\rho_{bf}}. \tag{4.20}
$$

To attain the general solution of Eqs. (4.17)-(4.19), we shall restrict this study under the assumptions of long wavelength and low Reynolds number. The non-dimensional equations can be written as:

$$
\frac{dp}{dr} = 0, \tag{4.21}
$$

$$\frac{dp}{dz} - \frac{1}{(1-\phi)^{2.5}} \left(\frac{1}{r}\frac{dw}{dr} + \frac{d^2w}{dr^2} \right) + Ha^2 \cos(\Theta)\,(w+1) = 0, \qquad (4.22)$$

$$\left(\Psi_{4.10} + \frac{4}{3}Rn \right)\left(\frac{d^2\theta}{dr^2} + \frac{1}{r}\frac{d\theta}{dr} \right) + \frac{2Br}{(1-\phi)^{2.5}}\left(\frac{dw}{dr} \right)^2 + \Omega = 0. \qquad (4.23)$$

The convenient boundary conditions are:

$$\left. \begin{array}{ll} \dfrac{\partial w}{\partial r} = 0, \quad \dfrac{\partial \theta}{\partial r} = 0, & \text{at } r = 0, \\[2mm] w = \dfrac{-2\pi\epsilon\alpha\beta\cos(2\pi z)}{1 - 2\pi\epsilon\alpha\beta\cos(2\pi z)} - 1, \quad \theta = 0 & \text{at } r = h(z) = 1 + \epsilon\cos(2\pi z). \end{array} \right\} \qquad (4.24)$$

4.2.1 Second Law Analysis The volumetric entropy generation term S_G can be written as follows [116]:

$$S_G = \frac{k_{nf}}{\bar{\theta}_0^2}\left(\left(\frac{\partial \bar{T}}{\partial \bar{r}} \right)^2 + \left(\frac{\partial \bar{T}}{\partial \bar{z}} \right)^2 \right) + \frac{\bar{\bar{\Phi}}}{\bar{\theta}_0} + \frac{\sigma_{bf}B_0^2}{\bar{\theta}_0}\cos(\Theta)(\bar{w}+c)^2. \qquad (4.25)$$

The dimensional viscous dissipation term $\bar{\bar{\Phi}}$ is given as

$$\bar{\bar{\Phi}} = \mu_{nf}\left[2\left(\frac{\partial \bar{u}}{\partial \bar{z}} \right)^2 + 2\left(\frac{\partial \bar{w}}{\partial \bar{r}} \right)^2 + \left(\frac{\partial^2 \bar{u}}{\partial \bar{r}} + \frac{\partial^2 \bar{w}}{\partial \bar{z}} \right)^2 \right], \qquad (4.26)$$

whereas the dimensionless entropy generation rate Eg is given as:

$$\begin{aligned} Eg =& \frac{S_G}{S_g} \\ =& \Psi_{4.10}\left(\frac{\partial \theta}{\partial r} \right)^2 + \frac{\Lambda\,Br}{(1-\phi)^{2.5}}\left(\frac{\partial w}{\partial r} \right)^2 + \Lambda\,Br\,Ha^2\cos(\Theta)\,(w+1)^2, \qquad (4.27) \end{aligned}$$

or

$$Eg = E_H + E_V + E_M. \qquad (4.28)$$

Eq. (4.25) clearly displays the three different roots for the generation of entropy:

- First term appears due to heat transfer E_H irreversibility.

- Second term appears because of the presence of the viscous dissipation E_V effect.

- Third term develops because of the magnetic field E_M.

The characteristic entropy generation, the finite temperature difference and Hartman number are given, respectively, as:

$$S_g = \frac{k_{bf}T_0^2}{\bar{\theta}_0^2 e^2}, \quad \Lambda = \frac{\bar{\theta}_0}{T_0}, \quad Ha^2 = \frac{e^2 B_0^2 \sigma_{bf}}{\mu_{bf}}. \tag{4.29}$$

Bejan number is introduced to examine the irreversibility distribution [107].

$$Be = \frac{\text{heat transfer irreversibility}}{\text{total irreversibility}}$$
$$= \frac{E_H}{E_H + E_V + E_M}. \tag{4.30}$$

4.3 Exact Solution

This segment presents the closed form exact solutions to the ordinary differential Eqs. (4.22) and (4.23) together with the boundary condition (4.24). The constitutive boundary layer equations for the considered flow analysis are coupled nonlinear partial differential equations. Similarity variables have been introduced to transform the governing system into the ordinary differential equations. The obtained system is now linear, 2nd order inhomogeneous ordinary differential system. The exact solution of ordinary differential system presented in Eqs. (4.31), (4.33) and (4.34) is acquired by the function "DSolve" designed in the computational software MATHEMATICA. The general solution of inhomogeneous differential equations comprises of the complementary and particular parts. For complementary solution, "DSolve" chooses the Bessel functions, because the homogeneous part of Eq. (4.22) corresponds to the standard form of Bessel equation of order zero., i.e. $r^2 w''(r) + rw'(r) + r^2 w(r) = 0$. Once, we are successful in obtaining the complementary solution, "DSolve" straightforwardly proceeds for the particular solution using variation of parameter method. The general solution of the temperature

Eq. (4.23) is obtained by using reduction of order technique. The "reduction of order technique" is a technique for transforming any linear differential equation to another linear differential equation of lower order, and then formulating the general solution to the principal differential equation. The expressions of the velocity, pressure gradient and temperature are computed as:

$$w(r,z) = \left(\frac{F\Psi_{4.2}I_0\left[\Psi_{4.3}Ha\sqrt{\Psi_{4.1}}\sqrt{\cos\Theta}\right] - (\Psi_{4.3}^2 + F\Psi_{4.2})I_0\left[r\,Ha\sqrt{\Psi_{4.1}}\sqrt{\cos\Theta}\right]}{\Psi_{4.3}^2\Psi_{4.2}I_2[\Psi_{4.3}Ha\sqrt{\Psi_{4.1}}\sqrt{\cos\Theta}} \right)$$
$$+ \Psi_{4.3}^2\left(\frac{{}_0\bar{F}_1\left[2,\frac{1}{4}\Psi_{4.3}^2Ha^2\Psi_{4.1}\cos\Theta\right]}{\Psi_{4.3}^2\Psi_{4.2}I_2[\Psi_{4.3}Ha\sqrt{\Psi_{4.1}}\sqrt{\cos\Theta}} \right). \tag{4.31}$$

The flow rate is given as [107]:

$$Q = 2\int\limits_0^{h(z)} rw(r,z)dr. \tag{4.32}$$

Now using (4.31) into (4.32), we have solution of dp/dz i.e.

$$\frac{dp}{dz} = \frac{Ha^2\cos\Theta\,(\Psi_{4.3}^2 - F)\,\Psi_{4.2}I_0\left(Ha\Psi_{4.3}\sqrt{\Psi_{4.1}}\sqrt{\cos\Theta}\right)}{\Psi_{4.3}^2I_2\left[\Psi_{4.3}\,Ha\sqrt{\Psi_{4.1}}\sqrt{\cos\Theta}\right](1 - 2\pi\epsilon\alpha\beta\cos[2\pi z])}$$
$$+ \frac{\Psi_{4.3}^2\,(\Psi_{4.2} - 1)\,{}_0\bar{F}_1\left[2,\frac{1}{4}\Psi_{4.3}^2\Psi_{4.1}\cos\Theta\right]}{\Psi_{4.3}^2I_2\left[\Psi_{4.3}\,Ha\sqrt{\Psi_{4.1}}\sqrt{\cos\Theta}\right](1 - 2\pi\epsilon\alpha\beta\cos[2\pi z])}. \tag{4.33}$$

$$\theta(r,z) = \frac{\left(Br\,(\Psi_{4.3}^2 + F\Psi_{4.2})^2\,(\Psi_{4.4} + Ha^2\Psi_{4.1}\Psi_{4.11}\cos\Theta) + \Psi_{4.9}\right)}{\left(4\Psi_{4.3}^4\Psi_{4.2}^2\Psi_{4.1}I_2[h\,Ha\sqrt{\Psi_{4.1}}\sqrt{\cos\Theta}]^2\,(Rn + \Psi_{4.10})\right)}. \tag{4.34}$$

The mean flow rate and the pressure rise can be calculted as [107]:

$$F = Q - \left[0.5 + \frac{\epsilon^2}{4}\right], \tag{4.35}$$

$$\Delta P = \int\limits_0^1 \frac{dp}{dz}dz, \tag{4.36}$$

where the expressions for $(\Psi_i, i = 4.1 - 4.11)$ are given as:

$$
\left.
\begin{aligned}
\Psi_{4.1} &= (1 - \phi)^{2.5}, \\
\Psi_{4.2} &= 1 - 2\pi\epsilon\alpha\beta\cos[2\pi z], \\
\Psi_{4.3} &= 1 + \epsilon\cos[2\pi z], \\
\Psi_{4.4} &= 2I_0[\Psi_{4.3}Ha\sqrt{\Psi_{4.1}}\sqrt{\cos\Theta}]^2 - 2I_0[r\,Ha\sqrt{\Psi_{4.1}}\sqrt{\cos\Theta}]^2, \\
\Psi_{4.5} &= -2I_1[\Psi_{4.3}Ha\sqrt{\Psi_{4.1}}\sqrt{\cos\Theta}] + 2I_0[\Psi_{4.3}Ha\sqrt{\Psi_{4.1}}\sqrt{\cos\Theta}], \\
\Psi_{4.6} &= \left(I_0[\Psi_{4.3}Ha\sqrt{\Psi_{4.1}}\sqrt{\cos\Theta}] + I_2[\Psi_{4.3}Ha\sqrt{\Psi_{4.1}}\sqrt{\cos\Theta}]\right), \\
\Psi_{4.7} &= -2I_1[r\,Ha\sqrt{\Psi_{4.1}}\sqrt{\cos\Theta}]^2 + 2I_0[r\,Ha\sqrt{\Psi_{4.1}}\sqrt{\cos\Theta}]^2, \\
\Psi_{4.8} &= \left(I_0[r\,Ha\sqrt{\Psi_{4.1}}\sqrt{\cos\Theta}] + 2I_2[r\,Ha\sqrt{\Psi_{4.1}}\sqrt{\cos\Theta}]\right), \\
\Psi_{4.9} &= \Psi_{4.3}^4\left(\Psi_{4.3}^2 - r^2\right)\Psi_{4.1}\Psi_{4.2}\Omega I_2[\Psi_{4.3}Ha\sqrt{\Psi_{4.1}}\sqrt{\cos\Theta}]^2\Psi_{4.10}, \\
\Psi_{4.10} &= \frac{k_p + 2k_{bf} + 2\left(k_p - k_{bf}\right)\phi\left(1 + \gamma\right)^3}{k_p + 2k_{bf} - 2\left(k_p - k_{bf}\right)\phi\left(1 + \gamma\right)^3}, \\
\Psi_{4.11} &= \left(-\Psi_{4.3}^2\left(\Psi_{4.5}\Psi_{4.6}\right) + r^2\left(\Psi_{4.7}\Psi_{4.8}\right)\right).
\end{aligned}
\right\}
\tag{4.37}
$$

4.4 Results and Discussion

The primary focus, here is to study the influence of Hartman number Ha, flow rate Q, radiation parameter Rn, Brinkmann number Br, angle of inclination Θ, wave number β and cilia length ϵ on the velocity field $w(r, z)$, temperature field $\theta(r, z)$, pressure gradient dp/dz, pressure rise ΔP, entropy number Eg and Bejan number Be.

For this purpose, the velocity field is plotted for different values of Ha and Q. Figure 4.2 clearly shows that as Ha develops the fluid velocity reduces effectively, because of the fact that the viscous forces are highly dominant against the electromagnetic forces, which retard the flow. It can be seen that velocity is at its maximum at $r = 0$ and the velocity starts to decrease near the ciliated walls. Figure 4.3 shows that for higher values of Q the fluid flow increases rapidly.

The energy profile is portrayed in Figures 4.4 and 4.5 for increasing values of Rn and Br. It is illustrated in Figure 4.4 that by an increasing the magnitude of the

radiation the temperature of the fluid starts to decrease. Physically, an increment in Rn implies a decrease in k^*, therefore less energy is absorbed by the fluid. On the other side, the $\theta(r, z)$ significantly increases for higher values of Brinkmann number as visualized from Figure 4.5. This behavior is obvious, as Brinkmann number Br describes the conduction of heat from a wall to a flowing fluid. So, as Br increases, the temperature profile also increases.

Figures 4.6 and 4.7 depict the pressure gradient versus the axial direction for different flow parameters. Increasing effect of Ha on dp/dz is recorded in the regions $[0.5, 1.0]$ and $[1.5, 2]$, whereas an opposite effect is seen in the regions $[0, 0.5]$, $[1, 1.5]$ and $z \in [2, 2.5]$ in Figure 4.6. Similarly, an increase in angle of the inclination Θ causes more rapid flow, which implies high pressure gradient as noticed from Figure 4.7.

Figures 4.8 and 4.9 portrays the variation of the ΔP versus Q for the flow parameter wave number β and the non-dimensional measure of cilia length ϵ. Figure 4.8 shows that an increase in β causes to decrease the pressure rise. Figure 4.9 shows that ϵ directly influences ΔP. The capability of flow increases, when ϵ is increased.

Figures 4.10 to 4.13 are developed to show the physical behavior of entropy in the radial direction for different parameters, i.e Brinkmann number, Hartmann number, dimensionless temperature difference and radiation parameter. Figures 4.10 to 4.12 show that by an increasing Br, Ha and Λ the entropy number also increases. As Br increases, heat transfer dominates fluid viscosity within the channel, which causes increase of the entropy. Small entropy is recorded at the bottom of the tube and larger entropy is recorded near the ciliated walls in all cases. The influence of the thermal radiation is examined in Figure 4.13. It is seen that, with the increase in $Rn = 0.0, 1.0, 2.0, 3.0$ the entropy number decreases but the values are almost same at the bottom of tube. From the graphical illustration, it is quite clear that the Eg is directly proportional to the Ha, Br and Λ, and inversely proportional to the radiation parameter.

Figures 4.14 to **??** are prepared to illustrate the physical insight of Be for increasing values of Ha, Br, Λ and Rn. It is found that Be is the increasing function of Br and decreasing function of Ha, Λ and Rn.

Trapping phenomenon is shown in Figures 4.18 to 4.21. From Figures 4.18 and 4.19 it is clear that by an increasing the inclination angle the bolus size shrinking, however the counting of trapped boluses increases. Figures 4.20 and 4.21 demonstrates that the amount of trapped boluses reduces and the bolus size enhances with an increment in the flow rate.

The variations in velocity and temperature profiles for multiple values of ϕ are presented in Table 4.2. The variation of entropy generation for numerous values of Rn and ϕ are presented in Table 4.3.
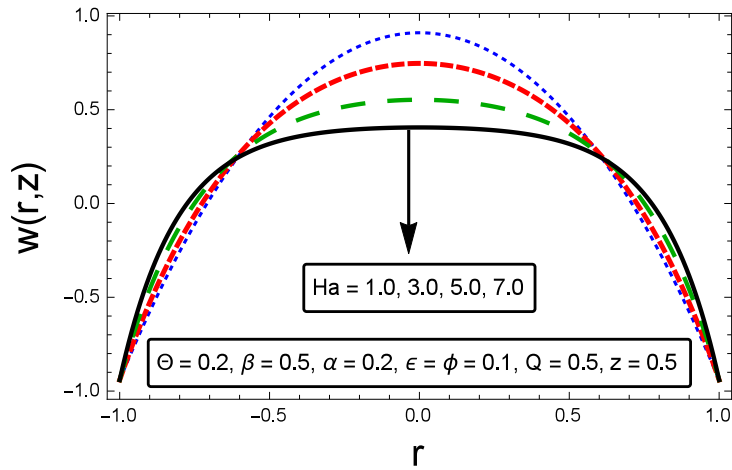
FIGURE 4.2: The impact of Ha on $w(r, z)$
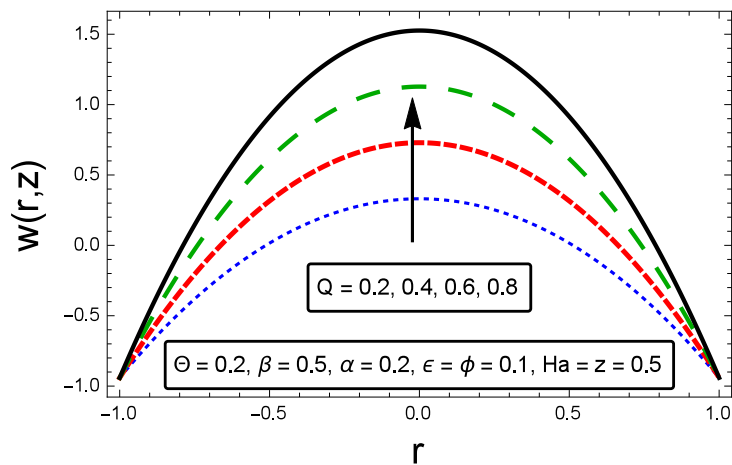
FIGURE 4.3: The impact of Q on $w(r, z)$
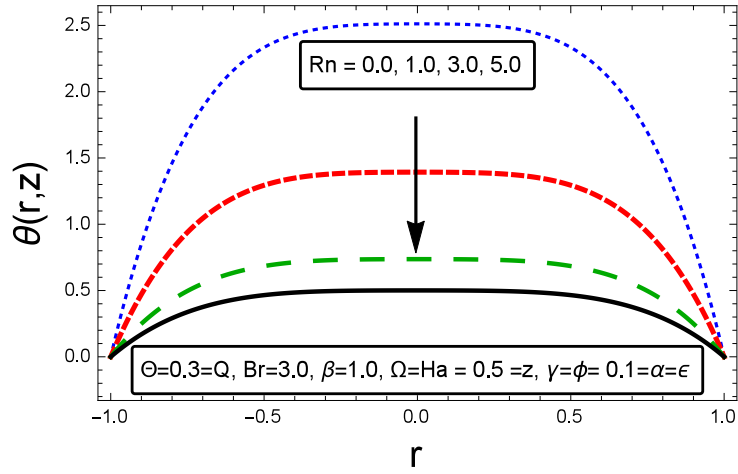
FIGURE 4.4: The impact of Rn on θ
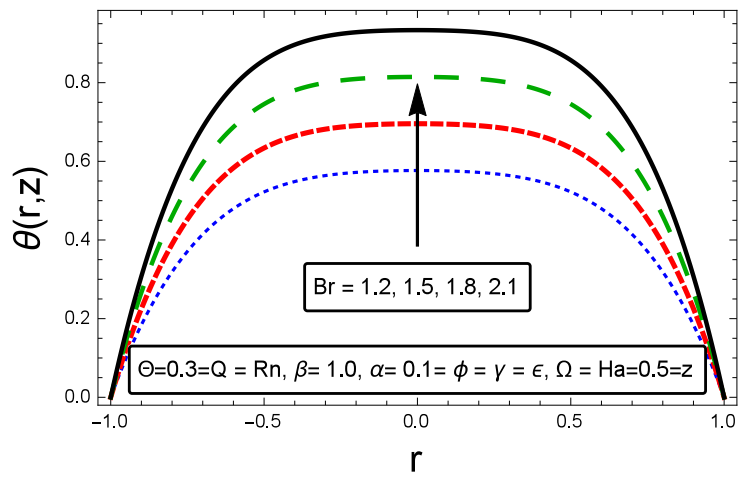
FIGURE 4.5: The impact of Br on θ
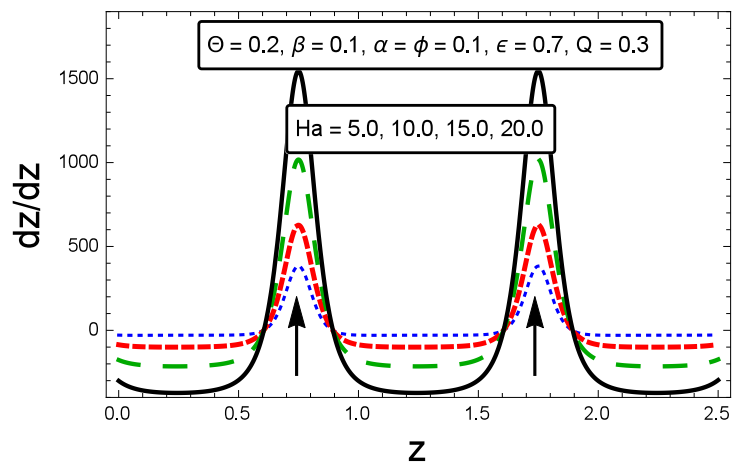
FIGURE 4.6: The impact of Ha on dp/dz
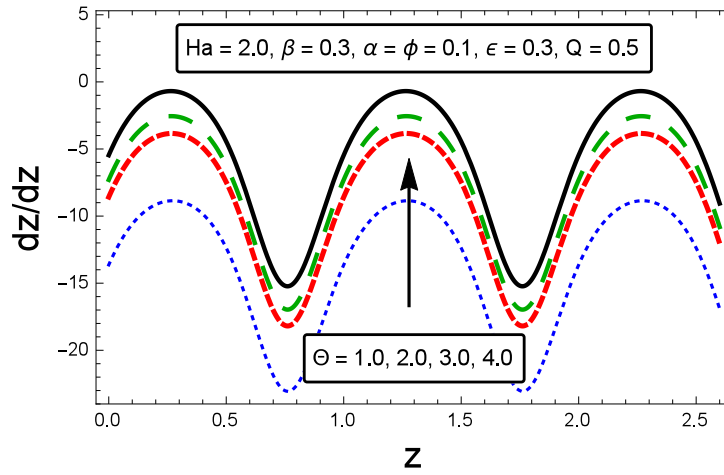
FIGURE 4.7: The impact of Θ on dp/dz
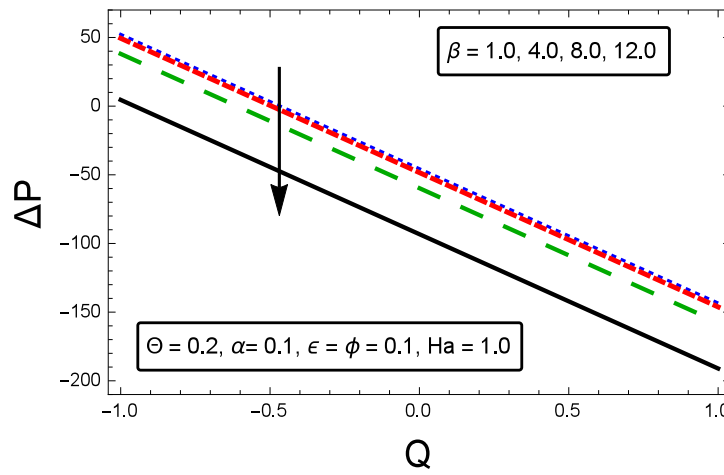
FIGURE 4.8: The impact of β on ΔP
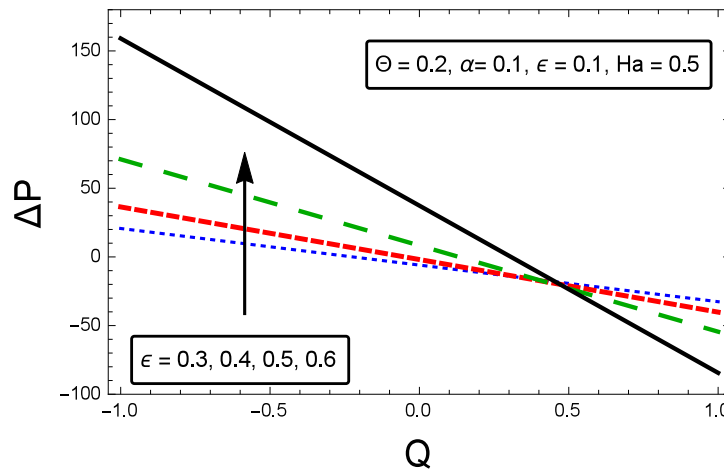
FIGURE 4.9: The impact of ϵ on ΔP

FIGURE 4.10: The impact of Br on Eg
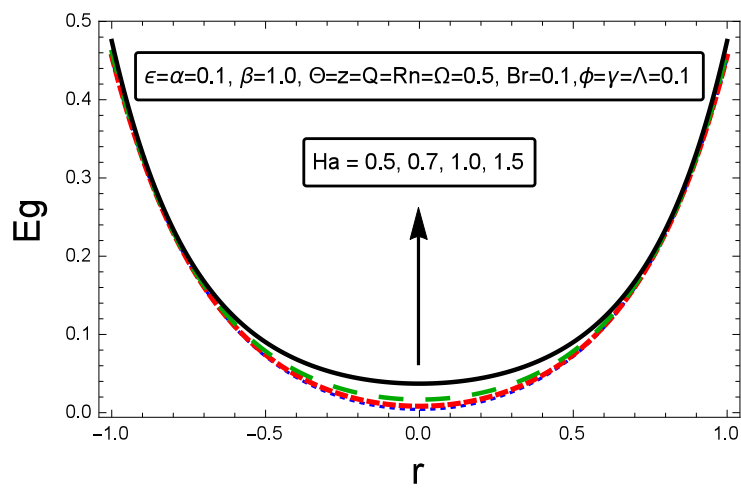
FIGURE 4.11: The impact of Ha on Eg
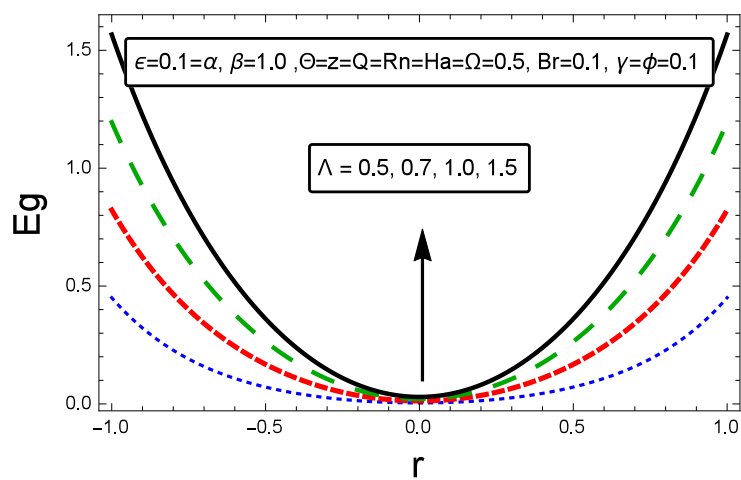
FIGURE 4.12: The impact of Λ on Eg
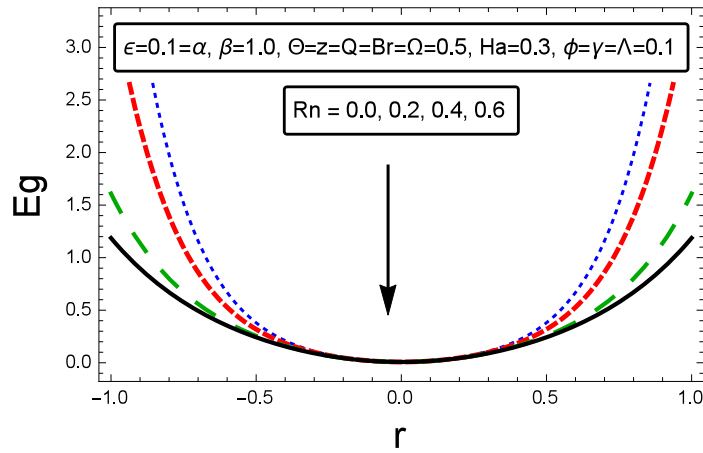
FIGURE 4.13: The impact of Rn on Eg
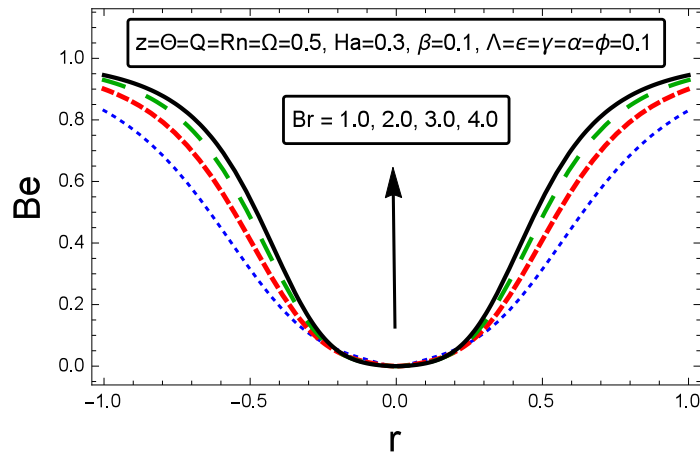
FIGURE 4.14: The impact of Br on Be
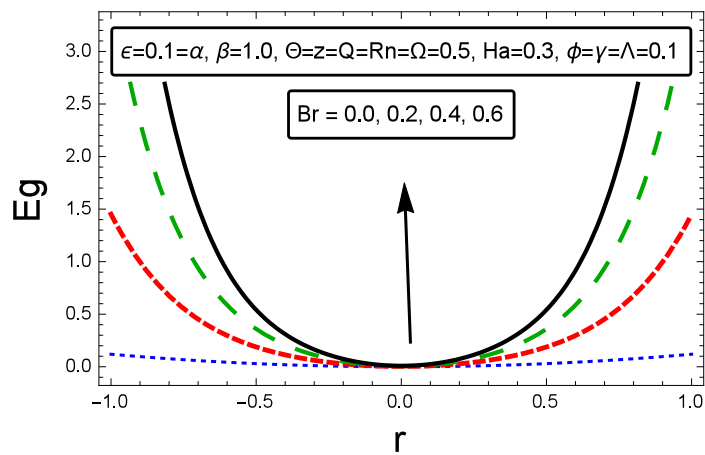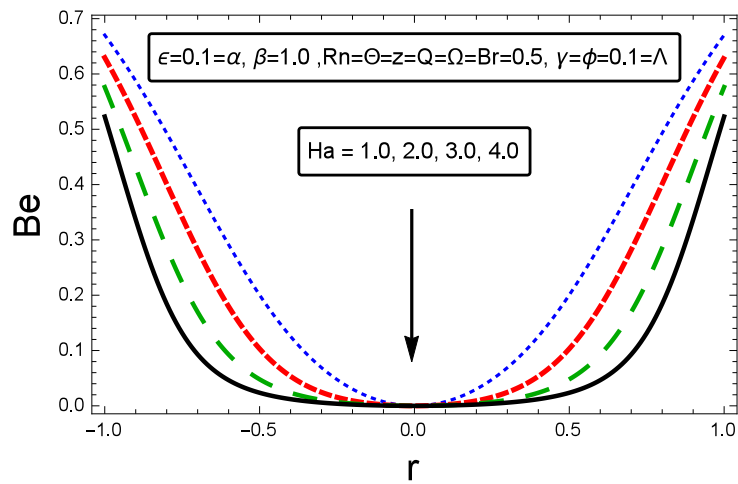

FIGURE 4.15: The impact of Ha on Be
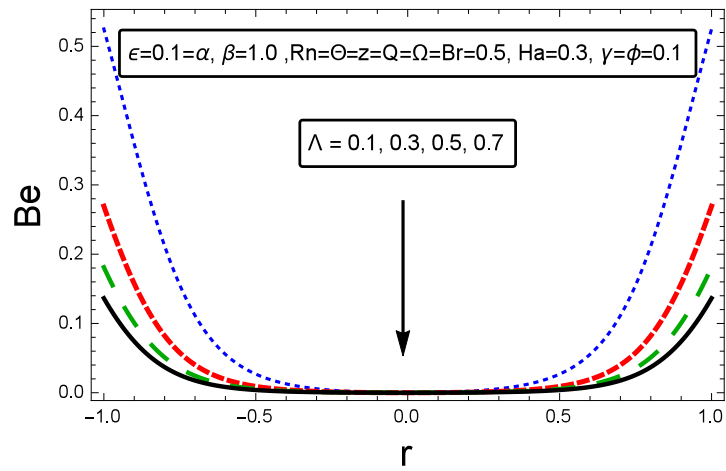
FIGURE 4.16: The impact of Λ on Be
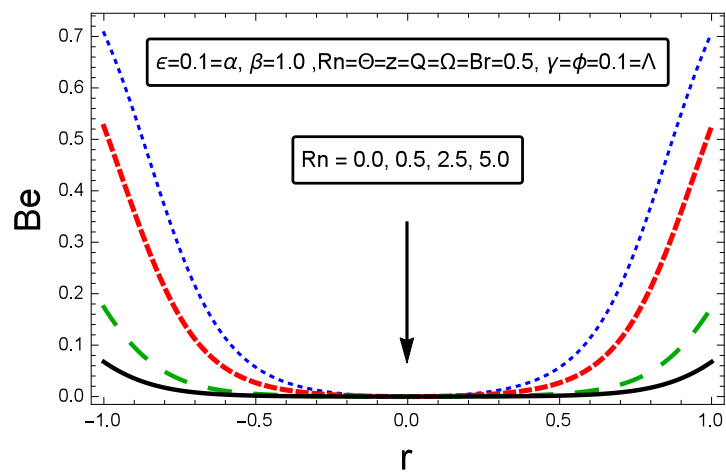
FIGURE 4.17: The impact of Rn on Be
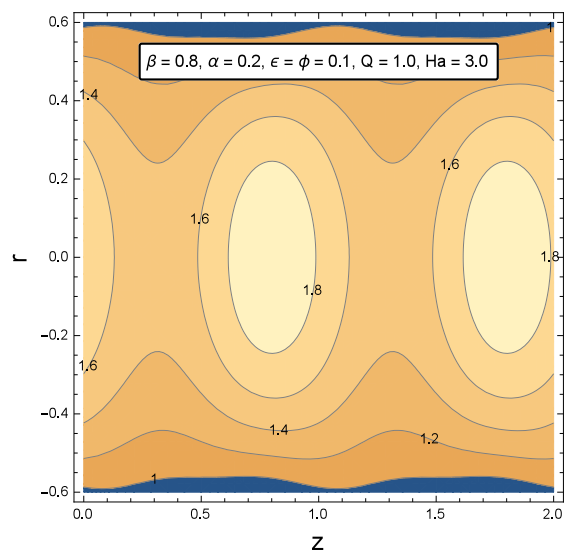
FIGURE 4.18: Streamlines for $\Theta = 0.5$
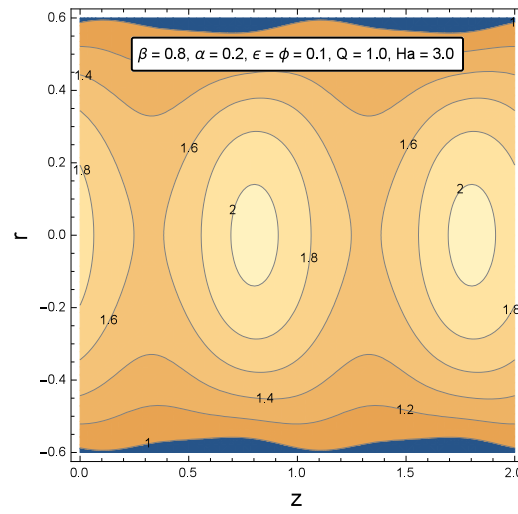
FIGURE 4.19: Streamlines for $\Theta = 1.0$
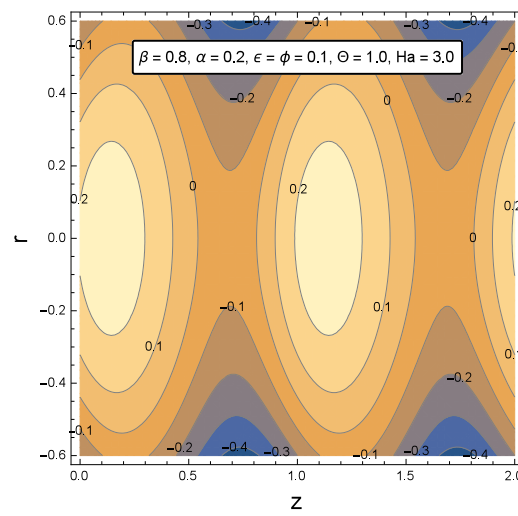
FIGURE 4.20: Streamlines for $Q = 0.1$
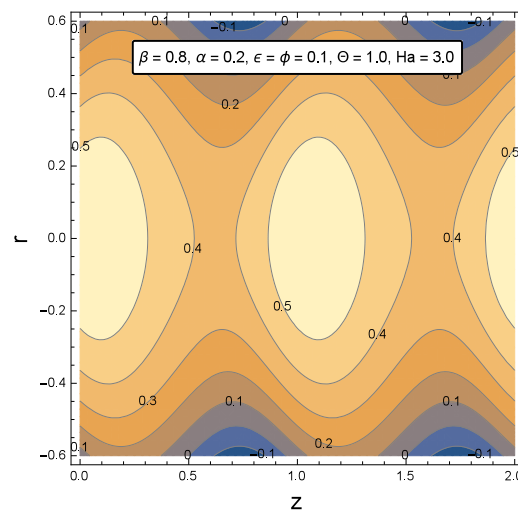
FIGURE 4.21: Streamlines for $Q = 0.3$

TABLE 4.2: Variation in w and θ for different values of ϕ while keeping the other particulars constant ($z = 0.1, \epsilon = 0.1, \alpha = 0.2, \beta = 0.5, \Theta = 0.5, Q = 0.3, Ha = 3.0., \gamma = 0.1, Rn = 0.5, \Omega = 0.5.$)

	$\phi = 0.0$		$\phi = 0.3$		$\phi = 0.5$	
r	w	θ	w	θ	w	θ
-1.00	-0.85876	0.00000	-0.86246	0.00000	-0.86395	0.00000
-0.75	-0.17509	0.18429	-0.18011	0.14054	-0.18216	0.00920
-0.50	0.29395	0.26639	0.29919	0.21019	0.30131	0.03167
-0.25	-0.17509	0.29631	-0.18011	0.23980	-0.18216	0.05147
0.00	0.65790	0.30310	0.67784	0.24766	0.68599	0.05912
0.25	-0.17509	0.29631	-0.18011	0.23980	-0.18216	0.05147
0.50	0.29395	0.26639	0.29919	0.21019	0.30131	0.03167
0.75	-0.17509	0.18429	-0.18011	0.14054	-0.18216	0.00920
1.00	-0.85876	0.00000	-0.86246	0.00000	-0.86395	0.00000

TABLE 4.3: Variation in Eg for various values of Rn and ϕ while setting the other particulars constant ($z = 0.5, \epsilon = 0.1, e = 0.5, Q = 0.5, Ha = 0.5, \gamma = 1.0, \beta = 1.0, \Theta = 0.1, \Lambda = 0.1, \Omega = 0.5, Br = 1.0$).

Rn	ϕ	$r = \pm 1.0$	$r = \pm 0.75$	$r = \pm 0.5$	$r = \pm 0.25$
0.0	0.0	15.66690	3.52975	0.68267	0.13833
1.0		04.99361	1.48760	0.45298	0.12839
2.0		03.01717	1.10985	0.41045	0.12644
3.0		02.32539	0.97751	0.39557	0.12578
0.0	0.1	00.86073	1.01024	0.46434	0.13054
1.0		00.52566	0.99819	0.45824	0.12351
2.0		-00.01107	0.97891	0.44845	0.11225
3.0		-00.95100	0.94513	0.43133	0.09254

Chapter 5

Entropy Formation Analysis for the Peristaltic Motion of Ferrofluids in the Presence of Joule Heating and Fluid Friction Phenomena in a Plumb Duct

5.1   Introduction

This chapter has been managed to evaluate the entropy growth during the peristaltic transport of ferrofluids in a plumb duct. The selected ferrofluids are made of magnetite Fe_3O_4 nanoparticles and engine oil. Moreover, heat transfer analysis is performed with Joule heating, thermal radiation and viscous dissipation effects. Mathematical formulation has been completed, which results into a set of ordinary differential equations. Closed form solutions has been computed for the momentum, energy and pressure gradient. Moreover, entropy formation because of heat transfer, thermal radiation, viscous dissipation and magnetic effects has been encountered. Graphical illustrations for the emerging flow parameters like

Hartmann number, Brinkmann number, radiation parameter and dimensionless temperature difference have been prepared in order to study the physical sense of these particulars. The central point of the second law of thermodynamics is achieved by increasing the magnitude of the radiation parameter.

5.2   Problem Statement

Considering, the peristaltic transport of two dimensional, incompressible axisymmetric flow of a magnetite nanofluid in a finite horizontal tube. A uniform magnetic field B_0 is applied normal to the circular tube. The selected ferrofluids are made of engine oil and magnetite nanoparticles. Heat transfer is targeted to be analyzed in the presence of Joule heating, viscous dissipation and thermal radiation. Cylindrical coordinate system $(\bar{R}, \bar{Z})$, is selected in such a manner such that $\bar{R}$-axis is perpendicular to the tube and $\bar{Z}$-axis lies along the center of the tube. The sinusoidal wave proliferates along the walls with a velocity c and wavelength λ. Figure 5.1 displays the physical aspects of the presented model and the coordinate system. The wall geometry is expressed as [116]:

$$\bar{R}_{wall} = \bar{h}(\bar{Z}, \bar{t}) = e + \epsilon \sin\left(\frac{2\pi}{\lambda}\left(\bar{Z} - c\bar{t}\right)\right), \tag{5.1}$$

where e and ϵ are the mean radius of the tube and amplitude of the wave respectively.
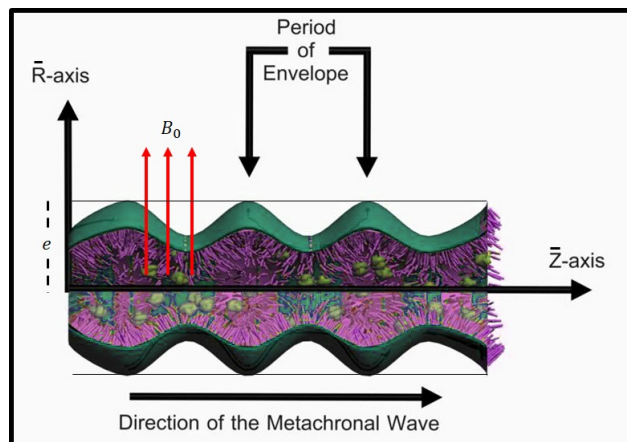
FIGURE 5.1: Geometrical view of the physical model

The governing model is expressed as [107]:

Continuity equation:

$$\frac{\partial \bar{U}}{\partial \bar{R}} + \frac{\bar{U}}{\bar{R}} + \frac{\partial \bar{W}}{\partial \bar{Z}} = 0. \tag{5.2}$$

Momentum equation in radial direction:

$$\rho_{nf} \left[\frac{\partial \bar{U}}{\partial \bar{t}} + \bar{U} \frac{\partial \bar{U}}{\partial \bar{R}} + \bar{W} \frac{\partial \bar{U}}{\partial \bar{Z}} \right] = - \frac{\partial \bar{P}}{\partial \bar{R}} + \mu_{nf} \left[2 \frac{\partial^2 \bar{U}}{\partial \bar{R}^2} + \frac{2}{\bar{R}} \left(\frac{\partial \bar{U}}{\partial \bar{R}} - \frac{\bar{U}}{\bar{R}} \right) \right]$$
$$+ \mu_{nf} \left[\frac{\partial}{\partial \bar{Z}} \left(\frac{\partial \bar{U}}{\partial \bar{R}} \right) + \frac{\partial^2 \bar{W}}{\partial \bar{Z}^2} \right]. \tag{5.3}$$

Momentum equation in axial direction:

$$\rho_{nf} \left[\frac{\partial \bar{W}}{\partial \bar{t}} + \bar{U} \frac{\partial \bar{W}}{\partial \bar{R}} + \bar{W} \frac{\partial \bar{W}}{\partial \bar{Z}} \right] = - \frac{\partial \bar{P}}{\partial \bar{Z}} + 2\mu_{nf} \left[\frac{\partial^2 \bar{W}}{\partial \bar{Z}^2} + \frac{1}{\bar{R}} \left(\frac{\partial \bar{U}}{\partial \bar{Z}} + \frac{\partial \bar{W}}{\partial \bar{R}} \right) \right]$$
$$+ \mu_{nf} \left[\frac{\partial}{\partial \bar{R}} \left(\frac{\partial \bar{U}}{\partial \bar{Z}} + \frac{\partial \bar{W}}{\partial \bar{R}} \right) \right]$$
$$- \sigma_{bf} B_0^2 \left[\bar{W} + c \right]. \tag{5.4}$$

Energy equation:

$$(\rho c_p)_{nf} \left[\frac{\partial \bar{T}}{\partial \bar{t}} + \bar{U} \frac{\partial \bar{T}}{\partial \bar{R}} + \bar{W} \frac{\partial \bar{T}}{\partial \bar{Z}} \right] = \left[k_{nf} + \frac{16 \sigma^* T_\infty^3}{3 k^*} \right] \frac{1}{\bar{R}} \frac{\partial}{\partial \bar{R}} \left(\bar{R} \frac{\partial \bar{T}}{\partial \bar{R}} \right) + k_{nf} \left[\frac{\partial^2 \bar{T}}{\partial \bar{Z}^2} \right]$$
$$+ \mu_{nf} \left[2 \left(\frac{\partial \bar{W}}{\partial \bar{R}} \right)^2 + \left(\frac{\partial \bar{U}}{\partial \bar{R}} + \frac{\partial \bar{W}}{\partial \bar{Z}} \right)^2 \right]$$
$$+ \sigma_{bf} B_0^2 \left[\bar{W} + c \right]^2 + 2\mu_{nf} \left(\frac{\partial \bar{U}}{\partial \bar{Z}} \right)^2. \tag{5.5}$$

The transformation between the frames are:

$$\bar{Z} = \bar{z} + c\bar{t}, \quad \bar{R} = \bar{r}, \quad \bar{P}(\bar{Z}, \bar{R}, \bar{t}) = \bar{p}(\bar{z}, \bar{r}, \bar{t}), \tag{5.6}$$

and the velocities inside the frames are:

$$\bar{U} = \bar{u}, \quad \bar{W} = \bar{w} + c. \tag{5.7}$$

The derived fundamental system of equations after invoking the above variables, is of the form:

$$\frac{\partial \bar{u}}{\partial \bar{r}} + \frac{\bar{u}}{\bar{r}} + \frac{\partial \bar{w}}{\partial \bar{z}} = 0, \tag{5.8}$$

$$\rho_{nf}\left[\bar{u}\frac{\partial \bar{u}}{\partial \bar{r}} + (\bar{w}+c)\frac{\partial \bar{u}}{\partial \bar{z}}\right] = \mu_{nf}\left[2\frac{\partial^2 \bar{u}}{\partial \bar{r}^2} + \frac{2}{\bar{r}}\left(\frac{\partial \bar{u}}{\partial \bar{r}} - \frac{\bar{u}}{\bar{r}}\right) + \frac{\partial}{\partial \bar{z}}\left(\frac{\partial \bar{u}}{\partial \bar{r}}\right) + \frac{\partial^2 \bar{w}}{\partial \bar{z}^2}\right]$$
$$- \frac{\partial \bar{p}}{\partial \bar{r}}, \tag{5.9}$$

$$\rho_{nf}\left[\bar{u}\frac{\partial \bar{w}}{\partial \bar{r}} + (\bar{w}+c)\frac{\partial \bar{w}}{\partial \bar{z}}\right] = 2\mu_{nf}\left[\frac{\partial^2 \bar{w}}{\partial \bar{z}^2} + \frac{1}{\bar{r}}\left(\frac{\partial \bar{u}}{\partial \bar{z}} + \frac{\partial \bar{w}}{\partial \bar{r}}\right) + \frac{\partial}{\partial \bar{r}}\left(\frac{\partial \bar{u}}{\partial \bar{z}} + \frac{\partial \bar{w}}{\partial \bar{r}}\right)\right]$$
$$- \sigma_{bf}B_0^2(\bar{w}+c) - \frac{\partial \bar{p}}{\partial \bar{z}}, \tag{5.10}$$

$$(\rho c_p)_{nf}\left[\bar{u}\frac{\partial \bar{T}}{\partial \bar{r}} + (\bar{w}+c)\frac{\partial \bar{T}}{\partial \bar{z}}\right] = \left[k_{nf} + \frac{16\sigma^* T_\infty^3}{3k^*}\right]\frac{1}{\bar{r}}\frac{\partial}{\partial \bar{r}}\left(\bar{r}\frac{\partial \bar{T}}{\partial \bar{r}}\right) + k_{nf}\left[\frac{\partial^2 \bar{T}}{\partial \bar{z}^2}\right]$$
$$+ \left[2\left(\frac{\partial \bar{u}}{\partial \bar{z}}\right)^2 + 2\left(\frac{\partial \bar{w}}{\partial \bar{r}}\right)^2 + \left(\frac{\partial \bar{u}}{\partial \bar{r}} + \frac{\partial \bar{w}}{\partial \bar{z}}\right)^2\right]\mu_{nf}$$
$$+ \sigma_{bf}B_0^2\left[\bar{w}+c\right]^2. \tag{5.11}$$

The boundary conditions:

$$\left.\begin{array}{ll}
\dfrac{\partial w}{\partial r} = 0, \quad \dfrac{\partial \theta}{\partial r} = 0, & \text{at} \quad r = 0, \\[2mm]
w = -1, \quad \theta = 0 & \text{at} \quad r = h(z) = \dfrac{e + \epsilon\sin(2\pi z)}{e},
\end{array}\right\} \tag{5.12}$$

where $\bar{u}$ and $\bar{w}$ are the velocity components in the radial and axial directions respectively. Further, B_0 the magnetic field, σ_{bf} the effective electrical conductivity. Thermal properties of the nanofluid are defined as follows [113].

$$\left.\begin{array}{l}
\mu_{nf} = \dfrac{\mu_{bf}}{(1-\phi)^{2.5}}, \\[3mm]
\rho_{nf} = (1-\phi)\rho_{bf} + \phi\rho_{bf}, \\[3mm]
(\rho c_p)_{nf} = (1-\phi)(\rho c_p)_{bf} + \phi(\rho c_p)_s, \\[3mm]
k_{nf} = \dfrac{k_s + 2k_{bf} + 2(k_s - k_{bf})\phi(1+\gamma)^3}{k_s + 2k_{bf} - 2(k_s - k_{bf})\phi(1+\gamma)^3}k_{bf},
\end{array}\right\} \tag{5.13}$$

Thermophysical properties of the engine oil and magnetite are presented in Table 5.1. The following transformations are found successful to convert the model into the dimensionless form:

$$
\left.
\begin{aligned}
r &= \frac{\bar{r}}{e}, \quad z = \frac{\bar{z}}{\lambda}, \quad w = \frac{\bar{w}}{c}, \\
u &= \frac{\lambda \bar{u}}{ec}, \quad p = \frac{e^2 \bar{p}}{c \lambda \mu_{bf}}, \\
h &= \frac{\bar{h}}{e}, \quad \theta = \frac{(\bar{T} - \bar{T}_0)}{T_0} \quad t = \frac{c\bar{t}}{\lambda},
\end{aligned}
\right\}
\tag{5.14}
$$

using (5.14) into (5.8)-(5.11), the mathematical model gets the following form:

$$
A_1 \, Re \, \beta^3 \left[u \frac{\partial u}{\partial r} + (w+1) \frac{\partial u}{\partial z} \right] = -\frac{\partial p}{\partial r} + \beta^2 \left[\frac{2}{(1-\phi)^{2.5}} \right] \left[\frac{\partial^2 u}{\partial r^2} + \frac{1}{r} \frac{\partial u}{\partial r} - \frac{u}{r^2} \right]
$$
$$
+ \left[\frac{\beta^3}{(1-\phi)^{2.5}} \right] \left[\frac{\partial^2 u}{\partial r \partial z} + \frac{\partial^2 w}{\partial z^2} \right],
\tag{5.15}
$$

$$
A_1 \, Re \, \beta \left[u \frac{\partial w}{\partial r} + (w+1) \frac{\partial w}{\partial z} \right] = -\frac{\partial p}{\partial z} + \beta^2 \left[\frac{1}{(1-\phi)^{2.5}} \right] \frac{\partial^2 w}{\partial z^2} + \frac{1}{(1-\phi)^{2.5}}
$$
$$
\times \left[\frac{1}{r} \left(\beta^2 \frac{\partial u}{\partial z} + \frac{\partial w}{\partial r} \right) + \beta^2 \frac{\partial^2 u}{\partial r \partial z} + \frac{\partial^2 w}{\partial r^2} \right]
$$
$$
- \frac{\sigma_{bf} B_0^2 e^2}{\mu_{bf}} (w+1),
\tag{5.16}
$$

$$
(\rho c_p)_{nf} \, e \, c \, \beta \left[u \frac{\partial \theta}{\partial r} + (w+1) \frac{\partial \theta}{\partial z} \right] = k_{nf} \left[\frac{\partial^2 \theta}{\partial r^2} + \frac{1}{r} \frac{\partial \theta}{\partial r} + \beta^2 \frac{\partial^2 \theta}{\partial z^2} \right] + \frac{2 c^2 \mu_{nf}}{T_0} \left(\frac{\partial w}{\partial r} \right)^2
$$
$$
+ \beta^2 c^2 \left[2e^2 \left(\frac{\partial u}{\partial z} \right)^2 + \left(\frac{\partial u}{\partial r} \right)^2 + \left(\frac{\partial w}{\partial z} \right)^2 \right] \mu_{nf}
$$
$$
+ \beta^2 c^2 \left[2 \frac{\partial u}{\partial r} \frac{\partial w}{\partial z} \right] + \mu_{nf} \frac{\sigma_{bf} B_0^2 c^2 e^2}{T_0} (w+1)^2
$$
$$
+ \frac{16 \sigma^* T_\infty^3}{3 k^*} \left[\frac{\partial^2 \theta}{\partial r^2} + \frac{1}{r} \frac{\partial \theta}{\partial r} \right],
\tag{5.17}
$$

where

$$
\left.
\begin{aligned}
Br &= \frac{c^2 \mu_{bf}}{k_{bf} T_0}, \quad Rn = \frac{4\sigma^*}{k^* k_{bf}} T_\infty^3, \quad Ha^2 = \frac{\sigma_{bf} B_0^2 e^2}{\mu_{bf}}, \\
\beta &= \frac{e}{\lambda}, \quad J_h = \frac{\sigma_{bf} c^2 e^2}{k_{bf} T_0} B_0^2, \quad A_1 = 1 - \phi + \phi \frac{\rho_s}{\rho_{bf}}.
\end{aligned}
\right\}
\tag{5.18}
$$

Here J_h is the Joule heating parameter. To achieve the general solution of the Eqs. (5.17)-(5.19), we shall restrict this study under the following assumptions:

- **Long wavelength**: the length of the wave is assumed to be infinite ($\lambda \to \infty$) as compared to the tube width.

- **Low Renyolds number**: inertial free flow ($Re \ll 1$) is considered i.e. inertial forces are minute as compared to viscous forces.

The set of Eqs. (5.15)-(5.17) after employing the above assumptions is reduced to the following set of equations:

$$\frac{dp}{dr} = 0, \tag{5.19}$$

$$\frac{dp}{dz} - \frac{1}{(1-\phi)^{2.5}} \left(\frac{1}{r}\frac{dw}{dr} + \frac{d^2w}{dr^2} \right) + Ha^2 \left(w + 1 \right) = 0, \tag{5.20}$$

$$\frac{d^2\theta}{dr^2} \left(1 + \frac{4Rn}{3\Psi_{5.1}} \right) + \frac{1}{r}\frac{d\theta}{dr} \left(1 + \frac{4Rn}{3\Psi_{5.1}} \right) + \frac{1}{\Psi_{5.1}} \frac{Br}{(1-\phi)^{2.5}} \left(\frac{dw}{dr} \right)^2$$
$$+ \frac{1}{\Psi_{5.1}} J_h \left(w + 1 \right)^2 = 0, \tag{5.21}$$

where
$$\Psi_{5.1} = \frac{k_s + 2k_{bf} + 2\left(k_s - k_{bf}\right)\phi\left(1+\gamma\right)^3}{k_s + 2k_{bf} - 2\left(k_s - k_{bf}\right)\phi\left(1+\gamma\right)^3}. \tag{5.22}$$

The wall conditions are given as:

$$\left. \begin{array}{ll} \dfrac{\partial w}{\partial r} = 0, \quad \dfrac{\partial \theta}{\partial r} = 0, & \text{at} \quad r = 0, \\[2mm] w = -1, \quad \theta = 0 & \text{at} \quad r = h(z) = \dfrac{e + \epsilon \sin(2\pi z)}{e}. \end{array} \right\} \tag{5.23}$$

TABLE 5.1: Thermophysical properties of magnetite and engine oil ([117, 118]).

item	$\rho(kg/m^3)$	$c_p(J/kgK)$	$k(W/mK)$
Magnetite	5180	670	9.7
Engine Oil	884	1910	0.144

5.2.1 Second Law Analysis

Non-equilibrium situation emerges as a result of exchange of momentum, temperature and magnetic field within the fluid and at the walls, which consequently produces the entropy. The volumetric entropy

generation rate S_G can be calculated by using the following formulae [116].

$$
S_G = \frac{1}{\bar{\theta}_0^2} \left[\overbrace{k_{nf} \left(\frac{\partial \bar{T}}{\partial \bar{r}} \right)^2}^{E_H} + \overbrace{\frac{16\sigma^* T_\infty^3}{3k^*} \left(\frac{\partial \bar{T}}{\partial \bar{r}} \right)^2}^{E_{Rn}} \right] + \overbrace{\frac{\sigma_{bf} B_0^2}{\bar{\theta}_0} (\bar{w} + c)^2}^{E_M}
$$

$$
+ \frac{\mu_{nf}}{\bar{\theta}_0} \left[\overbrace{2 \left(\frac{\partial \bar{u}}{\partial \bar{z}} \right)^2 + 2 \left(\frac{\partial \bar{w}}{\partial \bar{r}} \right)^2 + \frac{\partial^2 \bar{u}}{\partial \bar{r}^2} + \frac{\partial^2 \bar{w}}{\partial \bar{z}^2} + 2 \left(\frac{\partial \bar{u}}{\partial \bar{r}} \frac{\partial \bar{w}}{\partial \bar{z}} \right)}^{E_V} \right]. \quad (5.24)
$$

Eq. (5.24) reflects the contribution of four different factors causing the entropy generation. These are the heat transfer E_H, the thermal radiation E_{Rn}, the magnetic field E_M and the viscous dissipation E_V. Entropy gives the degree of disorder of the system and its surroundings and is given as:

$$
Eg = \left(\frac{k_{nf}}{k_{bf}} + \frac{4}{3} Rn \right) \left(\frac{\partial \theta}{\partial r} \right)^2 + \frac{2\Lambda Br}{(1 - \phi)^{2.5}} \left(\frac{\partial w}{\partial r} \right)^2 + \Lambda Br Ha^2 (w + 1)^2, \quad (5.25)
$$

where

$$
S_g = \frac{k_{bf} T_0^2}{\bar{\theta}_0^2 e^2}, \quad (5.26)
$$

$$
\Lambda = \frac{\bar{\theta}_0}{T_0}. \quad (5.27)
$$

The dimensionless Eg is computed on dividing S_G by S_g. Bejan number is introduced to investigates the irreversibility distribution:

$$
Be = \frac{E_H}{E_H + E_T + E_V + E_M}. \quad (5.28)
$$

5.3   Exact Solutions

In this segment, the exact solutions to the coupled ordinary differential Eqs. (5.20) and (5.21) together with the wall condition (5.23) are presented. The constitutive

boundary layer equations for the considered flow analysis incorporates continuity, momentum and energy equations. The exact solution of ordinary differential system presented in Eqs. (5.29), (5.31) and (5.32) is acquired by the function "DSolve" designed in the computational software MATHEMATICA. The general solution of inhomogeneous differential equations comprises of the complementary and particular parts. For complementary solution, "DSolve" chooses the Bessel functions, because the homogeneous part of Eq. (5.20) corresponds to the standard form of Bessel equation of order zero i.e. $r^2w''(r) + rw'(r) + r^2w(r) = 0$. Once, we are successful in obtaining the complementary solution, "DSolve" straightforwardly proceeds for the particular solution using variation of parameter method. The general solution of the temperature (5.21) is obtained by using reduction of order technique. The expressions for velocity, pressure gradient and temperature are computed as:

Velocity distribution:

$$w(r,z) = \left(-1 + \frac{(dp/dz)}{Ha^2} + \frac{(dp/dz)I_0\left[rHa\sqrt{1-\phi^{2.5}}\right]}{Ha^2 I_0\left[hHa\sqrt{1-\phi^{2.5}}\right]} \right). \tag{5.29}$$

Flow rate [107]:

$$Q = 2\pi \int_0^{h(z)} rw\,dr. \tag{5.30}$$

Pressure gradient:

Substituting (5.29) in (5.30), we have

$$\frac{dp}{dz} = -\frac{Ha^2\left(F + h^2\pi\right)I_0\left(hHa\sqrt{1-\phi^{2.5}}\right)}{h^2\pi I_2\left(hHa\sqrt{1-\phi^{2.5}}\right)}. \tag{5.31}$$

Temperature distribution:

$$\theta(r,z) = \left(F + h^2\pi\right)^2 \left(\frac{\left(\Psi_{5.2}\left(h^2\Psi_{5.3} + J_h r^2\left(1-\phi^{2.5}\right)\right)\right)I_0\left(hHa\sqrt{1-\phi^{2.5}}\right)^2}{4h^4 Ha^2\pi^2\left(1-\phi^{2.5}\right)I_2\left(h\sqrt{1-\phi^{2.5}}Ha\right)^2\left(Rn+\Psi_{5.1}\right)} \right)$$
$$+ \left(F + h^2\pi\right)^2 \left(\frac{I_0\left(hHa\sqrt{1-\phi^{2.5}}\right)\left(\Psi_{5.4} + \Psi_{5.5}I_1\left(hHa\sqrt{1-\phi^{2.5}}\right)\right)}{4h^4 Ha^2\pi^2\left(1-\phi^{2.5}\right)I_2\left(h\sqrt{1-\phi^{2.5}}Ha\right)^2\left(Rn+\Psi_{5.1}\right)} \right)$$

$$+ \left(F + h^2\pi\right)^2 \left(\frac{Ha\Psi_{5.6}I_1\left(rHa\sqrt{1 - \phi^{2.5}}\right)^2 + \Psi_{5.7}I_1\left(h\sqrt{1 - \phi^{2.5}}\right)}{4h^4 Ha^2\pi^2\left(1 - \phi^{2.5}\right)I_2\left(h\sqrt{1 - \phi^{2.5}}Ha\right)^2\left(Rn + \Psi_{5.1}\right)} \right)$$

$$+ \left(F + h^2\pi\right)^2 \left(\frac{\Psi_{5.8}\left(h^2 I_1\left(hHa\sqrt{1 - \phi^{2.5}}\right)^2 - r^2 I_2\left(rHa\sqrt{1 - \phi^{2.5}}\right)\right)}{4h^4 Ha^2\pi^2\left(1 - \phi^{2.5}\right)I_2\left(h\sqrt{1 - \phi^{2.5}}Ha\right)^2\left(Rn + \Psi_{5.1}\right)} \right).$$

$$(5.32)$$

Expressions for $\left(\Psi_i, i = 5.2, ..., 5.8\right)$ are given as:

$$\left.\begin{aligned}
\Psi_{5.2} &= -8J_h + 2BrHa^2 - Ha^2, \\
\Psi_{5.3} &= -3J_h + 2BrHa^2, \\
\Psi_{5.4} &= J_h I_0\left(rHa\sqrt{1 - \phi^{2.5}}\right), \\
\Psi_{5.5} &= 2hHa\left(-J_h + BrHa^2\right)\sqrt{1 - \phi^{2.5}}, \\
\Psi_{5.6} &= \left(-Br - J_h + BrHa^2\right)r^2\sqrt{1 - \phi^{2.5}}, \\
\Psi_{5.7} &= \left(J_h - BrHa^2\right)r\sqrt{1 - \phi^{2.5}}I_0\left(h\sqrt{1 - \phi^{2.5}}\right), \\
\Psi_{5.8} &= Ha\left(J_h - BrHa^2\right)\left(\sqrt{1 - \phi^{2.5}}\right).
\end{aligned}\right\}$$

$$(5.33)$$

5.4 Result and Discussion

An arrangement of figures in this section has been displayed to get a physical insight into the problem. Figure 5.2 displays the influence of Ha on w against the radial distance. It is found that as Ha increases the fluid velocity decreases. Actually, higher magnitude of Ha implies large Lorentz force (resistive force), therefore huge amount of resistance is faced by the fluid and hence retards the fluid motion. Figure 5.3 shows the impact of the flow rate Q on the $w(r, z)$. It is found that Q is directly proportional to the flow field. The increasing trend of thermal radiation parameter on the temperature field is shown in Figure 5.4. This graph shows that fluid temperature decreases gradually as radiation increases more quickly. Physically, an increase in Rn increases the mean absorption coefficient k^* which

consequently reduces the temperature. The behavior of the Joule heating parameter J_h on the temperature profile against the radial distance is presented in Figure 5.5. Basically, the effect of MHD produces the Joule heating effect. It is visualized that the temperature distribution enhances significantly for larger values of Joule heating. Effects of flow rate and amplitude ratio are portrayed in Figures 5.6 and 5.7 respectively. It is seen that the advancing flow rate gradually weakening the pressure gradient profile. Whereas, a uniform fluctuating behavior is examined in case of the amplitude ratio. Increasing trend of ϵ on the dp/dz is recorded in the regions $z \in [0, 0.5]$, $z \in [1, 1.5]$ and $z \in [2, 2.5]$, whereas an opposite trend is seen in the regions $z \in [0.5, 1.0]$ and $z \in [1.5, 2]$ in Figure 5.7. Figures 5.8 and 5.9 exhibits the variation of ΔP versus Q for wave number β and the Hartmann number Ha. Figure 5.8 shows that an increase in the β results causes to decrease the pressure rise. Figure 5.9 shows that ΔP is the decreasing function of Ha. Physically, when Ha is increased, the ability of fluid to flow is reduced, and so ΔP decreases automatically.

It is viewed in Figure 5.10 that the formation of entropy enhances with higher Ha. Moreover, maximum entropy is seen at the mid of tube, because in this portion the velocity is at its extreme and thus contribution to MHD flow is also at its extreme. Similarly, when Ha is large, low entropy is viewed near the walls of the tube, because high Ha implies low fluid friction irreversibility.

The influence of the thermal radiation Rn is demonstrated in Figure 5.11, we noticed that an increment in the radiation results to reduces the entropy. Physically, an increment in Rn give rise to a low buoyancy force which consequently decreases the entropy. Figure 5.12 depicts that the formation of entropy increases with the increasing Br.

Figure 5.13 shows the influence of the dimensionless temperature difference Λ on the entropy generation. It is seen that the entropy number increases for the increasing values of Λ.

Figures 5.14 to 5.17 are graphed to examine the nature of Be under the variations in different parameters. It is seen that the magnitude of Be reduces with an increase in the magnitude of Ha, Rn, Br and Λ, because the heat transfer

irreversibility E_H is small as compared with the total irreversibility i.e. $Eg = E_H + E_T + E_V + E_M$.

A very fascinating phenomenon in peristaltic movement, called trapping, is shown with respect to change in various parameters. Figures 5.18 and 5.19 reflect that the bolus size enlarges rapidly, however, the amount of trapped bolus start decreasing in size, as we increase the Q from 0.1 to 0.5. From Figures 5.20 and 5.21, it is clear that by increasing the ϵ from 0.3 to 0.5, the bolus size increases inside the streamlines but the count of trapped bolus reduces.

The variations in the velocity and temperature profiles for various values of ϕ is presented in Table 5.2. The variations in the temperature profile for various values of the Rn is presented in Table 5.3. Table 5.4 presents the dynamics of entropy for different values of Λ and Br.
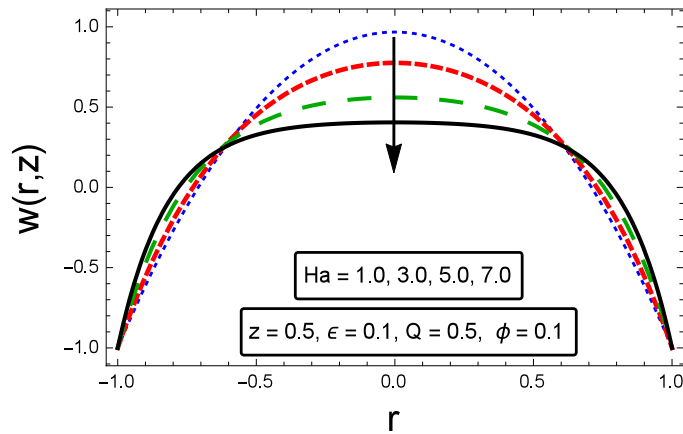
FIGURE 5.2: The impact of Ha on $w(r,z)$
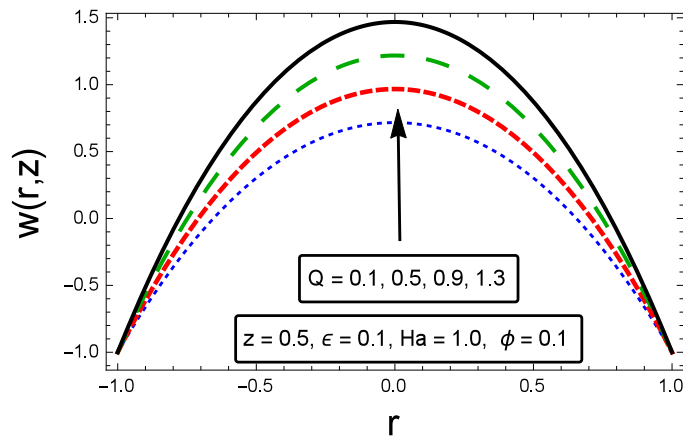
FIGURE 5.3: The impact of Q on $w(r,z)$
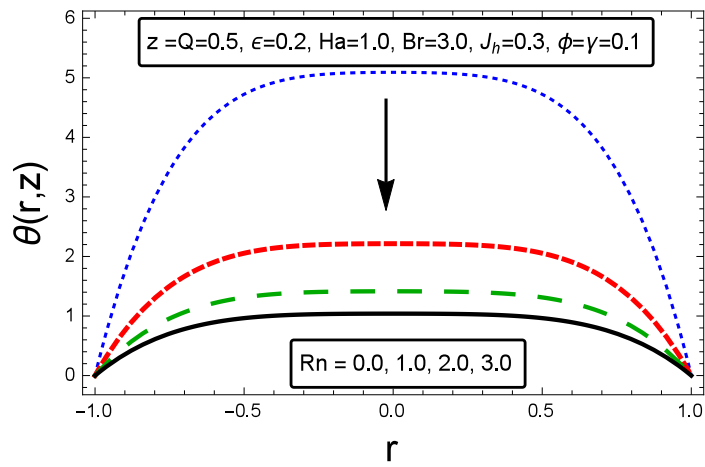
FIGURE 5.4: The impact of Rn on $\theta(r, z)$
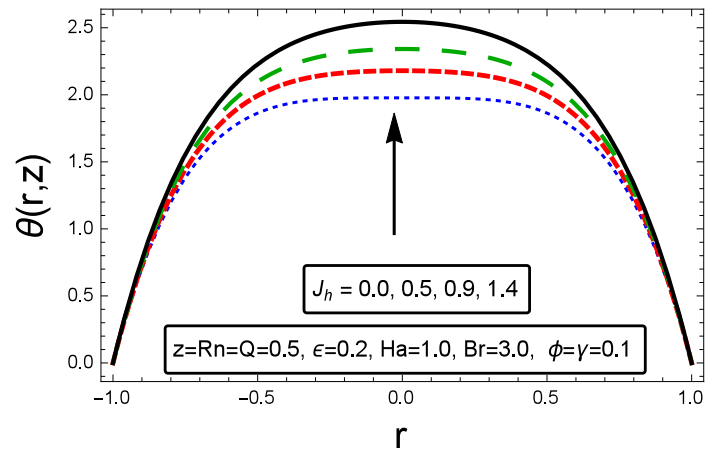
FIGURE 5.5: The impact of J_h on $\theta(r, z)$
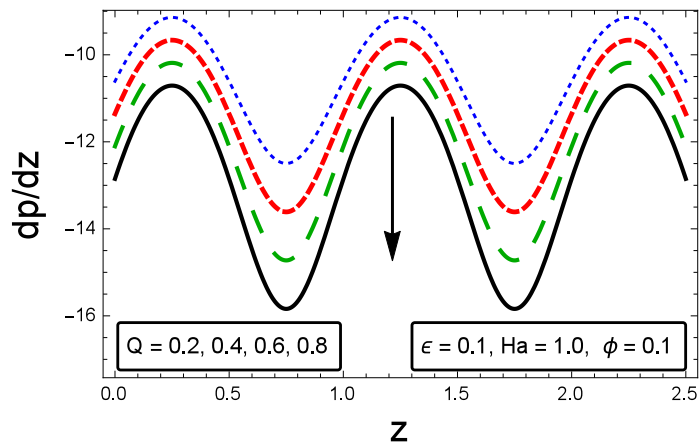
FIGURE 5.6: The impact of Q on dp/dz
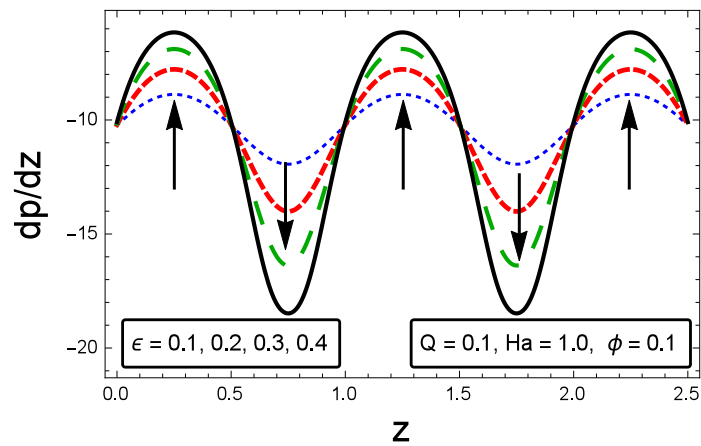
FIGURE 5.7: The impact of ϵ on dp/dz
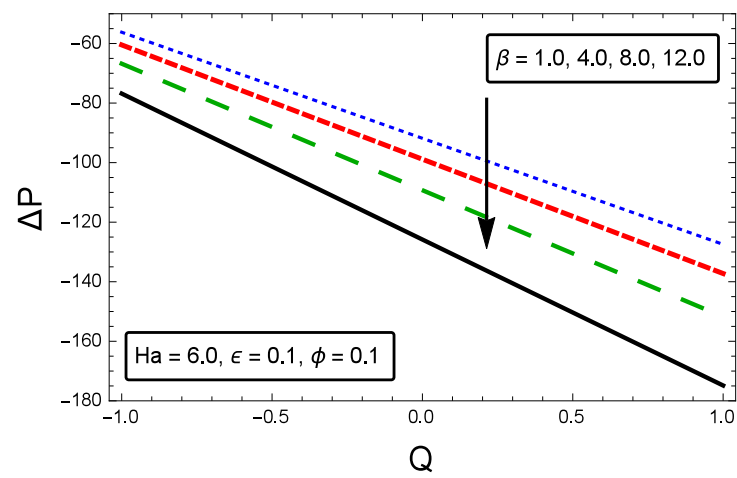
FIGURE 5.8: The impact of β on ΔP
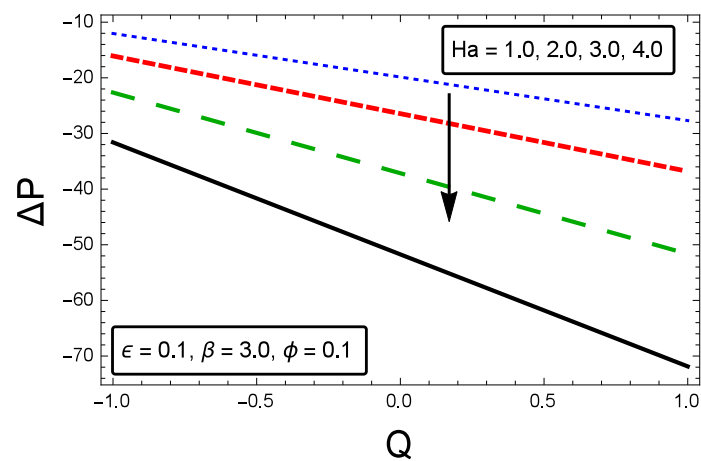
FIGURE 5.9: The impact of Ha on ΔP
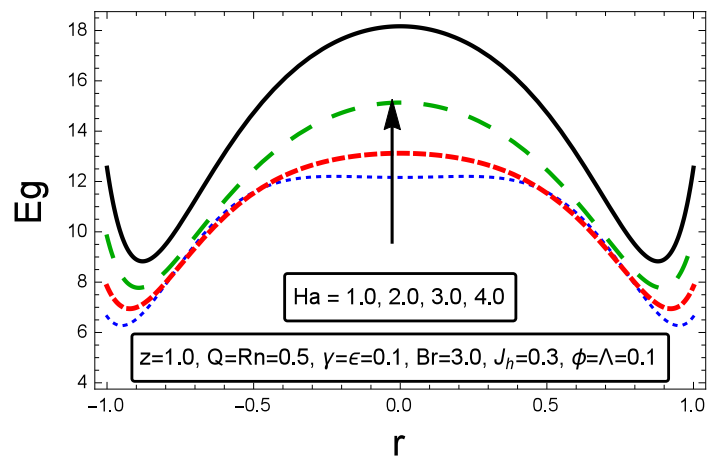
FIGURE 5.10: The impact of Ha on Eg
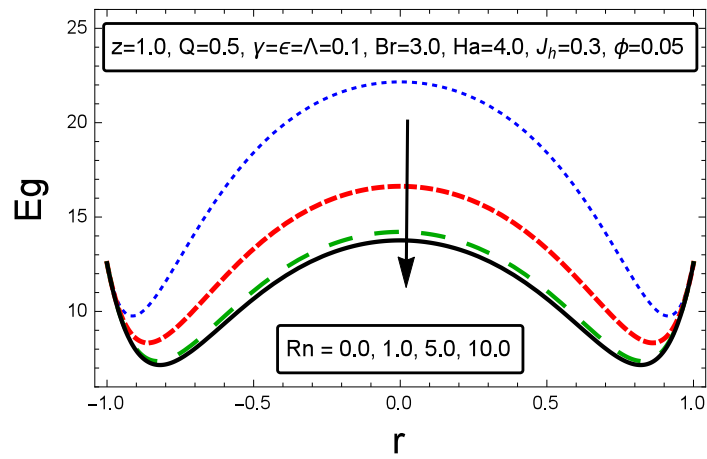
FIGURE 5.11: The impact of Rn on Eg
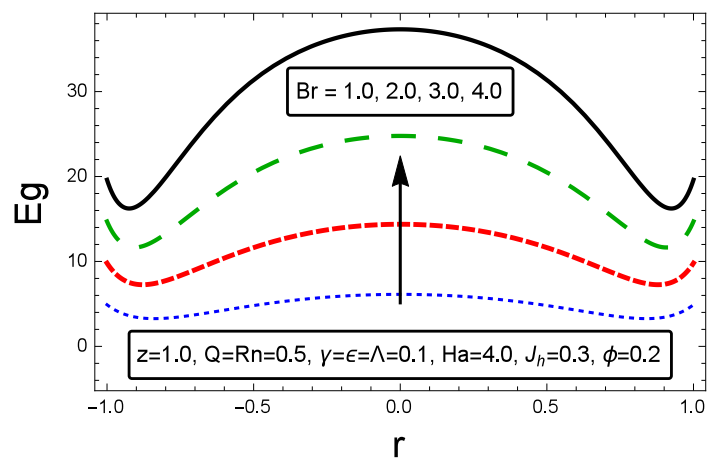
FIGURE 5.12: The impact of Br on Eg
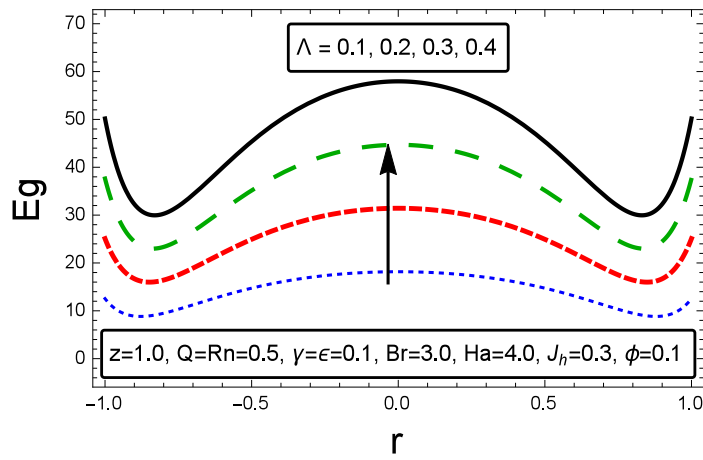
FIGURE 5.13: The impact of Λ on Eg
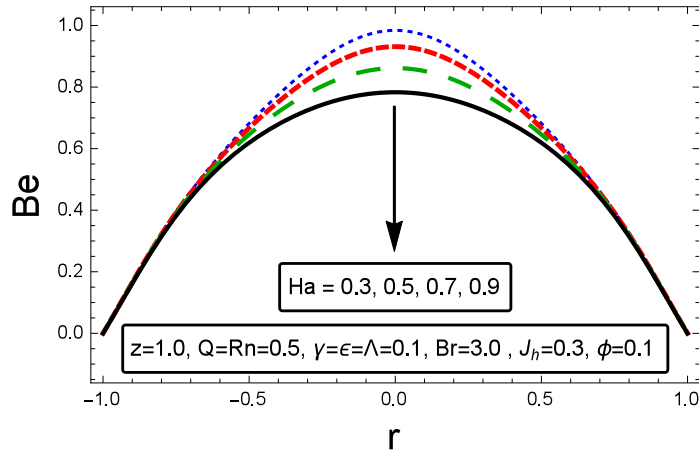
FIGURE 5.14: The impact of Ha on Be
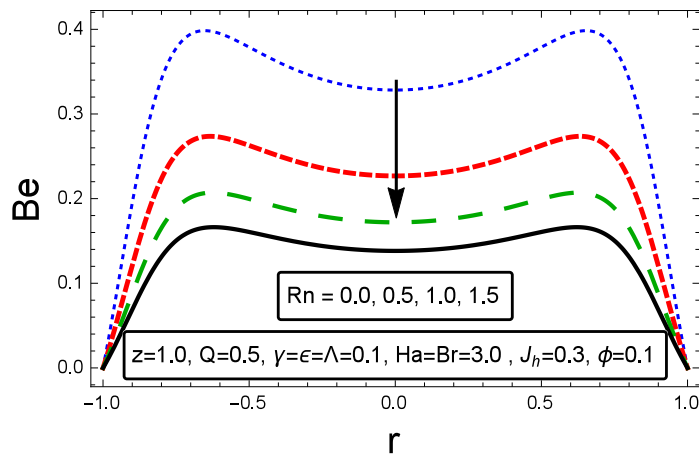
FIGURE 5.15: The impact of Rn on Be
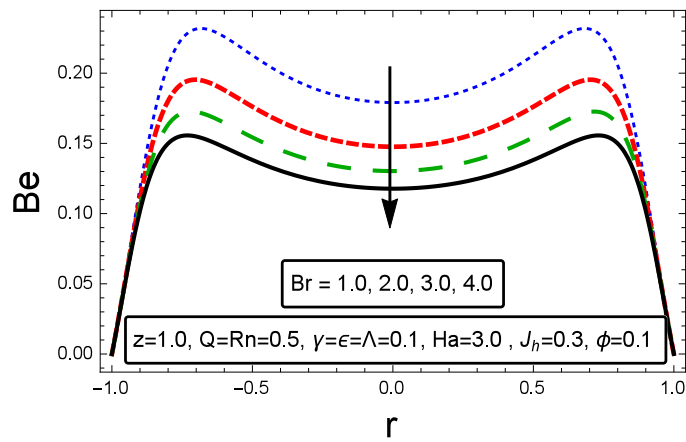
FIGURE 5.16: The impact of Br on Be
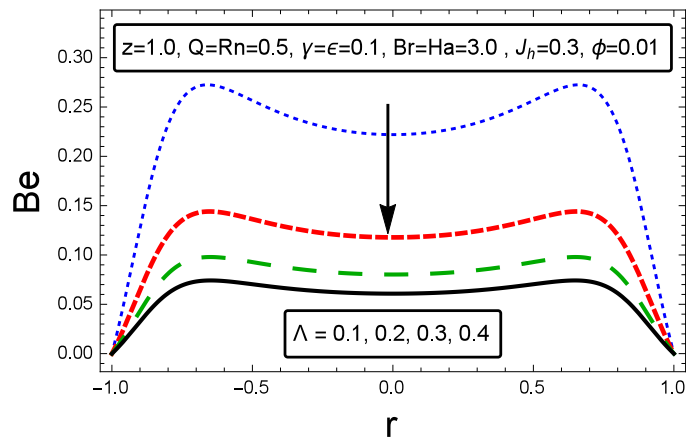
FIGURE 5.17: The impact of Λ on Be
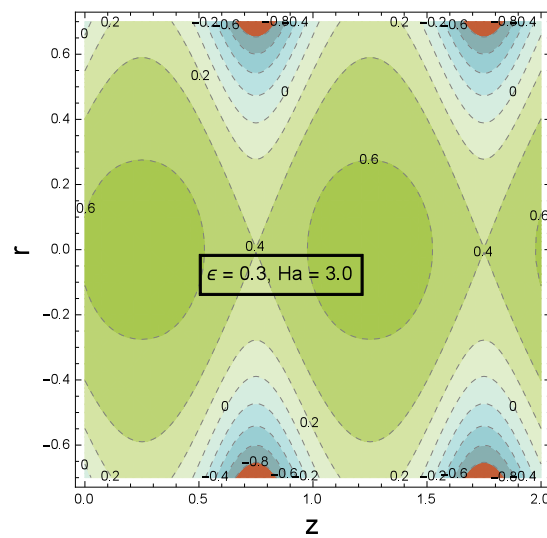
FIGURE 5.18: Streamlines for $Q = 0.1$
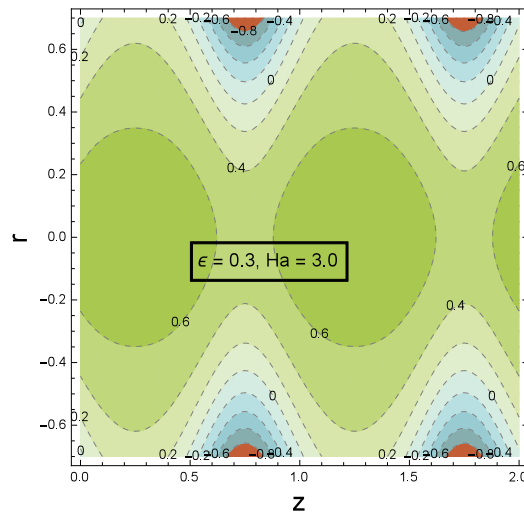
FIGURE 5.19: Streamlines for $Q = 0.5$
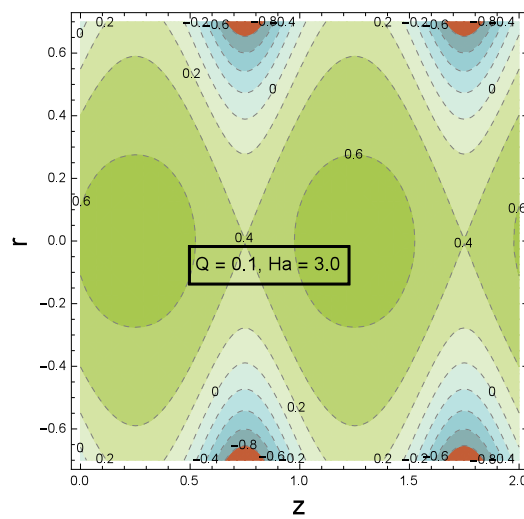
FIGURE 5.20: Streamlines for $\epsilon = 0.3$
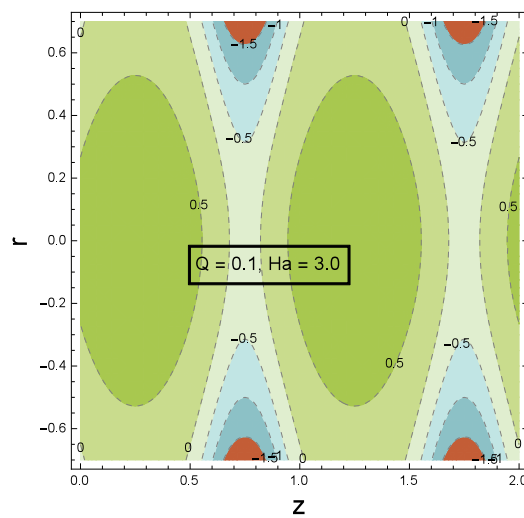
FIGURE 5.21: Streamlines for $\epsilon = 0.5$

TABLE 5.2: Variation in w and θ profiles for different values of ϕ while keeping the other particulars constant ($z = 0.5, \varepsilon = \gamma = 0.1, Q = 0.5 = Rn, Ha = 3.0, Br = J_h = 0.3$).

	$\phi = 0.0$		$\phi = 0.3$		$\phi = 0.5$	
r	w	θ	w	θ	w	θ
-1.00	-1.00000	0.00000	-1.00000	0.00000	-1.00000	0.00000
-0.75	-0.04152	1.25485	-0.08511	1.96078	-0.10689	5.11789
-0.50	0.43928	1.64699	0.47203	2.59566	0.48678	6.87813
-0.25	0.66228	1.64270	0.77119	2.62741	0.82599	7.12241
0.00	0.72709	1.75940	0.86539	2.77002	0.93630	7.33409
0.25	0.66228	1.64270	0.77119	2.62741	0.82599	7.12241
0.50	0.43928	1.64699	0.47203	2.59566	0.48678	6.87813
0.75	-0.04152	1.25485	-0.08511	1.96078	-0.10689	5.11789
1.00	-1.00000	0.00000	-1.00000	0.00000	-1.00000	0.00000

TABLE 5.3: Variation in θ profile for various values of Rn while setting the other particulars constant ($z = Q = 0.5, \epsilon = \gamma = 0.1, Ha = 2.0, Br = 3.0, \phi = J_h = 0.01$).

r	$Rn = 0.0$	$Rn = 1.0$	$Rn = 3.0$	$Rn = 5.0$
-1.00	0.00000	0.00000	0.00000	0.00000
- 0.75	1.93097	0.95292	0.47338	0.31490
- 0.50	2.49715	1.23232	0.61218	0.40724
- 0.25	2.60932	1.28768	0.63967	0.42553
0.00	2.61663	1.29128	0.64147	0.42672
0.25	2.60932	1.28768	0.63967	0.42553
0.50	2.49715	1.23232	0.61218	0.40724
0.75	1.93097	0.95292	0.47338	0.31490
1.00	0.00000	0.00000	0.00000	0.00000

TABLE 5.4: Variation in Eg for various values of Λ and Br while setting the other particulars constant ($z = 1.0, \varepsilon = 0.1, Q = 0.5, Ha = 4.0, \gamma = 0.1, Rn = 0.4, \phi = 0.01, J_h = 0.01$).

Λ	Br	$r = \pm1.0$	$r = \pm0.75$	$r = \pm0.5$	$r = \pm0.25$
0.0	1.0	0.00000	1.75142	2.36536	2.47188
1.0		111.927	68.2709	100.303	120.618
2.0		223.855	134.790	198.242	238.765
3.0		335.782	201.310	296.180	356.912
0.5	0.5	9.32729	5.59728	8.23972	9.93161
	1.0	18.6545	11.2896	16.6053	19.9926
	1.5	27.9818	17.0771	25.0976	30.1845
	2.0	37.3091	22.9599	33.7165	40.5072

Chapter 6

Entropy Analysis of SWCNT & MWCNT Flow Induced by Collecting Beating of Cilia with Porous Medium

6.1 Introduction

This chapter considers the thermodynamics analysis of creeping viscous nanofluid flow in a horizontal ciliated tube containing uniform magnetic field and porous medium. Moreover, energy analysis is performed in the presence of internal heat source and thermal radiation phenomena. The thermal conductivity of base fluid water is strengthened by considering the carbon nanotubes (CNTs). Mathematical formulations is established which result into a set of coupled partial differential equations. The governing differential system is transformed into ordinary differential system by considering the suitable similarity variables. Exact solution in the closed form is computed for the temperature, momentum and pressure gradient profiles. In this study, special attention is devoted to the term electrical conductivity of the considered CNTs. Streamlines patterns are also discussed to witnessed

the flow lines for different parameters. Thermodynamics analysis shows that entropy of the current flow system is increasing function of Brinkmann number, magnetic parameter, nanoparticle concentration parameter and Darcy number.

6.2 Problem Statement

This chapter investigates the axisymmetric flow of viscous nanofluid in a ciliated flexible horizontal tube. When the group of cilia operate together metachronal waves are produced, which move in the direction of effective stroke. These wave have wavy and beating motion. Flow is developed as a consequences of these wavy or beating motion of metachronal waves and due to no slip condition fluid is moving with the wave speed c. Further, the effects of uniform magnetic field, porous medium, internal heat source coefficient and thermal radiation are also considered. The cylindrical coordinate system $(\bar{R}, \bar{Z})$ has been introduced to present the geometry of the problem. Figure 6.1 depicts the systematic view of the under study peristaltic fluid model.
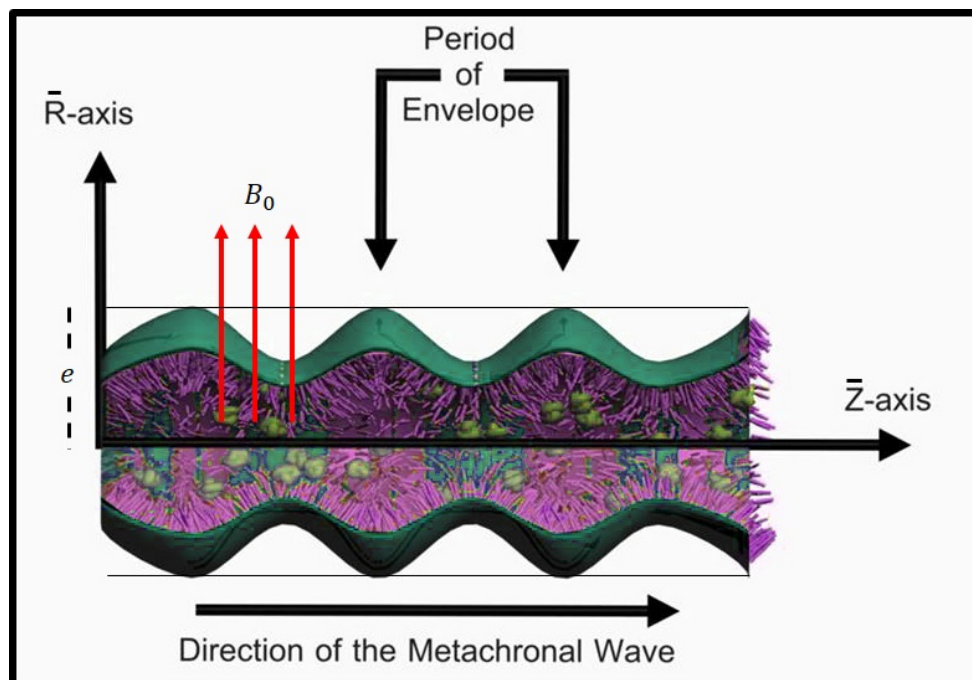
FIGURE 6.1: Geometrical view of the physical model

The shape of the cilia tips is supposed to obey the following pattern [105]-[106]:

$$\left.\begin{aligned}
\bar{R} = \bar{h} = \bar{f}(\bar{Z}, \bar{t}) &= e + e\epsilon \cos\left[\frac{2\pi}{\lambda}(\bar{Z} - c\bar{t})\right], \\
\bar{Z} = \bar{g}(\bar{Z}, \bar{Z}_0, \bar{t}) &= e + e\epsilon\alpha \sin\left[\frac{2\pi}{\lambda}(\bar{Z} - c\bar{t})\right],
\end{aligned}\right\} \tag{6.1}$$

where e denotes the mean radius of the tube, ϵ the wave amplitude, Z_0 the reference position of cilia, c the wave speed, λ the wavelength, and α the measure of the eccentricity. No slip condition indicates that the cilia tips and fluid closed to it, have equal velocity, thus radial and axial velocities are given as:

$$\left.\begin{aligned}
\bar{U} = \left(\frac{\partial\bar{R}}{\partial\bar{t}}\right)_{\bar{Z}_0} = \left(\frac{\partial\bar{f}}{\partial\bar{t}}\right) + \left(\frac{\partial\bar{f}}{\partial\bar{Z}}\right)\left(\frac{\partial\bar{Z}}{\partial\bar{t}}\right) = \left(\frac{\partial\bar{f}}{\partial\bar{t}}\right) + \left(\frac{\partial\bar{f}}{\partial\bar{Z}}\right)\bar{W}, \\
\bar{W} = \left(\frac{\partial\bar{Z}}{\partial\bar{t}}\right)_{\bar{Z}_0} = \left(\frac{\partial\bar{g}}{\partial\bar{t}}\right) + \left(\frac{\partial\bar{g}}{\partial\bar{Z}}\right)\left(\frac{\partial\bar{Z}}{\partial\bar{t}}\right) = \left(\frac{\partial\bar{g}}{\partial\bar{t}}\right) + \left(\frac{\partial\bar{g}}{\partial\bar{Z}}\right)\bar{W}.
\end{aligned}\right\} \tag{6.2}$$

Combining (6.1) and (6.2), the radial and axial velocities of the cilia are given as:

$$\left.\begin{aligned}
\bar{U} &= \frac{\left(\frac{2\pi}{\lambda}\right)\left[\epsilon\alpha c e \sin\left(\frac{2\pi}{\lambda}(\bar{Z} - c\bar{t})\right)\right]}{1 - \frac{2\pi}{\lambda}\left[\epsilon\alpha e \cos\left(\frac{2\pi}{\lambda}(\bar{Z} - c\bar{t})\right)\right]}, \\
\bar{W} &= \frac{\left(\frac{-2\pi}{\lambda}\right)\left[\epsilon\alpha c e \cos\left(\frac{2\pi}{\lambda}(\bar{Z} - c\bar{t})\right)\right]}{1 - \frac{2\pi}{\lambda}\left[\epsilon\alpha e \cos\left(\frac{2\pi}{\lambda}(\bar{Z} - c\bar{t})\right)\right]}.
\end{aligned}\right\} \tag{6.3}$$

The governing bounadry layer equations for the laminar, viscous nanofluid flow in a fixed frame are given as [107]:

$$\frac{\partial\bar{U}}{\partial\bar{R}} + \frac{\bar{U}}{\bar{R}} + \frac{\partial\bar{W}}{\partial\bar{Z}} = 0. \tag{6.4}$$

$$\rho_{nf}\left[\frac{\partial\bar{U}}{\partial\bar{t}} + \bar{U}\frac{\partial\bar{U}}{\partial\bar{R}} + \bar{W}\frac{\partial\bar{U}}{\partial\bar{Z}}\right] = -\frac{\partial\bar{P}}{\partial\bar{R}} + \mu_{nf}\left[2\frac{\partial^2\bar{U}}{\partial\bar{R}^2} + \frac{2}{\bar{R}}\left(\frac{\partial\bar{U}}{\partial\bar{R}} - \frac{\bar{U}}{\bar{R}}\right)\right]$$
$$+ \mu_{nf}\left[\frac{\partial}{\partial\bar{Z}}\left(\frac{\partial\bar{U}}{\partial\bar{R}}\right) + \frac{\partial^2\bar{W}}{\partial\bar{Z}^2}\right]$$
$$- \sigma_{nf}B_0^2\left(\bar{U} + c\right). \tag{6.5}$$

$$\rho_{nf}\left[\frac{\partial \bar{W}}{\partial \bar{t}} + \bar{U}\frac{\partial \bar{W}}{\partial \bar{R}} + \bar{W}\frac{\partial \bar{W}}{\partial \bar{Z}}\right] = -\frac{\partial \bar{P}}{\partial \bar{Z}} + 2\mu_{nf}\left[\frac{\partial^2 \bar{W}}{\partial \bar{Z}^2} + \frac{1}{\bar{R}}\left(\frac{\partial \bar{U}}{\partial \bar{Z}} + \frac{\partial \bar{W}}{\partial \bar{R}}\right)\right]$$
$$+ \mu_{nf}\left[\frac{\partial}{\partial \bar{R}}\left(\frac{\partial \bar{U}}{\partial \bar{Z}} + \frac{\partial \bar{W}}{\partial \bar{R}}\right)\right]$$
$$- \left(\sigma_{nf}B_0^2 + \frac{\mu_{nf}}{K}\right)(\bar{W} + c)$$
$$+ \rho_{nf}g\alpha^*(\bar{T} - \bar{T}_0). \tag{6.6}$$

$$(\rho c_p)_{nf}\left[\frac{\partial \bar{T}}{\partial \bar{t}} + \bar{U}\frac{\partial \bar{T}}{\partial \bar{R}} + \bar{W}\frac{\partial \bar{T}}{\partial \bar{Z}}\right] = k_{nf}\left[\frac{1}{\bar{R}}\frac{\partial}{\partial \bar{R}}\left(\bar{R}\frac{\partial \bar{T}}{\partial \bar{R}}\right) + \frac{\partial^2 \bar{T}}{\partial \bar{Z}^2}\right] + Q_0$$
$$+ \frac{16\sigma^*T_\infty^3}{3k^*}\left[\frac{1}{\bar{R}}\frac{\partial}{\partial \bar{R}}\left(\bar{R}\frac{\partial \bar{T}}{\partial \bar{R}}\right)\right]. \tag{6.7}$$

The transformation between the frames are:

$$\bar{Z} = \bar{z} + c\bar{t}, \quad \bar{R} = \bar{r}, \quad \bar{P}(\bar{Z}, \bar{R}, \bar{t}) = \bar{p}(\bar{z}, \bar{r}, \bar{t}), \tag{6.8}$$

and the velocities inside the two frames are:

$$\bar{U} = \bar{u}, \quad \bar{W} = \bar{w} + c, \tag{6.9}$$

the derived fundamental system of equations after invoking the above variables are of the form:

$$\frac{\partial \bar{u}}{\partial \bar{r}} + \frac{\bar{u}}{\bar{r}} + \frac{\partial \bar{w}}{\partial \bar{z}} = 0, \tag{6.10}$$

$$\rho_{nf}\left[\bar{u}\frac{\partial \bar{u}}{\partial \bar{r}} + (\bar{w} + c)\frac{\partial \bar{u}}{\partial \bar{z}}\right] = \mu_{nf}\left[2\frac{\partial^2 \bar{u}}{\partial \bar{r}^2} + \frac{2}{\bar{r}}\left(\frac{\partial \bar{u}}{\partial \bar{r}} - \frac{\bar{u}}{\bar{r}}\right) + \frac{\partial}{\partial \bar{z}}\left(\frac{\partial \bar{u}}{\partial \bar{r}}\right) + \frac{\partial^2 \bar{w}}{\partial \bar{z}^2}\right]$$
$$- \frac{\partial \bar{p}}{\partial \bar{r}} - \sigma_{nf}B_0^2(\bar{u} + c), \tag{6.11}$$

$$\rho_{nf}\left[\bar{u}\frac{\partial \bar{w}}{\partial \bar{r}} + (\bar{w} + c)\frac{\partial \bar{w}}{\partial \bar{z}}\right] = 2\mu_{nf}\left[\frac{\partial^2 \bar{w}}{\partial \bar{z}^2} + \frac{1}{\bar{r}}\left(\frac{\partial \bar{u}}{\partial \bar{z}} + \frac{\partial \bar{w}}{\partial \bar{r}}\right) + \frac{\partial}{\partial \bar{r}}\left(\frac{\partial \bar{u}}{\partial \bar{z}} + \frac{\partial \bar{w}}{\partial \bar{r}}\right)\right]$$
$$- \frac{\partial \bar{p}}{\partial \bar{z}} - \left(\sigma_{nf}B_0^2 + \frac{\mu_{nf}}{K}\right)(\bar{w} + c)$$
$$+ \rho_{nf}g\alpha^*(\bar{T} - \bar{T}_0), \tag{6.12}$$

$$(\rho c_p)_{nf} \left[\bar{u} \frac{\partial \bar{T}}{\partial \bar{r}} + (\bar{w} + c) \frac{\partial \bar{T}}{\partial \bar{z}} \right] = k_{nf} \left[\frac{1}{\bar{r}} \frac{\partial}{\partial \bar{r}} \left(\bar{r} \frac{\partial \overline{T}}{\partial \bar{r}} \right) + \frac{\partial^2 \overline{T}}{\partial \bar{z}^2} \right] + Q_0$$

$$+ \frac{16\sigma^* T_\infty^3}{3k^*} \left[\frac{1}{\bar{r}} \frac{\partial}{\partial \bar{r}} \left(\bar{r} \frac{\partial \overline{T}}{\partial \bar{r}} \right) \right]. \qquad (6.13)$$

The boundary conditions are:

$$\left. \begin{array}{l} w'(r) = 0, \quad \theta'(r) = 0, \qquad\qquad\qquad \text{at } r = 0, \\[2mm] w = \dfrac{-2\pi\epsilon\alpha\beta\cos(2\pi z)}{1 - 2\pi\epsilon\alpha\beta\cos(2\pi z)} - 1, \quad \theta = 0 \quad \text{at } r = h(z) = 1 + \epsilon\cos(2\pi z). \end{array} \right\} \quad (6.14)$$

Here $\bar{u}$ and $\bar{w}$ are the velocity elements in the radial $\bar{r}$ and axial $\bar{z}$ directions, B_0 the total magnetic field, σ_{nf} the electric conductivity of nanofluid, K the permeability parameter, ρ_{nf} the effective density, k_{bf} the thermal conductivity of the fluid fraction, k_{CNT} the thermal conductivity of the solid nanoparticle, and k_{nf} the effective thermal conductivity, given as [119]:

$$\left. \begin{array}{l} \mu_{nf} = \dfrac{\mu_{bf}}{(1 - \phi)^{2.5}}, \\[4mm] \rho_{nf} = (1 - \phi)\rho_f + \phi\rho_{CNT}, \\[3mm] (\rho c_p)_{nf} = (1 - \phi)(\rho c_p)_{bf} + \phi(\rho c_p)_{CNT}, \\[4mm] \sigma_{nf} = \sigma_{bf} \left(1 + \dfrac{3 \left(\dfrac{\sigma_{CNT}}{\sigma_{bf}} - 1 \right) \phi}{\left(\dfrac{\sigma_{CNT}}{\sigma_{bf}} + 2 \right) - \left(\dfrac{\sigma_{CNT}}{\sigma_{bf}} - 1 \right) \phi} \right), \\[10mm] k_{nf} = k_{bf} \left(\dfrac{(1 - \phi) + \dfrac{2\phi k_{CNT}}{k_{CNT} - k_{bf}} log \left(\dfrac{k_{CNT} + k_{bf}}{2k_{bf}} \right)}{(1 - \phi) + \dfrac{2\phi k_{bf}}{k_{CNT} - k_{bf}} log \left(\dfrac{k_{CNT} + k_{bf}}{2k_{bf}} \right)} \right). \end{array} \right\} \quad (6.15)$$

Thermophysical properties of the base fluids and nanoparticles are given in Table 6.1. The following transformations are found fruitful to convert the model into the dimensionless form:

$$\left. \begin{array}{l} r = \dfrac{\bar{r}}{e}, \quad z = \dfrac{\bar{z}}{\lambda}, \quad w = \dfrac{\bar{w}}{c}, \quad u = \dfrac{\lambda\bar{u}}{ec}, \\[4mm] p = \dfrac{e^2\bar{p}}{c\lambda\mu_{bf}}, \quad t = \dfrac{c\bar{t}}{\lambda}, \quad \theta = \dfrac{(\bar{T} - \bar{T}_0)}{T_0}, \end{array} \right\} \quad (6.16)$$

substituting (6.16) into Eqs. (6.10)-(6.13), the mathematical model gets the following form:

$$\Psi_{6.2}\, Re\, \beta^3 \left[u\frac{\partial u}{\partial r} + (w+1)\frac{\partial u}{\partial z} \right] = -\frac{\partial p}{\partial r} + \beta^2 \left[\frac{2}{(1-\phi)^{2.5}} \right] \left[\frac{\partial^2 u}{\partial r^2} + \frac{1}{r}\frac{\partial u}{\partial r} - \frac{u}{r^2} \right]$$
$$+ \left[\frac{\beta^3}{(1-\phi)^{2.5}} \right] \left[\frac{\partial^2 u}{\partial r \partial z} + \frac{\partial^2 w}{\partial z^2} \right]$$
$$- \Psi_{6.1}\, \beta \left(\frac{\sigma_{bf}}{\mu_{bf}} \right) B_0^2 e^2 (\beta\, u + 1), \qquad (6.17)$$

$$\Psi_{6.2}\, Re\, \beta \left[u\frac{\partial w}{\partial r} + (w+1)\frac{\partial w}{\partial z} \right] = \beta^2 \left[\frac{1}{(1-\phi)^{2.5}} \right] \frac{\partial^2 w}{\partial z^2} - \Psi_{6.1}\frac{\sigma_{bf} B_0^2 e^2}{\mu_{bf}}(w+1)$$
$$- \frac{\mu_{nf}}{\mu_{bf}}\frac{e^2}{K} + \frac{\rho_{bf}}{\mu_{bf}}\frac{ge^2}{c}\Psi_{6.2}\,\alpha^*\, T_0\,\theta - \frac{\partial p}{\partial z}$$
$$+ \left[\frac{1}{r}\left(\beta^2\frac{\partial u}{\partial z} + \frac{\partial w}{\partial r} \right) + \beta^2\frac{\partial^2 u}{\partial r\partial z} + \frac{\partial^2 w}{\partial r^2} \right]$$
$$\times \frac{1}{(1-\phi)^{2.5}}, \qquad (6.18)$$

$$(\rho c_p)_{nf}\, e\, c\, \beta \left[u\frac{\partial\theta}{\partial r} + (w+1)\frac{\partial\theta}{\partial z} \right] = k_{nf}\left[\frac{\partial^2\theta}{\partial r^2} + \frac{1}{r}\frac{\partial\theta}{\partial r} + \beta^2\frac{\partial^2\theta}{\partial z^2} \right] + \frac{Q_0 e^2}{T_0}$$
$$+ \frac{16\sigma^* T_\infty^3}{3k^*}\left[\frac{\partial^2\theta}{\partial r^2} + \frac{1}{r}\frac{\partial\theta}{\partial r} \right], \qquad (6.19)$$

where

$$\left.\begin{aligned}
&\beta = \frac{e}{\lambda},\ Da = \frac{K}{e^2},\ Ha^2 = \frac{\sigma_{bf} B_0^2 e^2}{\mu_{bf}},\ Re = \frac{ce\rho_{bf}}{\mu_{bf}},\ h = \frac{\bar{h}}{e},\\
&Gr = \frac{\rho_{bf} g\alpha^* e^2 T_0}{c\mu_{bf}},\ \Omega = \frac{Q_0 e^2}{k_{bf}T_0},\ Rn = \frac{4\sigma^*}{k^* k_{bf}}T_\infty^3.
\end{aligned}\right\} \qquad (6.20)$$

To achieve the general solution of the Eqs. (6.17)-(6.19). we shall restrict this study under the following assumptions:

- **Long wavelength**: the length of the wave is assumed to be infinite $(\lambda \to \infty)$ as compared to the tube width.

- **Low Renyolds number**: inertial free flow $(Re \ll 1)$ is considered i.e. inertial forces are minute as compared to viscous forces.

$$\frac{dp}{dr} = 0, \qquad (6.21)$$

$$\frac{dp}{dz} - \left(\frac{1}{r}\frac{dw}{dr} + \frac{d^2w}{dr^2}\right)\frac{1}{(1-\phi)^{2.5}} + \left(\Psi_{6.1}Ha^2 + \frac{Da^{-1}}{(1-\phi)^{2.5}}\right)(w+1)$$

$$-\ \Psi_{6.2}\,Gr\,\theta = 0, \tag{6.22}$$

$$\frac{d^2\theta}{dr^2}\left(\Psi_{6.3} + \frac{4}{3}Rn\right) + \frac{1}{r}\frac{d\theta}{dr}\left(\Psi_{6.3} + \frac{4}{3}Rn\right) + \Omega = 0, \tag{6.23}$$

where

$$\left.\begin{aligned}
\Psi_{6.1} &= 1 + \frac{3\left(\frac{\sigma_{CNT}}{\sigma_{bf}} - 1\right)\phi}{\left(\frac{\sigma_{CNT}}{\sigma_{bf}} + 2\right) - \left(\frac{\sigma_{CNT}}{\sigma_{bf}} - 1\right)\phi}, \\[2mm]
\Psi_{6.2} &= 1 - \phi + \phi\frac{\rho_{CNT}}{\rho_{bf}}, \\[2mm]
\Psi_{6.3} &= \left(\frac{(1-\phi) + \frac{2\phi k_{CNT}}{k_{CNT} - k_{bf}}log\left(\frac{k_{CNT} + k_{bf}}{2k_{bf}}\right)}{(1-\phi) + \frac{2\phi k_{bf}}{k_{CNT} - k_{bf}}log\left(\frac{k_{CNT} + k_{bf}}{2k_{bf}}\right)}\right).
\end{aligned}\right\} \tag{6.24}$$

Here Gr is the Grashof number, Da the Darcy number and Ω the internal heat source parameter. The boundary conditions are given as:

$$\left.\begin{aligned}
w'(r) &= 0, \quad \theta'(r) = 0, && \text{at } r = 0, \\
w &= \frac{-2\pi\epsilon\alpha\beta\cos(2\pi z)}{1 - 2\pi\epsilon\alpha\beta\cos(2\pi z)} - 1, \quad \theta = 0 && \text{at } r = h(z) = 1 + \epsilon\cos(2\pi z).
\end{aligned}\right\} \tag{6.25}$$

TABLE 6.1: Thermophysical properties of CNTs and water ([120]

Physical properties	$\rho(kg/m^3)$	$c_p(J/kgK)$	$k(W/mK)$	$\sigma\,(S/m)$
SWCNT	2600	425	6600	1400
MWCNT	1600	796	3000	300
water	997.1	4179	0.613	0.05

6.2.1 Second Law Analysis

Non-equilibrium situation emerges as a result of exchange of momentum, temperature and magnetic effects within the fluid and at the walls which causes a continuous entropy generation. The volumetric

entropy generation term S_G can be calculated as follows:

$$S_G = \frac{1}{\bar{\theta}_0^2} \left(\overbrace{k_{nf} \left(\frac{\partial \bar{T}}{\partial \bar{r}} \right)^2}^{E_H} + \overbrace{\frac{16\sigma^* T_\infty^3}{3k^*} \left(\frac{\partial \bar{T}}{\partial \bar{r}} \right)^2}^{E_{Rn}} \right) + \overbrace{\frac{\sigma_{nf} B_0^2}{\bar{\theta}_0} \left(\bar{w} + c \right)^2}^{E_M}. \qquad (6.26)$$

Eq. (6.26) reflects the contribution of three distinct factors causing the entropy generation. These factors are heat transfer E_H, thermal radiation E_{Rn} and the magnetic field E_M. Entropy basically gives the degree of disorder of the system and its surroundings and the rate of dimensionless entropy formation $Eg = \dfrac{S_G}{S_g}$ is:

$$Eg = \left(\Psi_{6.3} + \frac{4Rn}{3} \right) \left(\frac{\partial \theta}{\partial r} \right)^2 + \Psi_{6.1} \Lambda \, Br \, Ha^2 \, (w + 1)^2 , \qquad (6.27)$$

where

$$\left. \begin{aligned} S_g &= \frac{k_{bf} \bar{T}_0^2}{\bar{\theta}_0^2 e^2}, \\ Br &= \frac{c^2 \mu_{bf}}{k_{bf} \bar{T}_0}, \\ \Lambda &= \frac{\bar{\theta}_0}{\bar{\bar{T}}_0}, \end{aligned} \right\} \qquad (6.28)$$

here Λ is the dimensionless temperature difference, Br the Brinkmann number. To figure out the irreversibility distribution, Bejan number Be, was introduced by Bejan, and is given as:

$$Be = \frac{E_H}{E_H + E_{Rn} + E_M}. \qquad (6.29)$$

6.3   Exact Solutions

In this segment, the exact solutions to the coupled ordinary differential Eqs. (6.20) and (6.21) together with the wall condition (6.23) are computed. The governing boundary layer equations includes continuity, momentum and energy equation. The exact analytical solution to the ordinary differential system is acquired by

using a computational software MATHEMATICA.

Temperature distribution:

$$\theta(r,z) = \left(\frac{3(h-r)(h+r)\Omega}{16Rn + 12\left(\dfrac{(1-\phi) + \dfrac{2\phi k_{CNT}}{k_{CNT}-k_f}log\left(\dfrac{k_{CNT}+k_f}{2k_f}\right)}{(1-\phi) + \dfrac{2\phi k_f}{k_{CNT}-k_f}log\left(\dfrac{k_{CNT}+k_f}{2k_f}\right)}\right)} \right). \qquad (6.30)$$

velocity distribution:

$$w(r,z) = \left(\frac{-1 - \Psi_{6.4}Da(1-\phi)^{2.5} + \dfrac{\left(1 + \Psi_{6.4}Da\Psi_{6.6} + \Psi_{6.5}Da\right)I_0[\sqrt{\Psi_{6.4}}]r}{I_0[\sqrt{\Psi_{6.4}}]h}}{\Psi_{6.4}Da} \right), \qquad (6.31)$$

the flow rate is described as

$$Q = 2 \int_0^{h(z)} rw(r)dr, \qquad (6.32)$$

now substituting Eq. (6.20) into Eq. (6.21) and then we have solution of dp/dz

$$\frac{dp}{dz} = \left(\frac{\left(-8(F+h^2)\Psi_{6.10}\Psi_{6.7}\Psi_{6.2}\Omega\right)\Psi_{6.8} + 8h^2\left(3Da^2GrT\Psi_{6.2}\Omega\right)\Psi_{6.9}}{h^4(1-\phi)^{2.5}\left((1+DaHa(1-\phi)^{2.5}\Psi_{6.1})^2\right)(4Rn + 3\Psi_{6.3})\Psi_{6.9}} \right). \qquad (6.33)$$

The mean flow rate can be calculated as:

$$F = Q - \left[0.5 + \frac{\epsilon^2}{4}\right], \qquad (6.34)$$

where the expression for $(\Psi_i, i = 6.4 - 6.10)$ are given as:

$$
\left.
\begin{aligned}
\Psi_{6.4} &= Ha(1-\phi)^{2.5}\Psi_{6.1} + \frac{1}{Da}, \\
\Psi_{6.5} &= \frac{dp}{dz} + Ha\Psi_{6.1} - \Psi_{6.2}Gr\left(\frac{3(h-r)(h+r)\Omega}{16Rn + 12\Psi_{6.3}}\right), \\
\Psi_{6.6} &= \frac{-2\pi\epsilon\beta\cos(2\pi z)}{1 - 2\pi\epsilon\beta\cos(2\pi z)} - 1, \\
\Psi_{6.7} &= (4Rn + 3\Psi_{6.3}) + 3DaGrh^2(1-\phi)^{2.5}(h^2 + Da(-8 + Ha\Psi_{6.1})), \\
\Psi_{6.8} &= I_0\left[h\sqrt{\frac{1}{Da}Ha(1-\phi)^{2.5}\Psi_{6.1}}\right] + 8h^2\left((1 + DaHa(1-\phi)^{2.5}\Psi_{6.1})^2\right), \\
\Psi_{6.9} &= {}_0F_1\left[\frac{h^2}{4}\left(\frac{1}{Da}Ha(1-\phi)^{2.5}\Psi_{6.1}\right)\right], \\
\Psi_{6.10} &= \left(1 + DaHa(1-\phi)^{2.5}\Psi_{6.1}\right)^2.
\end{aligned}
\right\}
$$

$$(6.35)$$

6.4   Result and Discussion

This segment highlights the dynamics of various pertinent flow parameters on streamlines, velocity field, temperature field, pressure gradient, and entropy number.

Consequence of Darcy number Da on momentum profile is depicted in Figure 6.2, and it is observed that the fluid velocity increases with an increase in Da. Physically, an increases in Da enhances the permeability of the medium, which corresponds to greater permeability and thus increases the velocity. Variation of magnetic parameter Ha on $w(r, z)$ is graphed in Figure 6.3. It is judged that an enhancement in Ha reduces the fluid velocity for both SWCNT and MWCNT. Physically, an increase in Ha accelerates the strength of the Lorentz force, which is a resistive force, therefore more resistance is offered to the fluid motion which consequently reduces the fluid velocity.

The variation of Ω and Rn on $\theta(r, z)$ is depicted in Figure 6.4 and 6.5. It is noted that when Ω is kept zero the over all heat transfer rate is zero, which is obvious see Eq. (6.27), while increasing behavior of fluid energy is found for $\Omega > 0$ for

both SWCNT and MWCNT see Figure 6.4. Figure 6.5 displays the effect of Rn on energy profile. It is seen that the fluid temperature decreases rapidly as there is an increase in the radiation parameter. Physically, an increase in the radiative parameter Rn increases the mean absorption coefficient k^* which reduces the fluid temperature significantly.

Figures 6.6 and 6.7 show the influence of Darcy parameter Da and flow rate Q on the pressure gradient profiles. The pressure gradient is a physical quantity that characterize in which direction and at what rate the pressure raises the most rapidly. It is witnessed that a uniform oscillating behavior is found for increasing values of Da and Q (for both SWCNT and MWCNT). Figure 6.6 shows that with higher values of Darcy number, the permeability of the medium also enhances, which correspondingly enhances the pressure gradient profile. Figure 6.7 shows that the pressure profile is decreasing function of flow rate.

Figure 6.8 shows that the entropy of the fluid system increases with an increase in the magnitude of the Brinkmann number Br. As Br enhances, energy transfer influences the viscosity of fluid within the tube, therefore increases the total entropy. Figure 6.9 shows that the fluid entropy increases for the greater values of the magnetic number Ha. Moreover, maximum entropy is seen at the central portion of the tube, because in this portion the velocity is at its extreme and thus contribution to MHD flow is also at its extreme. The impact of nanoparticles concentration ϕ on Eg is plotted in Figure 6.10. It is seen that the maximum entropy is noted at the boundaries and at the center of tube, which is due to the fact that the concentration of CNTs is minimum at these regions. The impact of Darcy number Da on Eg is plotted in Figure 6.11. It is seen that the total entropy of the system increases for variation in Darcy number.

A very interesting part of peristaltic motion, called trapping, is presented with respect to change in the various parameters. An internal circulating bolus is formed during the peristaltic transport which is forced to move in the direction of waves. The trapping phenomenon for variation in α and Gr is shown in Figures 6.12-6.15. It is seen that with an increase in α and Gr the number of bolus increases and size of bolus reduces while considering SWCNT and MWCNT, respectively.
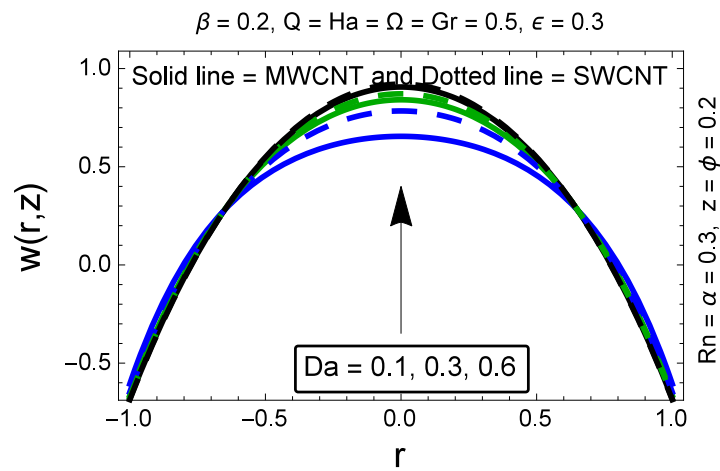
FIGURE 6.2: The impact of Da on $w(r,z)$
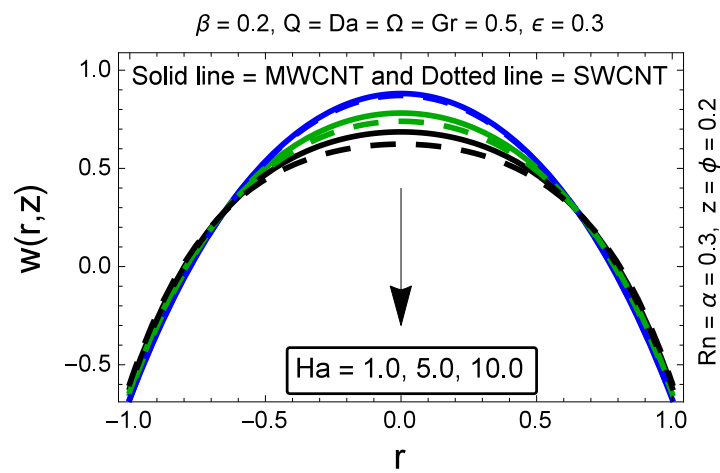
FIGURE 6.3: The impact of Ha on $w(r,z)$
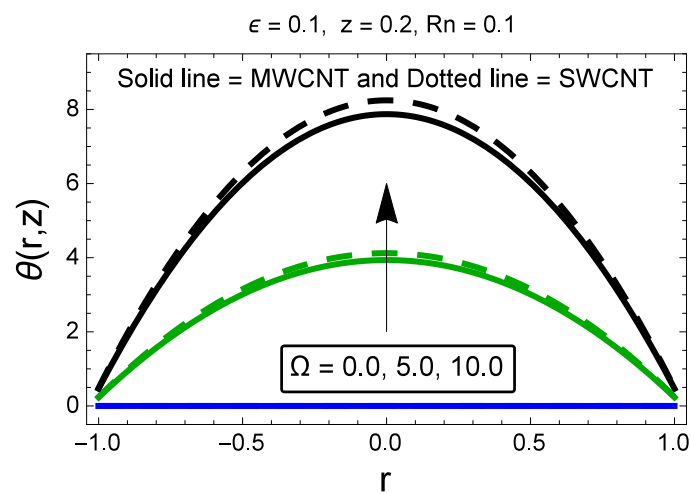
FIGURE 6.4: The impact of Ω on $\theta(r,z)$
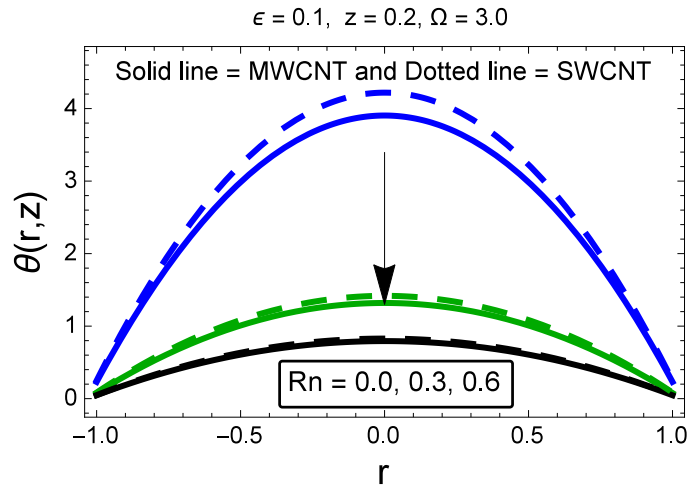
FIGURE 6.5: The impact of Rn on $\theta(r,z)$
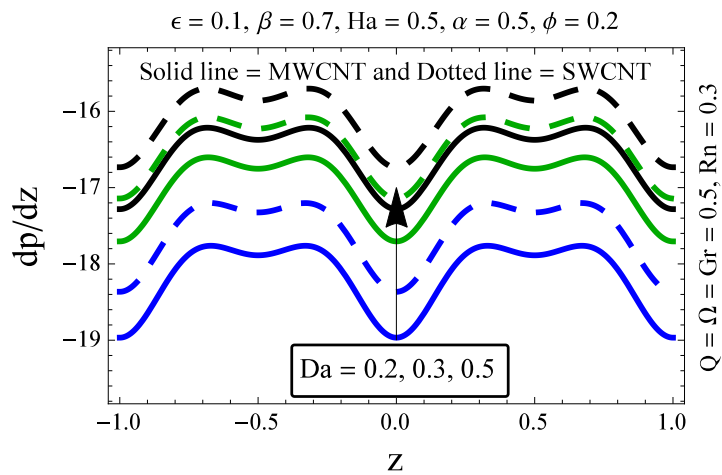
FIGURE 6.6: The impact of Da on dp/dz
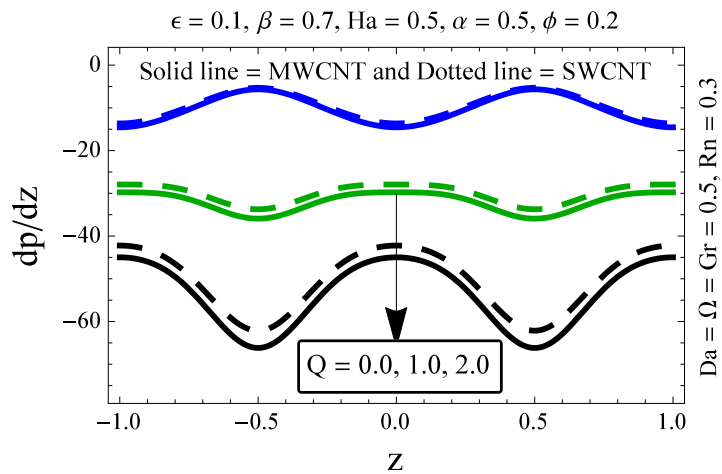
FIGURE 6.7: The impact of Q on dp/dz
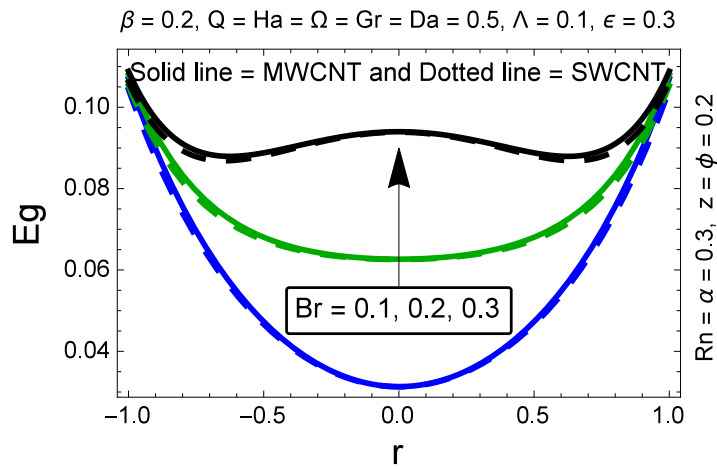
FIGURE 6.8: The impact of Br on Eg
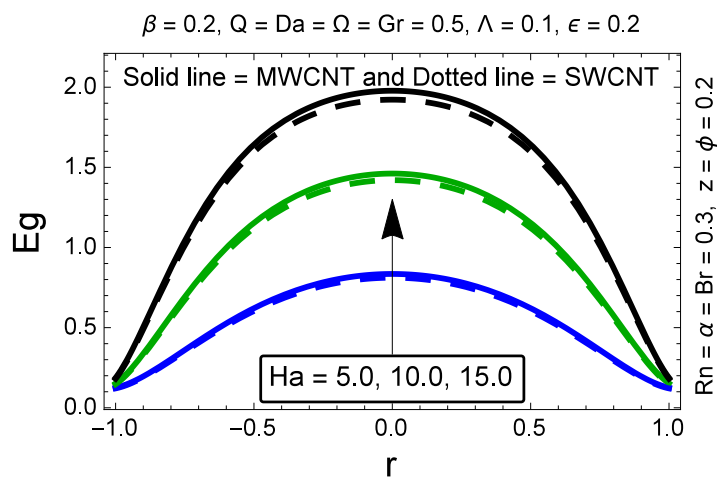
FIGURE 6.9: The impact of Ha on Eg
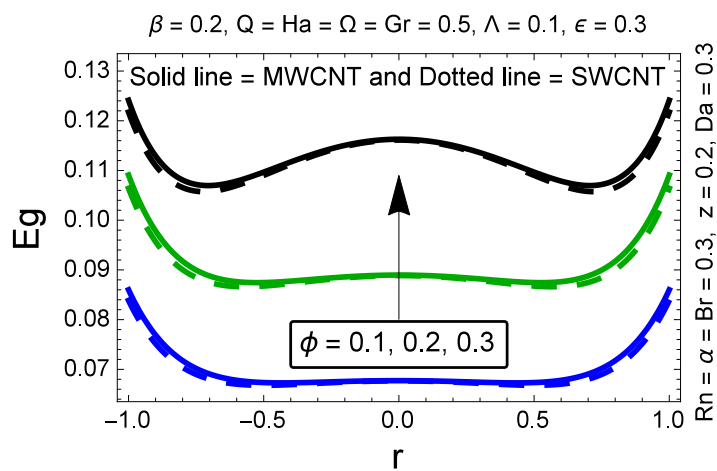
FIGURE 6.10: The impact of ϕ on Eg
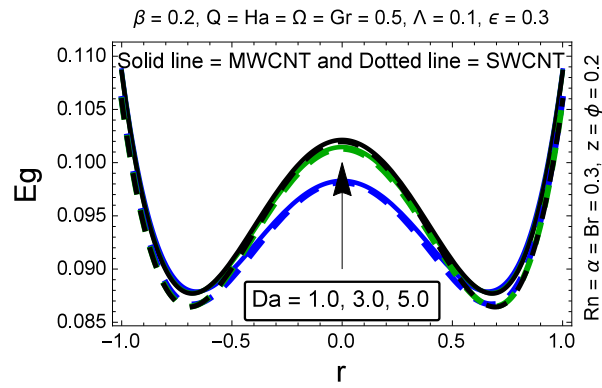
FIGURE 6.11: The impact of Da on Eg
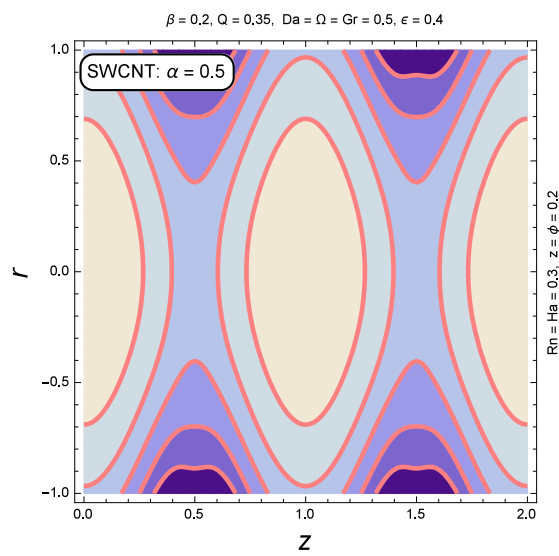
FIGURE 6.12: Streamlines for $\alpha = 0.5$
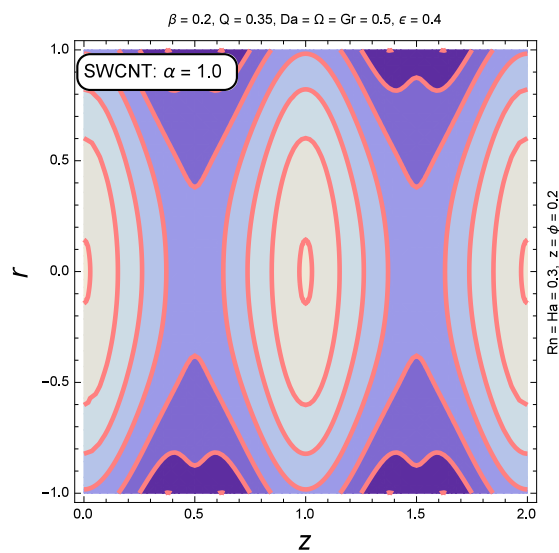
FIGURE 6.13: Streamlines for $\alpha = 1.0$
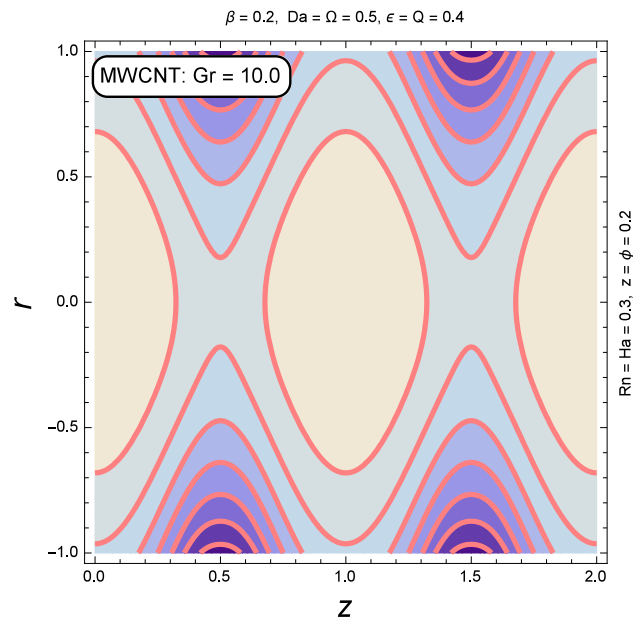
FIGURE 6.14: Streamlines for $Gr = 10.0$
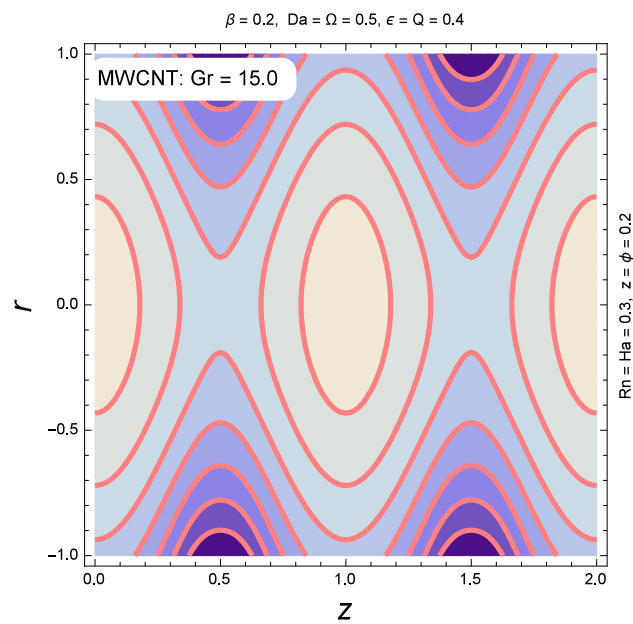
FIGURE 6.15: Streamlines for $Gr = 15.0$

Table 6.2 and 6.3 represents the numerical values of solid volume fraction of nanoparticle and Brinkmann number. It is seen that with an increase in solid volume fraction and Brinkmann number the irreversibility distribution parameter Bejan number decreases.

TABLE 6.2: Bejan profile for both SWCNT and MWCNT for variation in increasing values of solid volume fraction (ϕ) while setting $\beta = z = 0.2$, $Q = 0.5, \alpha = \epsilon = 0.3$, $Ha = Gr = \Omega = 0.5$, $Rn = Da = Br = 0.3$, $\Lambda = 0.1$.

r	$\phi = 0.1$		$\phi = 0.2$		$\phi = 0.3$	
	SWCNT	MWCNT	SWCNT	MWCNT	SWCNT	MWCNT
$\pm$ 1.00	0.97385	0.97307	0.97288	0.97216	0.96891	0.96826
$\pm$ 0.75	0.67197	0.66547	0.66352	0.65775	0.63120	0.62647
$\pm$ 0.50	0.31161	0.30545	0.30336	0.29811	0.27417	0.27033
$\pm$ 0.25	0.07779	0.07576	0.07503	0.07334	0.06572	0.06456
0.00	0.00000	0.00000	0.00000	0.00000	0.00000	0.00000

TABLE 6.3: Bejan profile for both SWCNT and MWCNT for variation in increasing values of Brinkmann number (Br) while setting $\beta = z = 0.2$, $Q = 0.5, \alpha = \epsilon = 0.3$, $Ha = Gr = \Omega = 0.5$, $Rn = Da = 0.3$, $\Lambda = 0.1$, $\phi = 0.2$.

r	$Br = 0.1$		$Br = 0.2$		$Br = 0.3$	
	SWCNT	MWCNT	SWCNT	MWCNT	SWCNT	MWCNT
$\pm$ 1.00	0.99154	0.99131	0.98323	0.98277	0.97505	0.97438
$\pm$ 0.75	0.85791	0.85474	0.75118	0.74633	0.66807	0.66233
$\pm$ 0.50	0.56111	0.55496	0.38996	0.38405	0.29881	0.29362
$\pm$ 0.25	0.18849	0.18479	0.10405	0.10180	0.07186	0.07025
0.00	0.00000	0.00000	0.00000	0.00000	0.00000	0.00000

Chapter 7

Conclusion and Future Work

7.1 Introduction

This thesis is managed to analyze the entropy generation during the peristaltic transport of creeping viscous nanofluid in an axisymmetric channel. The general solution of the governing equations are obtained under the assumptions of long wavelength and low Renyolds number. Below, we conclude the present study and indicate some possible future directions.

7.1.1 Conclusion

This thesis investigates the significance of creeping viscous nanofluid in an axisymmetric channel influenced by metachronical waves of cilia. The momentum analysis is performed along with the effects of uniform and inclined magnetic field, Hall current and gravitational field. Heat transport analysis is also computed while considering the impacts of thermal radiation, viscous dissipation, Joule heating and internal heat source phenomenons. Mathematical formulation have been operated and graphical results are also discussed. In some cases, present results are also compared with already published results. The fundamental points of the present investigation are:

- It is found that the flow field, the temperature field and the entropy generation are symmetric about the radial axis.

- It is acknowledged that extreme velocity happens at the middle of tube and falls off closed to the boundary.

- It is found that increasing magnitude of Hartmann number and Darcy number retards the fluid motion.

- It is seen that velocity field is the increasing function of flow rate parameter.

- It is observed that temperature profile is inversely proportional to the radiation parameter.

- A meaning full increment in the temperature profile is noticed with an increase in internal heat source parameter, Brinkmann number and Joule heating parameter.

- No temperature variation is seen, when the coefficient of internal heat source is kept zero.

- It is witnessed that pressure gradient exhibits uniform oscillating behavior against an increasing values of measure of the eccentricity, wave number and wave amplitude.

- We see that Hartmann number and angle of inclination both are increasing function of pressure gradient.

- Rapid decline is noticed in pressure rise against the higher magnitude of the wave and Harmtmann number.

- The engine oil is having the maximum thermal conductivity, where as the pure water have the least.

- By decreasing the magnitude of the Brinkmann number, Hartmann number, dimensionless temperature difference, solid volume fraction of nanopartlcles and Darcy parameters, we can achieve the main goal of the 2nd law of thermodynamics, i.e., the minimization of entropy generation.

- It is seen that entropy generation significantly reduces with variation in radiation parameter.

- It is seen that the total irreversibility distribution is high as compared with the heat transfer irreversibility.

- It is visualize that the number of trapped boluses decreases and the size bolus increases with an increment in the value of flow rate.

- Streamlines patterns for variation in Grashof number shows that number of bolus increases, while the size of bolus decrease for MWCNT.

7.1.2 Future Work In our daily life fluids are all around us, from a morning coffee to an evening bath. The industrial significance of peristalsis fluids flow are discussed in introduction and literature review section. In future, I have plan to explore the consequences of peristalsis fluids flow with non-Newtonian models. In short, I would like to proceed in the following possible directions:

- Entropy analysis of the peristalsis flow for Jeffery model in an inclined duct.

- Entropy analysis of the peristalsis flow of Williamson model in an inclined tube.

- Second law analysis of peristaltic flow of hyperbolic tangent fluid model in a duct.

- Entropy analysis of the peristaltic flow of Johnson- segalman model in an inclined tube.

Bibliography

[1] A. Bejan, "A study of entropy generation in fundamental convective heat transfer," *Journal of Heat Transfer*, vol. 101, no. 4, pp. 718–725, 1979.

[2] R. Robert, "A maximum-entropy principle for two-dimensional perfect fluid dynamics," *Journal of Statistical Physics*, vol. 65, no. 3-4, pp. 531–553, 1991.

[3] Z. Xu, S. Yang, and Z. Chen, "A modified entropy generation number for heat exchangers," *Journal of Thermal Science*, vol. 5, no. 4, pp. 257–263, 1996.

[4] A. Bejan, "Entropy generation minimization: The new thermodynamics of finite-size devices and finite-time processes," *Journal of Applied Physics*, vol. 79, no. 3, pp. 1191–1218, 1996.

[5] A. Nada, "Entropy generation due to laminar natural convection from a horizontal isothermal cylinder," *Heat and Mass Transfer*, vol. 29, pp. 573–592, 1998.

[6] M. Abu-Qudais and E. A. Nada, "Numerical prediction of entropy generation due to natural convection from a horizontal cylinder," *Energy*, vol. 24, no. 4, pp. 327–333, 1999.

[7] G. Naterer and J. Camberos, "Entropy and the second law fluid flow and heat transfer simulation," *Journal of Thermophysics and Heat Transfer*, vol. 17, no. 3, pp. 360–371, 2003.

[8] S. Mahmud and R. A. Fraser, "Flow, thermal, and entropy generation characteristics inside a porous channel with viscous dissipation," *International Journal of Thermal Sciences*, vol. 44, no. 1, pp. 21–32, 2005.

[9] E. Abu-Nada, "Numerical prediction of entropy generation in separated flows," *Entropy*, vol. 7, no. 4, pp. 234–252, 2005.

[10] P. Romatschke, "Relativistic viscous fluid dynamics and non-equilibrium entropy," *Classical and Quantum Gravity*, vol. 27, no. 2, p. 025006, 2009.

[11] Y. Aksoy, "Effects of couple stresses on the heat transfer and entropy generation rates for a flow between parallel plates with constant heat flux," *International Journal of Thermal Sciences*, vol. 107, pp. 1–12, 2016.

[12] D. Srinivasacharya and K. H. Bindu, "Entropy generation in a micropolar fluid flow through an inclined channel," *Alexandria Engineering Journal*, vol. 55, no. 2, pp. 973–982, 2016.

[13] A. Kamran, S. Hussain, M. Sagheer, and N. Akmal, "A numerical study of magnetohydrodynamics flow in Casson nanofluid combined with Joule heating and slip boundary conditions," *Results in Physics*, vol. 7, pp. 3037–3048, 2017.

[14] S. Hussain, S. E. Ahmed, and T. Akbar, "Entropy generation analysis in MHD mixed convection of hybrid nanofluid in an open cavity with a horizontal channel containing an adiabatic obstacle," *International Journal of Heat and Mass Transfer*, vol. 114, pp. 1054–1066, 2017.

[15] A. Anjum, N. Mir, M. Farooq, S. Ahmad, and N. Rafiq, "Optimization of entropy generation in thermally stratified polystyrene-water/kerosene nanofluid flow with convective boundary condition," *The European Physical Journal Plus*, vol. 134, no. 4, p. 176, 2019.

[16] S. Saleem and M. A. El-Aziz, "Entropy generation and convective heat transfer of radiated non-Newtonian power-law fluid past an exponentially moving

surface under slip effects," *The European Physical Journal Plus*, vol. 134, no. 4, p. 184, 2019.

[17] T. Latham, "Fluid motion in peristaltic pumps," Ph.D. dissertation, Thesis, MIT, Cambridge, MA, 1966.

[18] A. H. Shapiro, M. Y. Jaffrin, and S. L. Weinberg, "Peristaltic pumping with long wavelengths at low Reynolds number," *Journal of Fluid Mechanics*, vol. 37, no. 4, pp. 799–825, 1969.

[19] S. L. Weinberg, E. C. Eckstein, and A. H. Shapiro, "An experimental study of peristaltic pumping," *Journal of Fluid Mechanics*, vol. 49, no. 3, pp. 461–479, 1971.

[20] L. Srivastava and V. Srivastava, "Peristaltic transport of blood: Casson modelii," *Journal of Biomechanics*, vol. 17, no. 11, pp. 821–829, 1984.

[21] A. M. Siddiqui and W. Schwarz, "Peristaltic flow of a second-order fluid in tubes," *Journal of Non-Newtonian Fluid Mechanics*, vol. 53, pp. 257–284, 1994.

[22] V. Srivastava and M. Saxena, "A two-fluid model of non-Newtonian blood flow induced by peristaltic waves," *Rheologica Acta*, vol. 34, no. 4, pp. 406–414, 1995.

[23] D. Srinivasacharya, M. Mishra, and A. R. Rao, "Peristaltic pumping of a micropolar fluid in a tube," *Acta Mechanica*, vol. 161, no. 3-4, pp. 165–178, 2003.

[24] S. Srinivas and V. Pushparaj, "Non-linear peristaltic transport in an inclined asymmetric channel," *Communications in Nonlinear Science and Numerical Simulation*, vol. 13, no. 9, pp. 1782–1795, 2008.

[25] K. Vajravelu, S. Sreenadh, K. Rajanikanth, and C. Lee, "Peristaltic transport of a Williamson fluid in asymmetric channels with permeable walls," *Nonlinear Analysis: Real World Applications*, vol. 13, no. 6, pp. 2804–2822, 2012.

[26] D. Tripathi, "Study of transient peristaltic heat flow through a finite porous channel," *Mathematical and Computer Modelling*, vol. 57, no. 5-6, pp. 1270–1283, 2013.

[27] M. H. Kamel, I. M. Eldesoky, B. M. Maher, and R. M. Abumandour, "Slip effects on peristaltic transport of a particle-fluid suspension in a planar channel," *Applied Bionics and Biomechanics*, vol. 2015, 2015.

[28] T. Hayat, Quratulain, A. Alsaedi, M. Rafiq, and B. Ahmad, "Joule heating and thermal radiation effects on peristalsis in curved configuration," *Results in Physics*, vol. 6, pp. 1088–1095, 2016.

[29] K. S. Mekheimer, W. Hasona, R. Abo-Elkhair, and A. Zaher, "Peristaltic blood flow with gold nanoparticles as a third grade nanofluid in catheter: Application of Cancer Therapy," *Physics Letters A*, vol. 382, no. 2-3, pp. 85–93, 2018.

[30] R. Ellahi, A. Zeeshan, F. Hussain, and A. Asadollahi, "Peristaltic blood flow of couple stress fluid suspended with nanoparticles under the influence of chemical reaction and activation energy," *Symmetry*, vol. 11, no. 2, p. 276, 2019.

[31] K. K. Prasad and V. Ramanathan, "Heat transfer by free convection from a longitudinally vibrating vertical plate," *International Journal of Heat and Mass Transfer*, vol. 15, no. 6, pp. 1213–1223, 1972.

[32] B. Wang and X. Peng, "Experimental investigation on liquid forced-convection heat transfer through microchannels," *International Journal of Heat and Mass Transfer*, vol. 37, pp. 73–82, 1994.

[33] D. Rees and I. Pop, "Free convection induced by a horizontal wavy surface in a porous medium," *Fluid Dynamics Research*, vol. 14, no. 4, p. 151, 1994.

[34] S. U. Choi and J. A. Eastman, "Enhancing thermal conductivity of fluids with nanoparticles," Argonne National Lab., IL (United States), Tech. Rep., 1995.

[35] R. S. Shawgo, A. C. R. Grayson, Y. Li, and M. J. Cima, "Biomems for drug delivery," *Current Opinion in Solid State and Materials Science*, vol. 6, no. 4, pp. 329–334, 2002.

[36] D. L. Leslie-Pelecky and V. D. Labhasetwar, *Biomedical applications of nanotechnology.* John Wiley & Sons, 2007.

[37] K. Sefiane, J. Skilling, and J. Mac Gillivray, "Contact line motion and dynamic wetting of nanofluid solutions," *Advances in Colloid and Interface Science*, vol. 138, no. 2, pp. 101–120, 2008.

[38] S. S. Murshed, S.-H. Tan, and N.-T. Nguyen, "Temperature dependence of interfacial properties and viscosity of nanofluids for droplet-based microfluidics," *Journal of Physics D: Applied Physics*, vol. 41, no. 8, p. 085502, 2008.

[39] K. V. Wong and O. De Leon, "Applications of nanofluids: current and future," *Advances in Mechanical Engineering*, vol. 2, p. 519659, 2010.

[40] O. D. Makinde and A. Aziz, "Boundary layer flow of a nanofluid past a stretching sheet with a convective boundary condition," *International Journal of Thermal Sciences*, vol. 50, no. 7, pp. 1326–1332, 2011.

[41] A. Alsaedi, M. Awais, and T. Hayat, "Effects of heat generation/absorption on stagnation point flow of nanofluid over a surface with convective boundary conditions," *Communications in Nonlinear Science and Numerical Simulation*, vol. 17, no. 11, pp. 4210–4223, 2012.

[42] S. Nadeem and C. Lee, "Boundary layer flow of nanofluid over an exponentially stretching surface," *Nanoscale Research Letters*, vol. 7, no. 1, p. 94, 2012.

[43] M. Turkyilmazoglu and I. Pop, "Heat and mass transfer of unsteady natural convection flow of some nanofluids past a vertical infinite flat plate with radiation effect," *International Journal of Heat and Mass Transfer*, vol. 59, pp. 167–171, 2013.

[44] M. Sheikholeslami, M. G. Bandpy, R. Ellahi, and A. Zeeshan, "Simulation of MHD *CuO*-water nanofluid flow and convective heat transfer considering Lorentz forces," *Journal of Magnetism and Magnetic Materials*, vol. 369, pp. 69–80, 2014.

[45] M. Awais, T. Hayat, S. Iram, S. Siddiqa, and A. Alsaedi, "Thermophoresis and heat generation/absorption in flow of third grade nanofluid," *Current Nanoscience*, vol. 11, no. 3, pp. 394–401, 2015.

[46] M. Awais, T. Hayat, S. Irum, and A. Alsaedi, "Heat generation/absorption effects in a boundary layer stretched flow of Maxwell nanofluid: Analytic and numeric solutions," *PloS One*, vol. 10, no. 6, p. e0129814, 2015.

[47] M. Sheikholeslami, M. Rashidi, and D. Ganji, "Numerical investigation of magnetic nanofluid forced convective heat transfer in existence of variable magnetic field using two phase model," *Journal of Molecular Liquids*, vol. 212, pp. 117–126, 2015.

[48] M. Sheikholeslami and R. Ellahi, "Three dimensional mesoscopic simulation of magnetic field effect on natural convection of nanofluid," *International Journal of Heat and Mass Transfer*, vol. 89, pp. 799–808, 2015.

[49] S. Das and R. Jana, "Natural convective magneto-nanofluid flow and radiative heat transfer past a moving vertical plate," *Alexandria Engineering Journal*, vol. 54, no. 1, pp. 55–64, 2015.

[50] F. Abbasi, T. Hayat, and B. Ahmad, "Peristaltic transport of an aqueous solution of silver nanoparticles with convective heat transfer at the boundaries," *Canadian Journal of Physics*, vol. 93, no. 10, pp. 1190–1198, 2015.

[51] T. Hayat, S. Asad, and A. Alsaedi, "Flow of Casson fluid with nanoparticles," *Applied Mathematics and Mechanics*, vol. 37, no. 4, pp. 459–470, 2016.

[52] S. Iijima, "Helical microtubules of graphitic carbon," *Nature*, vol. 354, no. 6348, p. 56, 1991.

[53] H. Jeong, H. M. Gweon, B. J. Kwon, Y. Ahn, S. Lee, and J.-Y. Park, "Uncovering operational mechanisms of a single-walled carbon nanotube network device using local probe electrical characterizations," *Nanotechnology*, vol. 20, no. 34, p. 345202, 2009.

[54] J. Lee, A. Liao, E. Pop, and W. P. King, "Electrical and thermal coupling to a single-wall carbon nanotube device using an electrothermal nanoprobe," *Nano Letters*, vol. 9, no. 4, pp. 1356–1361, 2009.

[55] C. Fu and L. Gu, "Composite fibers from poly (vinyl alcohol) and poly (vinyl alcohol)-functionalized multiwalled carbon nanotubes," *Journal of Applied Polymer Science*, vol. 128, no. 2, pp. 1044–1053, 2013.

[56] T. C. Lin and B. R. Huang, "Temperature effect on hydrogen response for cracked carbon nanotube/nickel (CNT/Ni) composite film with horizontally aligned carbon nanotubes," *Sensors and Actuators B: Chemical*, vol. 185, pp. 548–552, 2013.

[57] D. Silambarasan, V. Surya, V. Vasu, and K. Iyakutti, "One-step process of hydrogen storage in single walled carbon nanotubes-tin oxide nano composite," *International Journal of Hydrogen Energy*, vol. 38, no. 10, pp. 4011–4016, 2013.

[58] L. Chen, K. Xia, L. Huang, L. Li, L. Pei, and S. Fei, "Facile synthesis and hydrogen storage application of nitrogen-doped carbon nanotubes with bamboo-like structure," *International Journal of Hydrogen Energy*, vol. 38, no. 8, pp. 3297–3303, 2013.

[59] S. Nallusamy, A. M. Babu, and N. M. Prabu, "Investigation on carbon nanotubes over review on other heat transfer nano fluids," *International Journal of Applied Engineering Research*, vol. 10, no. 62, pp. 112–117, 2015.

[60] M. Sabiha, R. Saidur, S. Hassani, Z. Said, and S. Mekhilef, "Energy performance of an evacuated tube solar collector using single walled carbon nanotubes nanofluids," *Energy Conversion and Management*, vol. 105, pp. 1377–1388, 2015.

[61] H. Eshgarf and M. Afrand, "An experimental study on rheological behavior of non-Newtonian hybrid nano-coolant for application in cooling and heating systems," *Experimental Thermal and Fluid Science*, vol. 76, pp. 221–227, 2016.

[62] M. Baratpour, A. Karimipour, M. Afrand, and S. Wongwises, "Effects of temperature and concentration on the viscosity of nanofluids made of single-wall carbon nanotubes in ethylene glycol," *International Communications in Heat and Mass Transfer*, vol. 74, pp. 108–113, 2016.

[63] N. S. Akbar, S. A. Abid, D. Tripathi, and N. A. Mir, "Nanostructures study of CNT nanofluids transport with temperature-dependent variable viscosity in a muscular tube," *The European Physical Journal Plus*, vol. 132, no. 3, p. 110, 2017.

[64] M. Bahiraei, M. Berahmand, and A. Shahsavar, "Irreversibility analysis for flow of a non-Newtonian hybrid nanofluid containing coated CNT/Fe_3O_4 nanoparticles in a minichannel heat exchanger," *Applied Thermal Engineering*, vol. 125, pp. 1083–1093, 2017.

[65] E. Shahsavani, M. Afrand, and R. Kalbasi, "Using experimental data to estimate the heat transfer and pressure drop of non-Newtonian nanofluid flow through a circular tube: applicable for use in heat exchangers," *Applied Thermal Engineering*, vol. 129, pp. 1573–1581, 2018.

[66] D. Wen and Y. Ding, "Formulation of nanofluids for natural convective heat transfer applications," *International Journal of Heat and Fluid Flow*, vol. 26, no. 6, pp. 855–864, 2005.

[67] D. Wen and Y. Ding, "Natural convective heat transfer of suspensions of titanium dioxide nanoparticles (nanofluids)," *IEEE Transactions on Nanotechnology*, vol. 5, no. 3, pp. 220–227, May 2006.

[68] W. Duangthongsuk and S. Wongwises, "Heat transfer enhancement and pressure drop characteristics of TiO_2-water nanofluid in a double-tube

counter flow heat exchanger," *International Journal of Heat and Mass Transfer*, vol. 52, no. 7-8, pp. 2059–2067, 2009.

[69] R. Saleh, N. Putra, R. E. Wibowo, W. N. Septiadi, and S. P. Prakoso, "Titanium dioxide nanofluids for heat transfer applications," *Experimental Thermal and Fluid Science*, vol. 52, pp. 19–29, 2014.

[70] M. Arulprakasajothi, K. Elangovan, K. H. Reddy, and S. Suresh, "Heat transfer study of water-based nanofluids containing titanium oxide nanoparticles," *Materials Today: Proceedings*, vol. 2, no. 4-5, pp. 3648–3655, 2015.

[71] N. Karapinar, "Magnetic separation of ferrihydrite from wastewater by magnetic seeding and high-gradient magnetic separation," *International Journal of Mineral Processing*, vol. 71, no. 1-4, pp. 45–54, 2003.

[72] J. Dobson, "Magnetic nanoparticles for drug delivery," *Drug Development Research*, vol. 67, no. 1, pp. 55–60, 2006.

[73] L. Blaney, "Magnetite (Fe_3O_4): Properties, synthesis, and applications," 2007.

[74] C. G. Hadjipanayis, R. Machaidze, M. Kaluzova, L. Wang, A. J. Schuette, H. Chen, X. Wu, and H. Mao, "Egfrviii antibody–conjugated iron oxide nanoparticles for magnetic resonance imaging–guided convection-enhanced delivery and targeted therapy of glioblastoma," *Cancer Research*, vol. 70, no. 15, pp. 6303–6312, 2010.

[75] P. I. Girginova, A. L. Daniel-da Silva, C. B. Lopes, P. Figueira, M. Otero, V. S. Amaral, E. Pereira, and T. Trindade, "Silica coated magnetite particles for magnetic removal of Hg2+ from water," *Journal of Colloid and Interface Science*, vol. 345, no. 2, pp. 234–240, 2010.

[76] R. K. Singh, T.-H. Kim, K. D. Patel, J. C. Knowles, and H.-W. Kim, "Biocompatible magnetite nanoparticles with varying silica-coating layer for use

in biomedicine: Physicochemical and magnetic properties, and cellular compatibility," *Journal of Biomedical Materials Research Part A*, vol. 100, no. 7, pp. 1734–1742, 2012.

[77] A. Atta, H. Al-Lohedan, and S. Al-Hussain, "Functionalization of magnetite nanoparticles as oil spill collector," *International Journal of Molecular Sciences*, vol. 16, no. 4, pp. 6911–6931, 2015.

[78] A. Atta, G. El-Mahdy, H. Al-Lohedan, and S. Al-Hussain, "Synthesis of environmentally friendly highly dispersed magnetite nanoparticles based on rosin cationic surfactants as thin film coatings of steel," *International Journal of Molecular Sciences*, vol. 15, no. 4, pp. 6974–6989, 2014.

[79] R. Hiergeist, W. Andrä, N. Buske, R. Hergt, I. Hilger, U. Richter, and W. Kaiser, "Application of magnetite ferrofluids for hyperthermia," *Journal of Magnetism and Magnetic Materials*, vol. 201, no. 1-3, pp. 420–422, 1999.

[80] S. Odenbach and S. Thurm, "Magnetoviscous effects in ferrofluids," in *Ferrofluids*. Springer, 2002, pp. 185–201.

[81] T. Voelker and S. Odenbach, "Thermodiffusion in ferrofluids in the presence of a magnetic field," *Physics of Fluids*, vol. 17, no. 3, p. 037104, 2005.

[82] Y. Xuan, Q. Li, and M. Ye, "Investigations of convective heat transfer in ferrofluid microflows using Lattice-Boltzmann approach," *International Journal of Thermal Sciences*, vol. 46, no. 2, pp. 105–111, 2007.

[83] A. Jafari, T. Tynjälä, S. Mousavi, and P. Sarkomaa, "CFD simulation of heat transfer in ferrofluids," *International Journal of Heat Fluid*, 2007.

[84] R. E. Rosensweig, *Ferrohydrodynamics*. Courier Corporation, 2013.

[85] N. Sandeep, A. J. Chamkha, and I. Animasaun, "Numerical exploration of magnetohydrodynamic nanofluid flow suspended with magnetite nanoparticles," *Journal of the Brazilian Society of Mechanical Sciences and Engineering*, vol. 39, no. 9, pp. 3635–3644, 2017.

[86] H. Alfvén, "Existence of electromagnetic-hydrodynamic waves," *Nature*, vol. 150, no. 3805, p. 405, 1942.

[87] K. S. Mekheimer and T. Al-Arabi, "Nonlinear peristaltic transport of MHD flow through a porous medium," *International Journal of Mathematics and Mathematical Sciences*, vol. 2003, no. 26, pp. 1663–1682, 2003.

[88] M. Elshahed and M. H. Haroun, "Peristaltic transport of Johnson-Segalman fluid under effect of a magnetic field," *Mathematical Problems in Engineering*, vol. 2005, no. 6, pp. 663–677, 2005.

[89] K. S. Mekheimer and Y. A. Elmaboud, "The influence of heat transfer and magnetic field on peristaltic transport of a newtonian fluid in a vertical annulus: application of an endoscope," *Physics Letters A*, vol. 372, no. 10, pp. 1657–1665, 2008.

[90] S. Srinivas and M. Kothandapani, "Peristaltic transport in an asymmetric channel with heat transfera note," *International Communications in Heat and Mass Transfer*, vol. 35, no. 4, pp. 514–522, 2008.

[91] S. Nadeem and S. Akram, "Magnetohydrodynamic peristaltic flow of a hyperbolic tangent fluid in a vertical asymmetric channel with heat transfer," *Acta Mechanica Sinica*, vol. 27, no. 2, pp. 237–250, 2011.

[92] S. Srinivas and R. Muthuraj, "Effects of chemical reaction and space porosity on MHD mixed convective flow in a vertical asymmetric channel with peristalsis," *Mathematical and Computer Modelling*, vol. 54, no. 5-6, pp. 1213–1227, 2011.

[93] K. Zakaria and N. Amin, "Peristaltic flow of a magnetohydrodynamic Oldroyd-B fluid in an asymmetric channel," *Int. J. of Appl. Math. and Mech*, vol. 8, no. 18, pp. 18–37, 2012.

[94] T. Hayat, S. Bibi, M. Rafiq, A. Alsaedi, and F. Abbasi, "Effect of an inclined magnetic field on peristaltic flow of Williamson fluid in an inclined channel

with convective conditions," *Journal of Magnetism and Magnetic Materials*, vol. 401, pp. 733–745, 2016.

[95] J. Prakash, E. Siva, D. Tripathi, S. Kuharat, and O. A. Bég, "Peristaltic pumping of magnetic nanofluids with thermal radiation and temperature-dependent viscosity effects: Modelling a solar magneto-biomimetic nanopump," *Renewable Energy*, vol. 133, pp. 1308–1326, 2019.

[96] D. A. Nield and A. Bejan, "Convection in Porous Media," vol. 3, 2006.

[97] Y. Cencel and J. Cimbala, "Fluid Mechanics-Fundamentals and Applications," 2006.

[98] F. M. White, "Viscous Fluid Flow, McGraw-Hill Mechanical Engineering," vol. 3, 2005.

[99] R. Bansal, "A Textbook of Fluid Mechanics and Hydraulic Machines," 2004.

[100] Y. A. Cengel, S. Klein, and W. Beckman, "Heat transfer: A practical approach," vol. 141, 1998.

[101] W. Yu and H. Xie, "A review on nanofluids: preparation, stability mechanisms, and applications," *Journal of Nanomaterials*, vol. 2012, p. 1, 2012.

[102] O. Maj, "A mathematical introduction to magnetohydrodynamics," in *Vorlesung (SS 2017)*, 2017.

[103] D. Halliday, J. Walker, and R. Resnick, "Fundamentals of Physics," 2013.

[104] J. Kunes, "Dimensionless Physical Quantities in Science and Engineering," 2012.

[105] M. A. Sleigh, "The Biology of Cilia and Flagella: International Series of Monographs on Pure and Applied Biology: Zoology," vol. 12, 1962.

[106] T. Lardner and W. Shack, "Cilia transport," *The Bulletin of Mathematical Biophysics*, vol. 34, no. 3, pp. 325–335, 1972.

[107] S. A. Noreen and A. W. Butt, "Physiological transportation of Casson fluid in a plumb duct," *Communications in Theoretical Physics*, vol. 63, no. 3, p. 347, 2015.

[108] T. Hayat, A. Kiran, M. Imtiaz, and A. Alsaedi, "Unsteady flow of carbon nanotubes with chemical reaction and Cattaneo-Christov heat flux model," *Results in Physics*, vol. 7, pp. 823–831, 2017.

[109] W. Khan, Z. Khan, and M. Rahi, "Fluid flow and heat transfer of carbon nanotubes along a flat plate with Navier slip boundary," *Applied Nanoscience*, vol. 4, no. 5, pp. 633–641, 2014.

[110] A. V. Kumar, M. Vankudre, and N. M. K. Bagwe, "Unsteady MHD free convection by passing cobalt nanoparticles past an accelerated vertical plate through porous medium of ethylene glycol," *International Journal of Engineering & Technology*, vol. 7, no. 4.10, pp. 619–623, 2018.

[111] S. P. Goqo, S. D. Oloniiju, H. Mondal, P. Sibanda, and S. S. Motsa, "Entropy generation in MHD radiative viscous nanofluid flow over a porous wedge using the bivariate spectral quasi-linearization method," *Case Studies in Thermal Engineering*, vol. 12, pp. 774–788, 2018.

[112] N. S. Akbar and A. W. Butt, "CNT suspended nanofluid analysis in a flexible tube with ciliated walls," *The European Physical Journal Plus*, vol. 129, no. 8, p. 174, 2014.

[113] W. Yu and S. Choi, "The role of interfacial layers in the enhanced thermal conductivity of nanofluids: a renovated Maxwell model," *Journal of Nanoparticle Research*, vol. 5, no. 1-2, pp. 167–171, 2003.

[114] A. Kasaeian and S. Nasiri, "Convection heat transfer modeling of nanofluid TiO_2 using different viscosity theories," *International Journal of Nanoscience and Nanotechnology*, vol. 11, no. 1, pp. 45–51, 2015.

[115] N. Akbar, M. Raza, and R. Ellahi, "Endoscopic effects with entropy generation analysis in peristalsis for the thermal conductivity of H_2O+Cu

nanofluid," *Journal of Applied Fluid Mechanics*, vol. 9, no. 4, pp. 1721–1730, 2016.

[116] N. Akbar, "Entropy generation analysis for a CNT suspension nanofluid in plumb ducts with peristalsis," *Entropy*, vol. 17, no. 3, pp. 1411–1424, 2015.

[117] T. Hayat, M. Rashid, and A. Alsaedi, "MHD convective flow of magnetite-Fe_3O_4 nanoparticles by curved stretching sheet," *Results in Physics*, vol. 7, pp. 3107–3115, 2017.

[118] R. U. Haq, F. Shahzad, and Q. M. Al-Mdallal, "MHD pulsatile flow of engine oil based carbon nanotubes between two concentric cylinders," *Results in Physics*, vol. 7, pp. 57–68, 2017.

[119] N. S. Akbar and Z. H. Khan, "Variable fluid properties analysis with water based CNT nanofluid over a sensor sheet: Numerical solution," *Journal of Molecular Liquids*, vol. 232, pp. 471–477, 2017.

[120] A. Lekawa-Raus, J. Patmore, L. Kurzepa, J. Bulmer, and K. Koziol, "Electrical properties of carbon nanotube based fibers and their future use in electrical wiring," *Advanced Functional Materials*, vol. 24, no. 24, pp. 3661–3682, 2014.